Rotating Cantilever Beams:

Finite Element Modeling and Vibration Analysis

Marco António Costa Fonseca Lima

Dissertação do MIEM

Orientador: Prof. Doutor José Dias Rodrigues

Faculdade de Engenharia da Universidade do Porto
Mestrado Integrado em Engenharia Mecânica

Julho de 2012

Resumo

No presente trabalho são analisadas vigas encastradas em rotação usando o método dos elementos finitos. São apresentados métodos de modelação para a análise das vibrações de flexão flapwise e chordwise usando as teorias de vigas de Euler-Bernoulli e Timoshenko. Estes métodos de modelação são baseados num novo conjunto de variáveis de deformação híbridas. As equações diferenciais lineares de movimento são obtidas usando o princípio de Hamilton, obtendo-se a partir destas as respectivas formas fracas. Parâmetros adimensionais são introduzidos e os seus efeitos são estudados. Efeitos de ressonância e instabilidade são também analisados.

Após a análise de vigas simples, um método de modelação para uma viga multicamada pré-torcida é introduzido utilizando a teoria layerwise. Os resultados são comparados com sucesso com aqueles obtidos para uma viga simples sem pré-torção. Os resultados para uma viga multicamada pré-torcida apenas puderam ser validados sob a condição de pequenos ângulos de torção.

Usando o modelo layerwise, os efeitos de amortecimento por tratamento viscoelástico são analisados para os dois movimentos de flexão usando a função de resposta em frequência. Finalmente, são efectudas alterações ao modelo layerwise para o caso de uma viga compósita laminada, onde os efeitos dos ângulos das fibras nos modos naturais são analisados.

Abstract

In the present work rotating cantilever beams are analyzed using the finite element method. Modeling methods for the analysis of flapwise and chordwise bending vibrations are presented using the Euler-Bernoulli and Timoshenko beam theories and also for a pre-twisted beam using Timoshenko theory. These modeling methods are based on a new set of hybrid deformation variables. The linear differential equations of motion are derived using Hamilton's principle from which the weak forms are derived. Dimensionless parameters are introduced and its effects on the natural frequencies are studied. Resonance and instability effects are also analyzed.

After the analysis of simple beams, a modeling method for a multilayer pre-twisted beam is introduced using the layerwise theory, its results are successfully compared with those obtained for a simple beam with no pre-twist. Results for the pre-twisted multilayer beam could only be validated under the condition of small pre-twist angle.

Using the layerwise model the effects of viscoelastic damping treatment are determined for both bending motions using the frequency response function. Finally, modifications of the layerwise model are made for the the case of a laminated composite beam, where the effects of the fiber angles over the natural modes are analyzed.

Contents

List of Figures

List of Tables

Chapter 1

Introduction

1.1 Motivation

Over the past years there has been a growing interest over the analysis of free vibrations characteristics of rotating structures that operate at a constant angular speed. Such interest comes from the obvious fact that numerous structural devices operate under such conditions, and the need of understanding and predicting the dynamic behaviour and characteristics of the same. Some pratical engineer examples of rotating structures are turbine, compressor and helicopter blades, robot manipulators and satellite antennas.

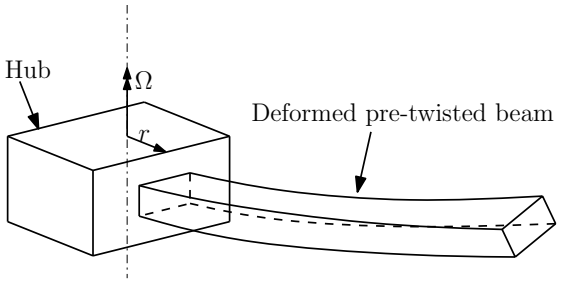

Figure 1.1: Scheme of a rotating cantilever beam

Since there are significant variations of the dynamic characteristics due to the rotational motion, in order to obtain an economical and reliable design as well as control of the system, the dynamic characteristics need to be determined in a accurate and efficient way, reason why this subject has been studied for many years.

1.2 Review of the Literature

According to Yoo et al. [1] the first modeling approach for rotating was introduced in the 1970s and it is somewhat referred to as classical linear Cartesian (CLC) modeling approach which is based on the classical linear elastic modeling, where both geometric as well as material linearity is assumed. The main advantage of this modeling approach is the ease of formulation as well as implementation. However it can only go so far as it produces erroneous results in numeric simulations when the structures undergo large overall motions as it is usually the case of a rotating beam.

To solve this problem other non-linear methods were introduced based on non-linear relations between the strains and displacements, as the defective results were attributed to the geometric linearity assumption. These methods indeed solved the lack of accuracy problem, but on the other hand the non-linearity created other problems like the large amount of computational effort needed to perform a dynamic analysis. With this in mind another modeling approach was developed using a set of hybrid coordinates (two Cartesian and one non-Cartesian), which will be better described later on.

This modeling method using hybrid deformation variable has been widely used by many authors since it showed itself efficient at resolving the lack of accuracy of the CLC method and also the inefficiency of the non-linear methods. Yoo et al. [1] used this modeling method to derive the linear equations of motion and compared results with the CLC approach establishing a limit of validity for this method. Yoo and Shin [2] derived the equations of motion approximating the hybrid set of variables using the Rayleigh-Ritz assumed mode method and analyzed the gyroscopic coupling effect between the stretch and bending motion and to what extent can it be neglected. Rao and Gupta [3] used the finite element method to determine the bending natural frequencies of a rotating twisted and double tapered beam, deriving the mass and stiffness matrices that included the effects of shear deformation, rotary inertia and centrifugal induced stiffness, although stretch deformation was not included. Chung and Yoo [4] also used the same hybrid modeling approach to derive the full non-linear equations of motion, which were then linearized and their respective weak forms were derived for application in the finite element method. Ozgumus and Kaya [5] studied the flapwise bending vibration and analyzed the effects of taper ratios of a double-tapered Timoshenko beam using a mathematical technique known as the differential transform method (DTM) to solve the governing differential equations of motion. Zhu [6] analyzed the chordwise and flapwise bending vibrations for a pre-twisted Timoshenko beam but gyroscopic effect was neglected, Yoo et al. [7] analyzed the same bending vibrations using an Euler-Bernoulli beam theory and in Yoo et al. [8] the effect of a concentrated mass was included. Yoo et al. [9] also analyzed the flapwise bending vibration for a multi-layered composite beam.

1.3 Objectives

The main objectives aimed by the present work are the following:

- Analyse and characterize the dynamic behaviour of rotating beams;
- Development and implementation of finite element models considering the effects that come from the rotating movement of the beam (centrifugal stiffening, gyroscopic effect);
- Modify the finite element models for multilayer beams so that the effects of superficial viscoelastic treatments can be analyzed as well as the effects of using composite materials.
- To contribute, through the development of modeling tools and parametric analysis, to the dynamic project of rotating beams.

1.4 Structure of the dissertation

This dissertation is organized in eight chapters each one regarding a different subject even though always related to the main issue which is the vibration of rotating beams.

In the present chapter 1 a literature review of the problem of rotating cantilever beams is made and the main objectives for this dissertation are presented.

In chapter 2 the displacement and velocity fields are carefully analyzed and a new hybrid coordinate, related the usual classic Cartesian deformation variables, is introduced and thoroughly derived. Using this new hybrid deformation variable, the linear differential equations of motion are derived utilizing Hamilton's principle.

From the differential equations the variational forms are obtained in chapter 3 and the global matrices that define the spatial model for the rotating beam problem are defined.

In chapter 4 using the global system of equations numeric results are obtained for the natural frequencies and mode shapes of the the rotating beam and the effects of the beam's geometry are analyzed.

In chapter 5 it is proposed a modeling method using a layerwise theory for a rotating pre-twisted beam composed of several layers (multilayer element).

Chapter 6 introduces a constitutive model for the behaviour of the viscoelastic material and implementation in the finite element method, it is then analyzed if the viscoelastic damping produces some control over the bending vibrations of the rotating beam.

In chapter 7 a modeling method for rotating laminated composite beams is introduced using the layerwise theory and the effects of the fibers' angles over the natural frequencies are determined.

In the last chapter some conclusions are drawn from the overall results obtained throughout this dissertation and some suggestions are left for further development of the present work.

Chapter 2

Equations of motion

2.1 Hamilton's principle: review

The extended Hamilton's principle will be used to derive the differential equations of motion. According to Meirovitch [10] the extended Hamilton's principle can be mathematically stated as

$$\delta \int_{t_i}^{t_f} (\mathfrak{L} + \mathcal{W})\, dt = 0 \tag{2.1.1}$$

where $\mathfrak{L}$ is known as the Lagrangian density function or Lagrangian functional, and $\mathcal{W}$ represents the work done on the system by non-conservative forces.

The Lagrangian functional $\mathfrak{L}$ is related to both kinetic and potential energy, T and Π respectively, and it is given by the following equation

$$\mathfrak{L} = T - \Pi \tag{2.1.2}$$

Replacing equation (2.1.2) in equation (2.1.1) and also taking into account that the variational and integration operators are interchangeable, Hamilton's principle can also be stated as

$$\int_{t_i}^{t_f} (\delta T - \delta\Pi + \delta\mathcal{W})\, dt = 0 \tag{2.1.3}$$

To determine the kinetic energy of a given mechanical system, one needs to know the velocity field of the system, which implies knowing the velocity of any generic point through a set of generalized coordinates. Let $\mathbf{v}_P$ be the velocity vector of any generic point P of the mechanical system, the kinetic energy can then be determined as follows

$$T = \frac{1}{2} \int_V \rho\, \mathbf{v}_P^T \cdot \mathbf{v}_P\, dV \tag{2.1.4}$$

with ρ as the material density.

As for the potential energy, it can easily be calculated knowing the strain and stress fields of the system. With $\boldsymbol{\varepsilon}$ as the strain field and $\boldsymbol{\sigma}$ as the stress field, the potential energy is then determined by the following relation

$$\Pi = \frac{1}{2} \int_V \boldsymbol{\varepsilon}^T \cdot \boldsymbol{\sigma}\, dV \tag{2.1.5}$$

The strain field is derived from the displacement field using Green's tensor whereas the stress field is calculated using the strains and the well known elastic constants from the generalized Hook's law.

2.2 Cartesian system of coordinates

In this section the displacement and the velocity fields of a rotating cantilever beam are derived with a Cartesian set of generalized coordinates.

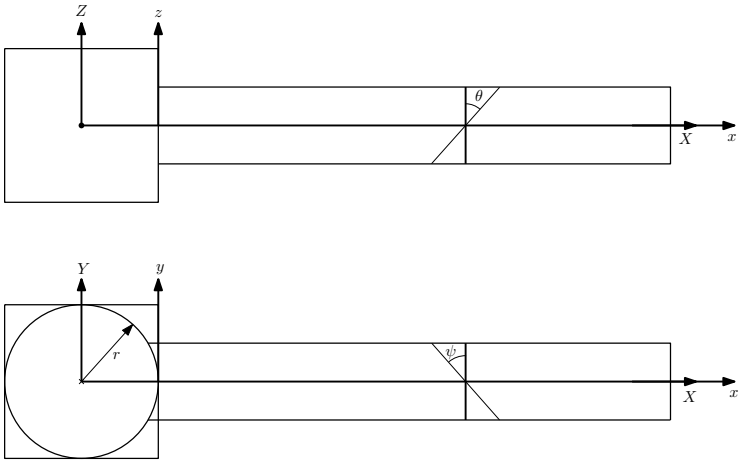

Figure 2.1: Axes system and rotation of the cross section

In the derivation of the displacement and velocity vectors two sets of axes will be used and they are represented in figure 2.1. Note that two sets of axes aren't actually coincident, while one (XYZ) is fixed, the other one (xyz) is attached to the rotating beam and moves with it. Thus we have one fixed referential, R_f, consisting in the XYZ axes and one movable referential, R_m, that accompanies the beam in its rotating movement consisting in the xyz axes. In the following equations every vectors are represented in the R_m referential.

2.2.1 Displacement and velocity fields

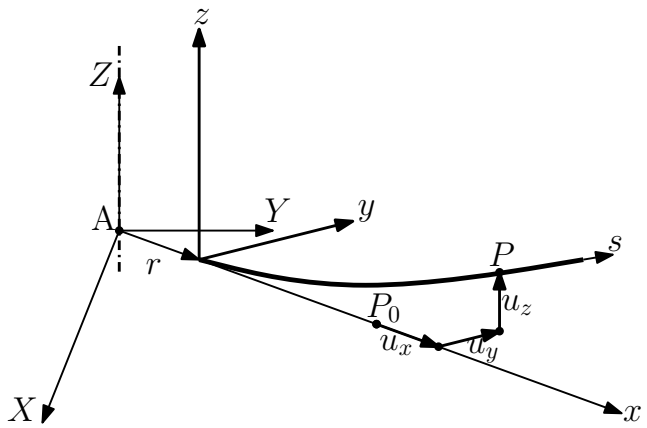

Figure 2.2: Displacement field of a generic point P

According to figure 2.2, the position vector of any point of the undeformed beam is

$$\overrightarrow{AP}_0 = \begin{Bmatrix} r+x \\ y \\ z \end{Bmatrix} \tag{2.2.1}$$

and after deformation of the beam, the position vector of the same point is

$$\overrightarrow{AP} = \begin{Bmatrix} r + x + u_x \\ y + u_y \\ z + u_z \end{Bmatrix} \tag{2.2.2}$$

Having these two vectors the displacement field can now easily be determined as follows

$$\mathbf{u} = \overrightarrow{AP} - \overrightarrow{AP}_0 = \begin{Bmatrix} u_x \\ u_y \\ u_z \end{Bmatrix} \tag{2.2.3}$$

To obtain the velocity vector one needs differentiate with respect to time the position vector $\overrightarrow{AP}$, but since we pretend the absolute velocity of any generic point and the position vector is represented in the referential R_m, a simple differentiation with respect to time will not suffice as it would lead us only to a relative velocity. Thus one needs to differentiate the position vector represented in the movable referential R_m with respect to the fixed referential R_f in order to obtain an absolute velocity vector that is still represented in the referential R_m, this is also known as the *Theorem of Relative Derivatives*.

Using said theorem, the absolute velocity vector $\mathbf{v}_P$ is determined as follows

$$\mathbf{v}_P\Big|_{R_m} = \overrightarrow{\dot{AP}}\Big|_{R_f}\Big|_{R_m} = \overrightarrow{\dot{AP}}\Big|_{R_m}\Big|_{R_m} + \overrightarrow{\omega}_{mf}\Big|_{R_m} \times \overrightarrow{AP}\Big|_{R_m} \tag{2.2.4}$$

where

$$\overrightarrow{\omega}_{mf}\Big|_{R_m} = \begin{Bmatrix} 0 \\ 0 \\ \Omega \end{Bmatrix} \tag{2.2.5}$$

represents the angular velocity vector of the rotating referential. Finally, the absolute velocity vector is given by

$$\mathbf{v}_P\Big|_{R_m} = \begin{Bmatrix} \dot{u}_x \\ \dot{u}_y \\ \dot{u}_z \end{Bmatrix} + \begin{Bmatrix} -\Omega(y + u_y) \\ \Omega(r + x + u_x) \\ 0 \end{Bmatrix} \tag{2.2.6}$$

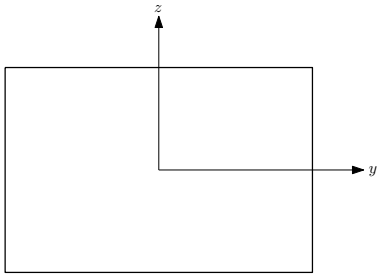

Figure 2.3: Cross section of a simple beam

Now, for a simple rotating beam, with the cross section presented in figure 2.3 and according to figure 2.1, the displacements u_x, u_y and u_z can be described through a set of generalized coordinates and the displacement vector $\mathbf{u}$ can be written as

$$\mathbf{u} = \begin{Bmatrix} u_x \\ u_y \\ u_z \end{Bmatrix} = \begin{Bmatrix} u(x,t) + z\theta(x,t) - y\psi(x,t) \\ v(x,t) \\ w(x,t) \end{Bmatrix} \tag{2.2.7}$$

where u, v and w are the displacements of any point at the neutral axis of the beam along the x, y and z axis respectively, θ and ψ represent the angular rotation of any cross section of the beam about the y and z axis respectively. Note that with this displacement field the generalized coordinates are assumed

constant for any point along a given cross section of the beam, since they depend only on the spatial variable x and the time variable t.

Replacing the displacement field (2.2.7) into the velocity field (2.2.6), the velocity field vector for a simple rotating beam becomes

$$\mathbf{v}_P = \begin{Bmatrix} \dot{u} + z\dot{\theta} - y\dot{\psi} - \Omega(y+v) \\ \dot{v} + \Omega(r+x+u+z\theta - y\psi) \\ \dot{w} \end{Bmatrix} \tag{2.2.8}$$

2.2.2 Strain field

According to Reddy [11], Green's strain tensor (also known as Green-Lagrange strain tensor) which was first introduced by Green and St. Venant is given by the following equation

$$L_{jk} = \frac{1}{2}\left(\frac{\partial u_j}{\partial X_k} + \frac{\partial u_k}{\partial X_j} + \frac{\partial u_i}{\partial X_j}\frac{\partial u_i}{\partial X_k}\right) \tag{2.2.9}$$

or in terms of mechanical strains

$$\varepsilon_{jk} = L_{jk}, \text{ if } j = k \tag{2.2.10a}$$
$$\gamma_{jk} = 2L_{jk}, \text{ if } j \neq k \tag{2.2.10b}$$

With $u_1, u_2, u_3 = u_x, u_y, u_z$ and $X_1, X_2, X_3 = x, y, z$ respectively, one gets the strain tensor as

$$\varepsilon_{xx} = \frac{1}{2}\left[2\frac{\partial u_x}{\partial x} + \left(\frac{\partial u_x}{\partial x}\right)^2 + \left(\frac{\partial u_y}{\partial x}\right)^2 + \left(\frac{\partial u_z}{\partial x}\right)^2\right] \tag{2.2.11a}$$
$$\varepsilon_{yy} = \frac{1}{2}\left[2\frac{\partial u_y}{\partial y} + \left(\frac{\partial u_x}{\partial y}\right)^2 + \left(\frac{\partial u_y}{\partial y}\right)^2 + \left(\frac{\partial u_z}{\partial y}\right)^2\right] \tag{2.2.11b}$$
$$\varepsilon_{zz} = \frac{1}{2}\left[2\frac{\partial u_z}{\partial z} + \left(\frac{\partial u_x}{\partial z}\right)^2 + \left(\frac{\partial u_y}{\partial z}\right)^2 + \left(\frac{\partial u_z}{\partial z}\right)^2\right] \tag{2.2.11c}$$
$$\gamma_{xy} = \frac{\partial u_x}{\partial y} + \frac{\partial u_y}{\partial x} + \frac{\partial u_x}{\partial x}\frac{\partial u_x}{\partial y} + \frac{\partial u_y}{\partial x}\frac{\partial u_y}{\partial y} + \frac{\partial u_z}{\partial x}\frac{\partial u_z}{\partial y} \tag{2.2.11d}$$
$$\gamma_{yz} = \frac{\partial u_y}{\partial z} + \frac{\partial u_z}{\partial y} + \frac{\partial u_x}{\partial y}\frac{\partial u_x}{\partial z} + \frac{\partial u_y}{\partial y}\frac{\partial u_y}{\partial z} + \frac{\partial u_z}{\partial y}\frac{\partial u_z}{\partial z} \tag{2.2.11e}$$
$$\gamma_{zx} = \frac{\partial u_z}{\partial x} + \frac{\partial u_x}{\partial z} + \frac{\partial u_x}{\partial z}\frac{\partial u_x}{\partial x} + \frac{\partial u_y}{\partial z}\frac{\partial u_y}{\partial x} + \frac{\partial u_z}{\partial z}\frac{\partial u_z}{\partial x} \tag{2.2.11f}$$

Keeping in mind that the generalized coordinates depend only on the spatial variable x and under the assumption of small displacements along the x direction comparatively to those along y and z directions or, in other words, $u_x < u_y$ and $u_x < u_z$, it follows that the strain equations (2.2.11) can be simplified by neglecting the terms involving the product of the derivative of u_x and other derivatives, and thus we have the following simplified strain field for a simple rotating beam

$$\varepsilon_{xx} = \frac{\partial u}{\partial x} + z\frac{\partial \theta}{\partial x} + y\frac{\partial \psi}{\partial x} + \frac{1}{2}\left(\frac{\partial v}{\partial x}\right)^2 + \frac{1}{2}\left(\frac{\partial w}{\partial x}\right)^2 \tag{2.2.12a}$$
$$\gamma_{xy} = \left(\frac{\partial v}{\partial x} - \psi\right) \tag{2.2.12b}$$
$$\gamma_{zx} = \left(\frac{\partial w}{\partial x} + \theta\right) \tag{2.2.12c}$$
$$\varepsilon_{yy} = \varepsilon_{zz} = \gamma_{yz} = 0 \tag{2.2.12d}$$

Note that the last two terms in equation 2.2.12a can not be neglected since geometric linearity is not valid when large overall motions are prescribed, as opposed to what is done in the CLC method.

2.2.3 Stress field

Using the appropriate elasticity relations between the stress and the strain fields, the first can be derived from the second, needing only to multiply the strains by the respective elastic constants that are derived from the generalized Hook's law, which results in the following constitutive law

$$\boldsymbol{\sigma} = \frac{E}{(1-2\nu)(1+\nu)} \begin{bmatrix} (1-\nu) & \nu & \nu & 0 & 0 & 0 \\ \nu & (1-\nu) & \nu & 0 & 0 & 0 \\ \nu & \nu & (1-\nu) & 0 & 0 & 0 \\ 0 & 0 & 0 & (1-2\nu) & 0 & 0 \\ 0 & 0 & 0 & 0 & (1-2\nu) & 0 \\ 0 & 0 & 0 & 0 & 0 & (1-2\nu) \end{bmatrix} \boldsymbol{\varepsilon} \tag{2.2.13}$$

which is only valid for materials with isotropic behaviour.

Since that for a beam the stresses σ_{yy}, σ_{zz} and τ_{yz} are assumed negligible, one gets the following stress fields for a simple rotating beam

$$\sigma_{xx} = E\varepsilon_{xx} \tag{2.2.14a}$$
$$\tau_{xy} = G\gamma_{xy} \tag{2.2.14b}$$
$$\tau_{zx} = G\gamma_{zx} \tag{2.2.14c}$$

with

$$G = \frac{E}{2(1+\nu)} \tag{2.2.15}$$

2.3 Hybrid coordinate system

As it was said in the introduction, a new set of generalized coordinates will be used in the derivation of the differential equations of movement. In this section a relation between the coordinates u and s is derived in order to apply it to both the strain and velocity fields and thus obtain the proper potential and kinetic expressions for the derivation of the equations of motion.

2.3.1 Relation between u and s

From figure 2.4 and considering *Pitagoras' theorem* the differential arc length of the neutral axis of the deformed beam can be given by the following expression

$$dS = \sqrt{(d\eta)^2 + (dv)^2 + (dw)^2} \tag{2.3.1}$$

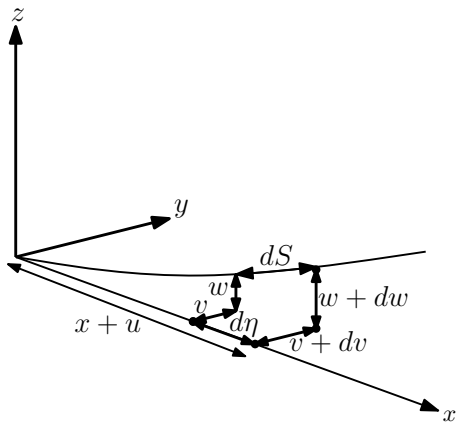

Figure 2.4: Differential arc of the neutral axis of the beam

with η being a variable that varies from 0 to $x+u$. Integration of equation (2.3.1) with respect to η between 0 and $x+u$ would lead us to the total arc length of the neutral axis of the deformed beam

$$S = \int_0^{x+u} \sqrt{(d\eta)^2 + (dv)^2 + (dw)^2} \tag{2.3.2}$$

However, this integration variable isn't the more appropriate one as it has analytical difficulties associated with it. In fact seeing that the integration limits depend explicitly on u, this actually complicates the main point of this procedure which is to find a simple relation between the displacements u and s. In order to surpass such difficulties another variable related to η is introduced as follows

$$\varphi = \eta - u \tag{2.3.3}$$

and after differentiating equation (2.3.3)

$$d\varphi = d\eta - du \tag{2.3.4}$$

which can be replaced back in equation (2.3.1) giving us

$$dS = \sqrt{(d\varphi + du)^2 + (dv)^2 + (dw)^2} \tag{2.3.5}$$

which is equivalent to

$$dS = \left[\left(d\varphi + \frac{\partial u}{\partial \varphi} d\varphi \right)^2 + \left(\frac{\partial v}{\partial \varphi} d\varphi \right)^2 + \left(\frac{\partial w}{\partial \varphi} d\varphi \right)^2 \right]^{\frac{1}{2}} \tag{2.3.6}$$

The total arc length can now be given by the integral of equation (2.3.6), but since integration is now taken with respect to φ one needs to change the integration limits. For $\eta = 0$ we have that $u = 0$, since the beam is fixed at the hub, and thus $\varphi = 0$. For $\eta = x + u$ it follows that $\varphi = x$. Having the new integration limits for the new variable φ, one can determine the total arc length as

$$S = \int_0^x dS = \int_0^x \left[\left(1 + \frac{\partial u}{\partial \varphi} \right)^2 + \left(\frac{\partial v}{\partial \varphi} \right)^2 + \left(\frac{\partial w}{\partial \varphi} \right)^2 \right]^{\frac{1}{2}} d\varphi \tag{2.3.7}$$

Considering only the first two terms of Taylor's expansion series of the first square term[1] in equation (2.3.7) yields

$$\left(1 + \frac{\partial u}{\partial \varphi} \right)^2 \approx 1 + 2\frac{\partial u}{\partial \varphi} \tag{2.3.8}$$

and introducing this approximation in equation (2.3.7) one gets

$$S \approx \int_0^x \left[1 + \left\{ 2\frac{\partial u}{\partial \varphi} + \left(\frac{\partial v}{\partial \varphi} \right)^2 + \left(\frac{\partial w}{\partial \varphi} \right)^2 \right\} \right]^{\frac{1}{2}} d\varphi \tag{2.3.9}$$

Approximating the integrand function by the first two terms of its Taylor expansion series[2] it follows that

$$S \approx \int_0^x \left\{ 1 + \frac{1}{2} \left[2\frac{\partial u}{\partial \varphi} + \left(\frac{\partial v}{\partial \varphi} \right)^2 + \left(\frac{\partial w}{\partial \varphi} \right)^2 \right] \right\} d\varphi \tag{2.3.10}$$

Now note that the total arc length of the neutral axis after deformation of the beam can be decomposed into the original length x before deformation and an additional stretch length s caused by deformation of the beam or, in other words, $S = x + s$. Replacing this relation in equation (2.3.10) and after integrating the first two terms of the right hand side of that same equation one gets

[1] $(1+x)^2 \approx (1+0)^2 + 2(1+0)(x-0) = 1 + 2x$

[2] $(1+x)^{\frac{1}{2}} \approx (1+0)^{\frac{1}{2}} + \frac{1}{2}(1+0)^{-\frac{1}{2}}(x-0) = 1 + \frac{1}{2}x$

$$x + s \approx x + u + \underbrace{\frac{1}{2}\int_0^x \left(\frac{\partial v}{\partial \varphi}\right)^2 d\varphi}_{h_v} + \underbrace{\frac{1}{2}\int_0^x \left(\frac{\partial w}{\partial \varphi}\right)^2 d\varphi}_{h_w} \tag{2.3.11}$$

and thus obtains an approximate relation between the displacements u and s as follows

$$u = s - h_v - h_w \tag{2.3.12}$$

Differentiation of equation (2.3.12) with respect to time lead us to

$$\frac{\partial u}{\partial t} = \underbrace{\frac{\partial s}{\partial t}}_{\dot{s}} - \underbrace{\int_0^x \frac{\partial v}{\partial \varphi}\frac{\partial}{\partial t}\left(\frac{\partial v}{\partial \varphi}\right) d\varphi}_{\dot{h}_v} - \underbrace{\int_0^x \frac{\partial w}{\partial \varphi}\frac{\partial}{\partial t}\left(\frac{\partial w}{\partial \varphi}\right) d\varphi}_{\dot{h}_w} \tag{2.3.13}$$

and differentiating equation (2.3.12) with respect to x and taking into account the *Fundamental Theorem of Calculus* it follows that

$$\frac{\partial u}{\partial x} = \frac{\partial s}{\partial x} - \frac{1}{2}\left(\frac{\partial v}{\partial x}\right)^2 - \frac{1}{2}\left(\frac{\partial w}{\partial x}\right)^2 \tag{2.3.14}$$

As it will be seen ahead, using the three conventional Cartesian variables the exact potential energy can only be expressed in a non-quadratic form leading to non-linear active forces in the equations of motion [1], which is how some non-linear modeling methods express the potential energy. The use of the stretch deformation facilitates the potential energy as it can be expressed in a quadratic form. However, the use of s complicates the formulation for the kinetic energy although, through linearization the final equations of motion can be obtained.

In the following sections the linear differential equations of motion will be derived for the Euler-Bernoulli , Timoshenko and pre-twisted Timoshenko beams. The material of the beam is assumed homogeneous and isotropic, the neutral and centroidal axes in the cross section are assumed coincident so that neither eccentricity nor torsion needs to be considered. Moreover, the hub where the beam is attached to is assumed undeformable and the beam is considered to rotate at constant speed so that no angular acceleration needs to be accounted for.

2.4 Euler-Bernoulli beam theory

In the Euler-Bernoulli beam theory (or slender beam theory) the shear strains and stresses are assumed negligible. To do so the strains γ_{xy} and γ_{zx} must vanish and the rotations of the cross section of the beam in each plane are expressed in terms of the displacements in the respective normal planes. In other words we have the rotation θ in the xz plane expressed in terms of the displacement w in the xy plane, and the rotation ψ in the xy plane expressed in terms of the displacement v in the xz plane as follows

$$\theta = -\frac{\partial w}{\partial x} \text{ and } \psi = \frac{\partial v}{\partial x} \tag{2.4.1}$$

With the rotations of the cross section defined as such, it is equivalent as assuming that the cross sections of the beam remain normal to the neutral axis. In this beam theory another basic assumption is the negligible rotary inertia, which has effect on the kinetic energy of the beam.

2.4.1 Kinetic energy

Replacing the relation between $\dot{u}$ and $\dot{s}$, derived in equation (2.3.13), in the velocity field (2.2.6) we get

$$\mathbf{v}_P = \begin{Bmatrix} \dot{s} - (\dot{h}_v + \dot{h}_w) + z\dot{\theta} - y\dot{\psi} - \Omega(y + v) \\ \dot{v} + \Omega(r + x + s + z\theta - y\psi) - \Omega(h_v + h_w) \\ \dot{w} \end{Bmatrix} \tag{2.4.2}$$

which is the velocity field expressed in terms of the new generalized coordinate s rather than u. Having the velocity field defined the kinetic energy can be expressed as

$$T = \frac{1}{2}\int_V \rho\Big\{\Big[\dot{s} - \Omega(y+v) + z\dot{\theta} - y\dot{\psi}\Big]^2 + y\Omega(\dot{h}_v + \dot{h}_w) + \Big[\dot{v} + \Omega(r+x+s+z\theta - y\psi)\Big]^2 - \Omega^2(r+x)(h_v+h_w) + \dot{w}^2\Big\} \tag{2.4.3}$$

and after integration over the cross sectional area of the beam and neglecting the rotary inertia, the kinetic energy can also be expressed as

$$T = \frac{1}{2}\int_0^L \rho A\Bigg\{\left(\frac{\partial s}{\partial t} - \Omega v\right)^2 + \left(\frac{\partial v}{\partial t} + \Omega(r+x+s)\right)^2 - \Omega^2(r+x)(h_v+h_w) + \left(\frac{\partial w}{\partial t}\right)^2\Bigg\} dx \tag{2.4.4}$$

Now note that some terms involving h_v and h_w were already neglected. In fact, h_v and h_w are assumed to be small quantities since they are already square terms, and as such any product of these terms and any other generalized displacement is neglected. Were these terms included in the formulation and one would obtain the full set of non-linear differential equations as it was done by Chung and Yoo [4]. However since the main point is to obtain linear differential equations for implementation in the finite element method, these terms can be neglected at this point of the formulation.

Applying the variational to the kinetic energy yields

$$\int_{t_i}^{t_f} \delta T\, dt = \int_0^L \rho A \int_{t_i}^{t_f} \Bigg\{\left(\frac{\partial s}{\partial t} - \Omega v\right)\frac{\partial}{\partial t}\delta s + \left(\frac{\partial s}{\partial t} - \Omega v\right)\delta\Big(-\Omega v\Big) + \left(\frac{\partial v}{\partial t} + \Omega(r+x+s)\right)\frac{\partial}{\partial t}\delta v + \left(\frac{\partial v}{\partial t} + \Omega(r+x+s)\right)\delta\Big(\Omega(r+x+s)\Big) - \Omega^2(r+x)\delta(h_v+h_w) + \frac{\partial w}{\partial t}\frac{\partial}{\partial t}\delta w\Bigg\} dt\, dx \tag{2.4.5}$$

According to Chung and Yoo [4] the penultimate term, after integration by parts is taken, can be given as

$$\int_{t_i}^{t_f}\int_0^L -\Omega^2(r+x)\delta(h_v+h_w)\, dt\, dx = \int_{t_i}^{t_f}\int_0^L \frac{\partial}{\partial x}\left[\Omega^2\rho A\Big(r(L-x) + \frac{1}{2}(L^2-x^2)\Big)\frac{\partial v}{\partial x}\right]\delta v + \frac{\partial}{\partial x}\left[\Omega^2\rho A\Big(r(L-x) + \frac{1}{2}(L^2-x^2)\Big)\frac{\partial w}{\partial x}\right]\delta w\, dt\, dx \tag{2.4.6}$$

Finally, after integrating the variational of the kinetic energy by parts with respect to time and knowing that by definition the displacements are null at the initial and final times t_i and t_f respectively it follows that

$$\begin{aligned}\int_{t_i}^{t_f} \delta T\, dt = \int_0^L \int_{t_i}^{t_f} \Bigg\{ \rho A \Bigg[&- \left(\frac{\partial^2 s}{\partial t^2} - \Omega \frac{\partial v}{\partial t}\right)\delta s - \left(\Omega \frac{\partial s}{\partial t} - \Omega^2 v\right)\delta v - \left(\frac{\partial^2 v}{\partial t^2} + \Omega \frac{\partial s}{\partial t}\right)\delta v \\ &+ \left(\Omega \frac{\partial v}{\partial t} + \Omega^2 s\right)\delta s + \Omega^2 (r+x)\delta s - \frac{\partial^2 w}{\partial t^2}\delta w \Bigg] \\ &+ \frac{\partial}{\partial x}\left[\Omega^2 \rho A \left(r(L-x) + \frac{1}{2}(L^2 - x^2)\right)\frac{\partial v}{\partial x}\right]\delta v \\ &+ \frac{\partial}{\partial x}\left[\Omega^2 \rho A \left(r(L-x) + \frac{1}{2}(L^2 - x^2)\right)\frac{\partial w}{\partial x}\right]\delta w \Bigg\}\, dt\, dx\end{aligned} \tag{2.4.7}$$

2.4.2 Potential energy

As it was already said, shear strains and stresses are assumed negligible in the Euler-Bernoulli beam theory and likewise, the potential energy is simply given as

$$\int_V E\varepsilon_{xx}^2\, dV = \int_V E\left[\frac{\partial u}{\partial x} + \frac{1}{2}\left(\frac{\partial v}{\partial x}\right)^2 + \frac{1}{2}\left(\frac{\partial w}{\partial x}\right)^2 + z\frac{\partial \theta}{\partial x} + y\frac{\partial \psi}{\partial x}\right] dV \tag{2.4.8}$$

Now note that the first three terms represent the actual stretch deformation as it was defined in equation (2.3.14) allowing the simplification of the expression for the potential energy. Replacing the relations for the cross section rotation and integrating over the cross sectional area of the beam, the potential energy can be expressed as

$$\Pi = \frac{1}{2}\int_0^L E\left[A\left(\frac{\partial s}{\partial x}\right)^2 + I_z\left(\frac{\partial^2 v}{\partial x^2}\right)^2 + I_y\left(\frac{\partial^2 w}{\partial x^2}\right)^2\right] dx \tag{2.4.9}$$

In the CLC modeling method the expression for the potential energy would simply be

$$\Pi = \frac{1}{2}\int_0^L E\left[A\left(\frac{\partial u}{\partial x}\right)^2 + I_z\left(\frac{\partial^2 v}{\partial x^2}\right)^2 + I_y\left(\frac{\partial^2 w}{\partial x^2}\right)^2\right] dx \tag{2.4.10}$$

which now can be seen that it is obviously approximated since there are two terms in equation (2.4.8) that are neglected because of the assumption of geometric linearity, which is clearly not valid when large overall motions are prescribed.

Applying the variational to the potential energy and integrating from t_i to t_f one gets

$$\int_{t_i}^{t_f} \delta\Pi\, dt = \int_{t_i}^{t_f}\int_0^L E\left[A\frac{\partial s}{\partial x}\frac{\partial}{\partial x}\delta s + I_z\frac{\partial^2 v}{\partial x^2}\frac{\partial^2}{\partial x^2}\delta v + I_y\frac{\partial^2 w}{\partial x^2}\frac{\partial^2}{\partial x^2}\delta w\right] dx\, dt \tag{2.4.11}$$

and after integrating twice by parts with respect to the spatial variable x

$$\begin{aligned}\int_{t_i}^{t_f} \delta\Pi\, dt = \int_{t_i}^{t_f} \Bigg\{ &EA\frac{\partial s}{\partial x}\delta s\Big|_0^L + EI_z\frac{\partial^2 v}{\partial x^2}\frac{\partial}{\partial x}\delta v\Big|_0^L + EI_y\frac{\partial^2 w}{\partial x^2}\frac{\partial}{\partial x}\delta w\Big|_0^L - \frac{\partial}{\partial x}\left(EI_z\frac{\partial^2 v}{\partial x^2}\right)\delta v\Big|_0^L \\ &- \frac{\partial}{\partial x}\left(EI_y\frac{\partial^2 w}{\partial x^2}\right)\delta w\Big|_0^L \\ &+ \int_0^L -\frac{\partial}{\partial x}\left(EA\frac{\partial s}{\partial x}\right)\delta s + \frac{\partial^2}{\partial x^2}\left(EI_z\frac{\partial^2 v}{\partial x^2}\right)\delta v + \frac{\partial^2}{\partial x^2}\left(EI_y\frac{\partial^2 w}{\partial x^2}\right)\delta w\, dx \Bigg\}\, dt\end{aligned} \tag{2.4.12}$$

Finally considering the boundary conditions of the system

$$\int_{t_i}^{t_f} \delta\Pi \, dt = \int_{t_i}^{t_f} \int_0^L -\frac{\partial}{\partial x}\left(EA\frac{\partial s}{\partial x}\right)\delta s + \frac{\partial^2}{\partial x^2}\left(EI_z\frac{\partial^2 v}{\partial x^2}\right)\delta v + \frac{\partial^2}{\partial x^2}\left(EI_y\frac{\partial^2 w}{\partial x^2}\right)\delta w \, dx \, dt \tag{2.4.13}$$

and the boundary conditions are

$$s = v = w = \frac{\partial w}{\partial x} = \frac{\partial v}{\partial x} = 0, \text{ at } x = 0 \tag{2.4.14a}$$

$$EA\frac{\partial s}{\partial x} = EI_z\frac{\partial^2 v}{\partial x^2} = EI_y\frac{\partial^2 w}{\partial x^2} = \frac{\partial}{\partial x}\left(EI_y\frac{\partial^2 w}{\partial x^2}\right) = \frac{\partial}{\partial x}\left(EI_z\frac{\partial^2 v}{\partial x^2}\right) = 0, \text{ at } x = L \tag{2.4.14b}$$

2.4.3 Work of non-conservative forces

The work done by external distributed forces can expressed as

$$\mathcal{W} = f_s(x,t)s + f_v(x,t)v + f_w(x,t)w \tag{2.4.15}$$

and the virtual work becomes

$$\delta\mathcal{W} = f_s\delta s + f_v\delta v + f_w\delta w \tag{2.4.16}$$

2.4.4 Differential equations of movement

Introducing in the Hamilton principle (2.1.3) the variational of the kinetic energy as defined in equation (2.4.7) as well as the variational of the potential energy as defined in equation (2.4.13) and the virtual work done by external forces (2.4.16), yields the final linear partial differential equations of motion for the Euler-Bernoulli beam

$$\rho A\left(\frac{\partial^2 s}{\partial t^2} - 2\Omega\frac{\partial v}{\partial t} - \Omega^2 s\right) - \frac{\partial}{\partial x}\left(EA\frac{\partial s}{\partial x}\right) = \rho A\Omega^2(r+x) + f_s \tag{2.4.17}$$

$$\begin{aligned}\rho A\left(\frac{\partial^2 v}{\partial t^2} + 2\Omega\frac{\partial s}{\partial t} - \Omega^2 v\right) + \frac{\partial^2}{\partial x^2}\left(EI_z\frac{\partial^2 v}{\partial x^2}\right) \\ - \frac{\partial}{\partial x}\left[\Omega^2\rho A\left(r(L-x) + \frac{1}{2}(L^2 - x^2)\right)\frac{\partial v}{\partial x}\right] = f_v\end{aligned} \tag{2.4.18}$$

$$\begin{aligned}\rho A\frac{\partial^2 w}{\partial t^2} + \frac{\partial^2}{\partial x^2}\left(EI_y\frac{\partial^2 w}{\partial x^2}\right) \\ - \frac{\partial}{\partial x}\left[\Omega^2\rho A\left(r(L-x) + \frac{1}{2}(L^2 - x^2)\right)\frac{\partial w}{\partial x}\right] = f_w\end{aligned} \tag{2.4.19}$$

Now note that equations (2.4.17) and (2.4.18) are coupled through gyroscopic coupling and both equations define what will be called from now on the **chordwise motion**; on the other hand equation (2.4.19) which is uncoupled from the other two, defines what will be called the **flapwise motion**.

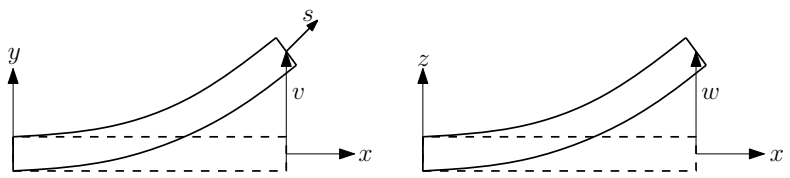

(a) Chordwise motion (b) Flapwise motion

Figure 2.5: Comparison between the chordwise and flapwise motions

As it can be seen from figure 2.5, while the chordwise motion is defined by a bending deformation in the xy plane and a stretch deformation of the neutral axis of the beam, the flapwise motion is characterized by a bending deformations in the xz plane.

2.5 Timoshenko beam theory

In this section the partial differential equations of movement for the Timoshenko beam theory will be derived. The main differences comparatively to the Euler-Bernoulli theory lie in the fact that the rotations of the cross section are independent degrees of freedom which allows for the consideration of the shear strains and stresses, having an effect on the potential energy of the beam. Also in the Timoshenko beam theory the rotary inertia of the cross section of the beam is usually considered, which has an effect on the kinetic energy of the beam.

2.5.1 Kinetic energy

The velocity vector is in every way identical to that defined for the Euler-Bernoulli theory. Replacing the relation between the displacements s and u and velocity vector becomes

$$\mathbf{v}_P = \begin{Bmatrix} \dot{s} - (\dot{h}_v + \dot{h}_w) + z\dot{\theta} - y\dot{\psi} - \Omega(y+v) \\ \dot{v} + \Omega(r+x+s+z\theta - y\psi) - \Omega(h_v + h_w) \\ \dot{w} \end{Bmatrix} \tag{2.5.1}$$

and under the same assumptions of small quantities for the h_v and h_w functions and neglecting any product of these terms and other generalized displacements the kinetic energy can be simplified into

$$\begin{aligned} T = \frac{1}{2}\int_V \rho\Big\{ &\Big[\dot{s} - \Omega v - \Omega y + z\dot{\theta} - y\dot{\psi}\Big]^2 + \Omega y(\dot{h}_v + \dot{h}_w) \\ &+ \Big[\dot{v} + \Omega(r+x+s+z\theta - y\psi)\Big]^2 - \Omega^2(r+x)(h_v+h_w) + \dot{w}^2\Big\}\, dV \end{aligned} \tag{2.5.2}$$

Integrating over the cross section of the beam and considering the rotary inertia, the kinetic energy for the rotating Timoshenko beam is given as follows

$$\begin{aligned} T = \frac{1}{2}\int_0^L \rho\Big\{ &A\Big[\left(\frac{\partial s}{\partial t} - \Omega v\right)^2 + \left(\frac{\partial v}{\partial t} + \Omega(r+x+s)\right)^2 - \Omega^2(r+x)(h_v+h_w) + \left(\frac{\partial w}{\partial t}\right)^2\Big] \\ &+ I_y\left(\frac{\partial \theta}{\partial t}\right)^2 + I_z\left(\frac{\partial \psi}{\partial t}\right)^2 + \Omega^2(I_y\theta^2 + I_z\psi^2 + I_z) + 2\Omega I_z\frac{\partial \psi}{\partial t}\Big\}\, dx \end{aligned} \tag{2.5.3}$$

Applying the variational to the knetic energy

$$\begin{aligned} \int_{t_i}^{t_f} \delta T\, dt = \int_0^L \rho \int_{t_i}^{t_f} \Big\{ &A\Big[\left(\frac{\partial s}{\partial t} - \Omega v\right)\frac{\partial}{\partial t}\delta s + \left(\frac{\partial s}{\partial t} - \Omega v\right)\delta\Big(-\Omega v\Big) \\ &+ \left(\frac{\partial v}{\partial t} + \Omega(r+x+s)\right)\frac{\partial}{\partial t}\delta v + \left(\frac{\partial v}{\partial t} + \Omega(r+x+s)\right)\delta\Big(\Omega(r+x+s)\Big) \\ &- \Omega^2(r+x)\delta(h_v+h_w) + \frac{\partial w}{\partial t}\frac{\partial}{\partial t}\delta w\Big] \\ &I_y\frac{\partial \theta}{\partial t}\frac{\partial}{\partial t}\delta\theta + I_z\frac{\partial \psi}{\partial t}\frac{\partial}{\partial t}\delta\psi + \Omega^2(I_y\theta\delta\theta + I_z\psi\delta\psi) + \Omega I_z\frac{\partial}{\partial t}\delta\psi\Big\}\, dt\, dx \end{aligned} \tag{2.5.4}$$

and after taking integration by parts and knowing that the displacements are by definition null at times t_i and t_f, the variational form for the kinetic energy becomes

$$\begin{aligned}\int_{t_i}^{t_f} \delta T\, dt = \int_0^L \rho \int_{t_i}^{t_f} \Bigg\{ A\Bigg[&- \left(\frac{\partial^2 s}{\partial t^2} - \Omega\frac{\partial v}{\partial t}\right)\delta s - \left(\Omega\frac{\partial s}{\partial t} - \Omega^2 v\right)\delta v - \left(\frac{\partial^2 v}{\partial t^2} + \Omega\frac{\partial s}{\partial t}\right)\delta v \\ &+ \left(\Omega\frac{\partial v}{\partial t} + \Omega^2 s\right)\delta s + \Omega^2(r+x)\delta s - \frac{\partial^2 w}{\partial t^2}\delta w\Bigg] \\ &+ \frac{\partial}{\partial x}\left[\Omega^2\rho A\Big(r(L-x) + \frac{1}{2}(L^2 - x^2)\Big)\frac{\partial v}{\partial x}\right]\delta v \\ &+ \frac{\partial}{\partial x}\left[\Omega^2\rho A\Big(r(L-x) + \frac{1}{2}(L^2 - x^2)\Big)\frac{\partial w}{\partial x}\right]\delta w \\ &- I_y\frac{\partial^2\theta}{\partial t^2}\delta\theta - I_z\frac{\partial^2\psi}{\partial t^2}\delta\psi + \Omega^2(I_y\theta\delta\theta + I_z\psi\delta\psi)\Bigg\}\, dt\, dx\end{aligned} \tag{2.5.5}$$

2.5.2 Potential energy

Since that in the Timoshenko beam theory the shear strains and stresses are considered, the potential energy is given by the following expression

$$\Pi = \frac{1}{2}\int_V (E\varepsilon_{xx}^2 + G\gamma_{xy}^2 + G\gamma_{zx}^2)\, dV \tag{2.5.6}$$

which after replacement of the stretch deformation defined in (2.3.14) and integration over the area of the cross section results in

$$\begin{aligned}\Pi = \frac{1}{2}\int_0^L \Bigg\{ &E\left[A\left(\frac{\partial s}{\partial x}\right)^2 + I_y\left(\frac{\partial\theta}{\partial x}\right)^2 + I_z\left(\frac{\partial\psi}{\partial x}\right)^2\right] \\ &+ G\left[A_y^*\left(\frac{\partial v}{\partial x} - \psi\right)^2 + A_z^*\left(\frac{\partial w}{\partial x} + \theta\right)^2\right]\Bigg\}\, dx\end{aligned} \tag{2.5.7}$$

where A_y^* and A_z^* represent the reduced shear areas in both directions and are given by $A_y^* = \kappa_y A$ and $A_z^* = \kappa_z A$, with κ_y and κ_z as the shear correction factors.

Applying the variational to the potential energy and integrating it from t_i to t_f

$$\begin{aligned}\int_{t_i}^{t_f} \delta\Pi\, dt = \int_{t_i}^{t_f}\int_0^L \Bigg\{ &E\left[A\frac{\partial s}{\partial x}\frac{\partial}{\partial x}\delta s + I_y\frac{\partial\theta}{\partial x}\frac{\partial}{\partial x}\delta\theta + I_z\frac{\partial\psi}{\partial x}\frac{\partial}{\partial x}\delta\psi\right] \\ &+G\left[A_y^*\left(\frac{\partial v}{\partial x} - \psi\right)\left(\frac{\partial}{\partial x}\delta v - \delta\psi\right) + A_z^*\left(\frac{\partial w}{\partial x} + \theta\right)\left(\frac{\partial}{\partial x}\delta w + \delta\theta\right)\right]\Bigg\}\, dx\, dt\end{aligned} \tag{2.5.8}$$

and after integrating once by parts with respect to the spatial variable x

$$\begin{aligned}\int_{t_i}^{t_f} \delta\Pi\, dt = \int_{t_i}^{t_f} \Bigg\{ &E\left[A\frac{\partial s}{\partial x}\delta s + I_y\frac{\partial\theta}{\partial x}\delta\theta + I_z\frac{\partial\psi}{\partial x}\delta\psi\right]_0^L + G\left[A_z^*\left(\frac{\partial w}{\partial x} + \theta\right)\delta w + A_y^*\left(\frac{\partial v}{\partial x} - \psi\right)\delta v\right]_0^L \\ &+ \int_0^L -\frac{\partial}{\partial x}\left(EA\frac{\partial s}{\partial x}\right)\delta s - \frac{\partial}{\partial x}\left(EI_y\frac{\partial\theta}{\partial x}\right)\delta\theta - \frac{\partial}{\partial x}\left(EI_z\frac{\partial\psi}{\partial x}\right)\delta\psi \\ &- \frac{\partial}{\partial x}\left[GA_z^*\left(\frac{\partial w}{\partial x} + \theta\right)\right]\delta w - \frac{\partial}{\partial x}\left[GA_y^*\left(\frac{\partial v}{\partial x} - \psi\right)\right]\delta v \\ &+ GA_z^*\left(\frac{\partial w}{\partial x} + \theta\right)\delta\theta - GA_y^*\left(\frac{\partial v}{\partial x} - \psi\right)\delta\psi\, dx\Bigg\}\, dt\end{aligned} \tag{2.5.9}$$

taking into account the boundary conditions and grouping the terms by displacements, the variational form of the potential energy for the Timoshenko beam can finally be given by

$$\begin{aligned}\int_{t_i}^{t_f} \delta\Pi\, dt = \int_{t_i}^{t_f}\int_0^L \Bigg\{ &- \frac{\partial}{\partial x}\left(EA\frac{\partial s}{\partial x}\right)\delta s - \frac{\partial}{\partial x}\left[GA_y^*\left(\frac{\partial v}{\partial x} - \psi\right)\right]\delta v - \frac{\partial}{\partial x}\left[GA_z^*\left(\frac{\partial w}{\partial x} + \theta\right)\right]\delta w \\ &+ \left[GA_z^*\left(\frac{\partial w}{\partial x} + \theta\right) - \frac{\partial}{\partial x}\left(EI_y\frac{\partial \theta}{\partial x}\right)\right]\delta\theta \\ &+ \left[-GA_y^*\left(\frac{\partial v}{\partial x} - \psi\right) - \frac{\partial}{\partial x}\left(EI_z\frac{\partial \psi}{\partial x}\right)\right]\delta\psi\Bigg\}\, dx\, dt\end{aligned} \tag{2.5.10}$$

and the boundary conditions for the rotating Timoshenko beam are

$$s = v = w = \theta = \psi = 0 \text{ at } x = 0 \tag{2.5.11a}$$

$$EA\frac{\partial s}{\partial x} = EI_y\frac{\partial \theta}{\partial x} = EI_z\frac{\partial \psi}{\partial x} = GA_z^*\left(\frac{\partial w}{\partial x} + \theta\right) = GA_y^*\left(\frac{\partial v}{\partial x} - \psi\right) = 0 \text{ at } x = L \tag{2.5.11b}$$

2.5.3 Work of non-conservative forces

The work of non-conservative forces for the Timoshenko beam can expressed as

$$\mathcal{W} = f_s(x,t)s + f_v(x,t)v + f_w(x,t)w + f_\theta(x,t)\theta + f_\psi(x,t)\psi \tag{2.5.12}$$

and the virtual work of the same forces becomes

$$\delta\mathcal{W} = f_s\delta s + f_v\delta v + f_w\delta w + f_\theta\delta\theta + f_\psi\delta\psi \tag{2.5.13}$$

2.5.4 Differential equations of movement

The differential equations of movement obtained for the Timoshenko rotating beam are fairly similar to those derived for the Euler-Bernoulli beam, only now since the rotations of the cross section are independent degrees of freedom, two more differential equations appear resulting in five differential equations of movement.

$$\rho A\left(\frac{\partial^2 s}{\partial t^2} - 2\Omega\frac{\partial v}{\partial t} - \Omega^2 s\right) - \frac{\partial}{\partial x}\left(EA\frac{\partial s}{\partial x}\right) = \rho A\Omega^2(r + x) + f_s \tag{2.5.14}$$

$$\begin{aligned}\rho A\left(\frac{\partial^2 v}{\partial t^2} + 2\Omega\frac{\partial s}{\partial t} - \Omega^2 v\right) &- \frac{\partial}{\partial x}\left[GA_y^*\left(\frac{\partial v}{\partial x} - \psi\right)\right] \\ &- \frac{\partial}{\partial x}\left[\Omega^2\rho A\left(r(L - x) + \frac{1}{2}(L^2 - x^2)\right)\frac{\partial v}{\partial x}\right] = f_v\end{aligned} \tag{2.5.15}$$

$$\rho I_z\left(\frac{\partial^2 \psi}{\partial t^2} - \Omega^2\psi\right) - GA_y^*\left(\frac{\partial v}{\partial x} - \psi\right) - \frac{\partial}{\partial x}\left(EI_z\frac{\partial \psi}{\partial x}\right) = f_\psi \tag{2.5.16}$$

$$\begin{aligned}\rho A\frac{\partial^2 w}{\partial t^2} &- \frac{\partial}{\partial x}\left[GA_z^*\left(\frac{\partial w}{\partial x} + \theta\right)\right] \\ &- \frac{\partial}{\partial x}\left[\Omega^2\rho A\left(r(L - x) + \frac{1}{2}(L^2 - x^2)\right)\frac{\partial w}{\partial x}\right] = f_w\end{aligned} \tag{2.5.17}$$

$$\rho I_y\left(\frac{\partial^2 \theta}{\partial t^2} - \Omega^2\theta\right) + GA_z^*\left(\frac{\partial w}{\partial x} + \theta\right) - \frac{\partial}{\partial x}\left(EI_y\frac{\partial \theta}{\partial x}\right) = f_\theta \tag{2.5.18}$$

One can observe how the five differential equations relate to each other. While equations (2.5.14), (2.5.15) and (2.5.16) are coupled with each other defining the chordwise motion for the Timoshenko rotating beam, equations (2.5.17) and (2.5.18) are coupled between them and define the flapwise motion for the Timoshenko rotating beam.

2.6 Pre-twisted Timoshenko beam

In this section the partial differential equations of movement for a pre-twisted Timoshenko beam will be derived. The process is quite similar to that in the previous section, being the main difference now the fact that, since the cross sections of the beam are pre-twisted, there is no longer a line of symmetry (as it can be seen in figure 2.6) and as such $\int_A xy\,dA \neq 0$, as a result the product of inertia need to be accounted for in both the kinetic and potential energies.

Even though in this work the pre-twisted beam analysis is done solely using the Timoshenko beam theory, the equations of motion could easily be derived using the Euler-Bernoulli beam theory as well (Yoo et al. [7]).

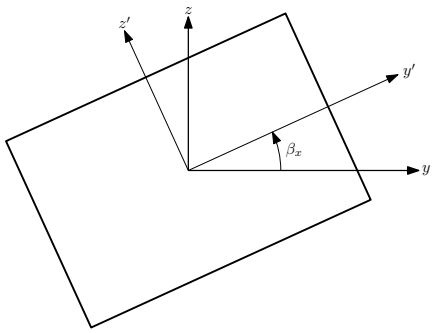

Figure 2.6: Pre-twisted cross section of the beam

As it can be seen in figure 2.6 the generic cross section of the pre-twisted beam can be defined by an angle β_x which can be determined as follows

$$\beta_x = \frac{x}{L}\beta_L \tag{2.6.1}$$

where β_L is the angle of the beam at the free-end. With the angle β_x defined as such, it is assumed that it has a linear variation from $x = 0$ until $x = L$. Furthermore the moments of inertia and the product of inertia need to be determined for each cross section as

$$I_y = I_{z'} \sin^2 \beta_x + I_{y'} \cos^2 \beta_x \tag{2.6.2a}$$
$$I_z = I_{z'} \cos^2 \beta_x + I_{y'} \sin^2 \beta_x \tag{2.6.2b}$$
$$I_{yz} = (I_{z'} - I_{y'}) \sin \beta_x \cos \beta_x \tag{2.6.2c}$$

2.6.1 Kinetic energy

The velocity vector is identical to that defined in the previous section and as such the kinetic energy is very similar to that defined for the Timoshenko beam needing only to introduce the product of inertia when integrating over the cross section of the beam. Thus, the kinetic energy for the Timoshenko pre-twisted beam is given by the following expression

$$T = \frac{1}{2}\int_0^L \rho\Bigg\{A\Bigg[\left(\frac{\partial s}{\partial t} - \Omega v\right)^2 + \left(\frac{\partial v}{\partial t} + \Omega(r+x+s)\right)^2 - \Omega^2(r+x)(h_v+h_w) + \left(\frac{\partial w}{\partial t}\right)^2\Bigg] + I_y\left(\frac{\partial \theta}{\partial t}\right)^2 + I_z\left(\frac{\partial \psi}{\partial t}\right)^2 + \Omega^2(I_y\theta^2 + I_z\psi^2 - 2I_{yz}\theta\psi + I_z) - 2I_{yz}\frac{\partial \theta}{\partial t}\frac{\partial \psi}{\partial t} + 2\Omega(I_z\frac{\partial \psi}{\partial t} - I_{yz}\frac{\partial \theta}{\partial t})\Bigg\} dx \tag{2.6.3}$$

After applying the variational to the kinetic energy and taking integration by parts it becomes

$$\begin{aligned}\int_{t_i}^{t_f} \delta T\, dt = \int_0^L \rho \int_{t_i}^{t_f} \Bigg\{A\Bigg[&- \left(\frac{\partial^2 s}{\partial t^2} - \Omega\frac{\partial v}{\partial t}\right)\delta s - \left(\Omega\frac{\partial s}{\partial t} - \Omega^2 v\right)\delta v - \left(\frac{\partial^2 v}{\partial t^2} + \Omega\frac{\partial s}{\partial t}\right)\delta v \\ &+ \left(\Omega\frac{\partial v}{\partial t} + \Omega^2 s\right)\delta s + \Omega^2(r+x)\delta s - \frac{\partial^2 w}{\partial t^2}\delta w\Bigg] \\ &+ \frac{\partial}{\partial x}\left[\Omega^2\rho A\Big(r(L-x) + \frac{1}{2}(L^2-x^2)\Big)\frac{\partial v}{\partial x}\right]\delta v \\ &+ \frac{\partial}{\partial x}\left[\Omega^2\rho A\Big(r(L-x) + \frac{1}{2}(L^2-x^2)\Big)\frac{\partial w}{\partial x}\right]\delta w \\ &+ \left(-I_y\frac{\partial^2\theta}{\partial t^2} + I_{yz}\frac{\partial^2\psi}{\partial t^2}\right)\delta\theta + \left(-I_z\frac{\partial^2\psi}{\partial t^2} + I_{yz}\frac{\partial^2\theta}{\partial t^2}\right)\delta\psi \\ &+ \Omega^2[I_y\theta\delta\theta + I_z\psi\delta\psi - I_{yz}(\psi\delta\theta + \theta\delta\psi)]\Bigg\} dt\, dx\end{aligned} \tag{2.6.4}$$

2.6.2 Potential energy

The basic form of the potential energy for the pre-twisted beam is also identical to that defined for the Timoshenko beam and after integration over the cross sectional area of the pre-twisted beam the potential energy is defined as

$$\begin{aligned}\Pi = \frac{1}{2}\int_0^L \Bigg\{&E\Bigg[A\left(\frac{\partial s}{\partial x}\right)^2 + I_y\left(\frac{\partial \theta}{\partial x}\right)^2 + I_z\left(\frac{\partial \psi}{\partial x}\right)^2 - 2I_{yz}\frac{\partial\theta}{\partial x}\frac{\partial\psi}{\partial x}\Bigg] \\ &+ GA^*\left[\left(\frac{\partial v}{\partial x} - \psi\right)^2 + \left(\frac{\partial w}{\partial x} + \theta\right)^2\right]\Bigg\} dx\end{aligned} \tag{2.6.5}$$

After applying the variational, integrating by parts and considering the boundary conditions the final variationl form for the pre-twisted Timoshenko rotating beam becomes

$$\begin{aligned}\int_{t_i}^{t_f} \delta\Pi\, dt = \int_{t_i}^{t_f}\int_0^L \Bigg\{ &- \frac{\partial}{\partial x}\left(EA\frac{\partial s}{\partial x}\right)\delta s - \frac{\partial}{\partial x}\left[GA_y^*\left(\frac{\partial v}{\partial x} - \psi\right)\right]\delta v - \frac{\partial}{\partial x}\left[GA_z^*\left(\frac{\partial w}{\partial x} + \theta\right)\right]\delta w \\ &+ \left[GA_z^*\left(\frac{\partial w}{\partial x} + \theta\right) - \frac{\partial}{\partial x}\left(EI_y\frac{\partial\theta}{\partial x}\right) + \frac{\partial}{\partial x}\left(EI_{yz}\frac{\partial\psi}{\partial x}\right)\right]\delta\theta \\ &+ \left[-GA_y^*\left(\frac{\partial v}{\partial x} - \psi\right) - \frac{\partial}{\partial x}\left(EI_z\frac{\partial\psi}{\partial x}\right) + \frac{\partial}{\partial x}\left(EI_{yz}\frac{\partial\theta}{\partial x}\right)\right]\delta\psi\Bigg\} dx\, dt\end{aligned} \tag{2.6.6}$$

with the boundary conditions as follows

$$s = v = w = \theta = \psi = 0 \text{ at } x = 0 \tag{2.6.7a}$$

$$\begin{aligned} EA\frac{\partial s}{\partial x} = EI_y\frac{\partial \theta}{\partial x} = EI_z\frac{\partial \psi}{\partial x} = EI_{yz}\frac{\partial \theta}{\partial x} = EI_{yz}\frac{\partial \psi}{\partial x} \\ = GA_y^*\left(\frac{\partial v}{\partial x} - \psi\right) = GA_z^*\left(\frac{\partial w}{\partial x} + \theta\right) = 0 \text{ at } x = L \end{aligned} \tag{2.6.7b}$$

2.6.3 Differential equations of movement

Introducing the variational forms of the kinetic and potential energy, (2.6.4) and (2.6.6) respectively, and also the virtual work done by external forces in Hamilton principle (2.1.1) leads to partial differential equations for the pre-twisted Timoshenko beam as follows

$$\rho A\left(\frac{\partial^2 s}{\partial t^2} - 2\Omega\frac{\partial v}{\partial t} - \Omega^2 s\right) - \frac{\partial}{\partial x}\left(EA\frac{\partial s}{\partial x}\right) = \rho A\Omega^2(r + x) + f_s \tag{2.6.8}$$

$$\begin{aligned} \rho A\left(\frac{\partial^2 v}{\partial t^2} + 2\Omega\frac{\partial s}{\partial t} - \Omega^2 v\right) - \frac{\partial}{\partial x}\left[GA_y^*\left(\frac{\partial v}{\partial x} - \psi\right)\right] \\ - \frac{\partial}{\partial x}\left[\rho A\Omega^2\left(r(L - x) + \frac{1}{2}(L^2 - x^2)\right)\frac{\partial v}{\partial x}\right] = f_v \end{aligned} \tag{2.6.9}$$

$$\begin{aligned} \rho I_z\left(\frac{\partial^2 \psi}{\partial t^2} - \Omega^2\psi\right) - \rho I_{yz}\left(\frac{\partial^2 \theta}{\partial t^2} - \Omega^2\theta\right) \\ - \frac{\partial}{\partial x}\left(EI_z\frac{\partial \psi}{\partial x}\right) + \frac{\partial}{\partial x}\left(EI_{yz}\frac{\partial \theta}{\partial x}\right) - GA_y^*\left(\frac{\partial v}{\partial x} - \psi\right) = f_\psi \end{aligned} \tag{2.6.10}$$

$$\begin{aligned} \rho A\frac{\partial^2 w}{\partial t^2} - \frac{\partial}{\partial x}\left[GA_z^*\left(\frac{\partial w}{\partial x} + \theta\right)\right] \\ - \frac{\partial}{\partial x}\left[\rho A\Omega^2\left(r(L - x) + \frac{1}{2}(L^2 - x^2)\right)\frac{\partial w}{\partial x}\right] = f_w \end{aligned} \tag{2.6.11}$$

$$\begin{aligned} \rho I_y\left(\frac{\partial^2 \theta}{\partial t^2} - \Omega^2\theta\right) - \rho I_{yz}\left(\frac{\partial^2 \psi}{\partial t^2} - \Omega^2\psi\right) \\ - \frac{\partial}{\partial x}\left(EI_y\frac{\partial \theta}{\partial x}\right) + \frac{\partial}{\partial x}\left(EI_{yz}\frac{\partial \psi}{\partial x}\right) + GA_z^*\left(\frac{\partial w}{\partial x} + \theta\right) = f_\theta \end{aligned} \tag{2.6.12}$$

Note that now, unlike the differential equations defined in the previous sections, all the partial differential equations of movement are coupled due to the product of inertia introduced by the pre-twist angle of the beam, which means that both flapwise and chordwise movements are also coupled.

Chapter 3

Finite element analysis

In this chapter the weak forms (also known as variational forms) are derived for application in the finite element method. The weak forms are derived from the strong forms (defined by the system of partial differential equations of movement and respective boundary conditions) using the weighted-residuals method.

3.1 Beam finite element

In order to solve the system of differential equations using the finite element method, the beam needs to be discretized into several elements as in figure 3.1.

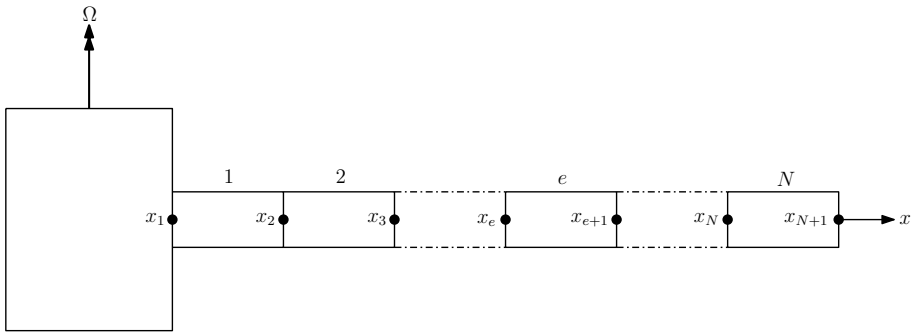

Figure 3.1: Discretization of the beam in finite elements

It is usually convenient to define the domain of the beam element in terms of a natural coordinate ξ, rather than a system global coordinate x, so that its domain is always the same for any element of the beam which facilitates numerical integration of the element matrices using the Gauss quadrature. The natural coordinate system has its origin at the center of the element and the element domain is $-1 < \xi < +1$ as it is shown in figure 3.2.

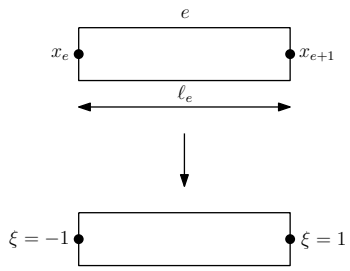

Figure 3.2: Natural coordinate

The global coordinate x can then be determined from the natural coordinate ξ as follows

$$x(\xi) = N_1 x_e + N_2 x_{e+1} = \begin{bmatrix} N_1 & N_2 \end{bmatrix} \begin{bmatrix} x_e \\ x_{e+1} \end{bmatrix} = \mathbf{N}\mathbf{x}^{\mathbf{e}} \tag{3.1.1}$$

where N_1 and N_2 are shape functions defined in the natural coordinate system that interpolate the geometry of the beam and are given by

$$N_1 = \frac{1-\xi}{2} \tag{3.1.2a}$$

$$N_2 = \frac{1+\xi}{2} \tag{3.1.2b}$$

To obtain the derivative of a shape function defined in the natural coordinate system with respect to the global spatial variable x one can do as follows

$$\frac{dN}{d\xi} = \frac{dN}{dx} \underbrace{\frac{dx}{d\xi}}_{\mathbf{J}} \tag{3.1.3}$$

$$\frac{dN}{dx} = \frac{dN}{d\xi}\mathbf{J}^{-1} \tag{3.1.4}$$

with $\mathbf{J}$ as the Jacobian transformation defined for the beam element as

$$\mathbf{J} = \frac{d}{d\xi}\left(\begin{bmatrix} N_1 & N_2 \end{bmatrix} \begin{bmatrix} x_e \\ x_{e+1} \end{bmatrix} \right) = \begin{bmatrix} \frac{dN_1}{d\xi} & \frac{dN_2}{d\xi} \end{bmatrix} \begin{bmatrix} x_e \\ x_{e+1} \end{bmatrix} \tag{3.1.5}$$

To derive the weak forms in the following sections, the differential equations of motion are multiplied by the weighting functions and integrated from $x = 0$ to $x = L$ and then integrated by parts. It is seen that the natural boundary conditions are already satisfied by the weak forms and as such the weighting functions need only to meet the requirements set by the essential boundary conditions. For the simple beam case (either Euler-Bernoulli or Timoshenko beam), two weak forms are derived since there are two main types of motion. As for the pre-twisted beam, only one weak form is derived since both motion types are coupled.

3.2 Euler-Bernoulli element

The shape functions used to interpolate the element bending displacements, w and v, in the Euler-Bernoulli beam theory are known as the Hermite cubic interpolation functions and are given by (see for instance [12] and [13]).

$$H_1 = \frac{1}{4}(2 - 3\xi + \xi^3) \tag{3.2.1a}$$

$$H_2 = \frac{\ell_e}{8}(1 - \xi - \xi^2 + \xi^3) \tag{3.2.1b}$$

$$H_3 = \frac{1}{4}(2 + 3\xi - \xi^3) \tag{3.2.1c}$$

$$H_4 = \frac{\ell_e}{8}(-1 - \xi + \xi^2 + \xi^3) \tag{3.2.1d}$$

The reason for the shape functions to be cubic is because the polynomial function from which they are derived, which is used to approximate the displacements v and w, has to be cubic so that there are four parameters in the polynomial in order to satisfy all four essential boundary conditions. Also, from the Euler-Bernoulli potential energy one can see that the bending displacements need to be twice differentiable so that the bending potential energy isn't null; on the other hand bending displacements need to cubic to yield nonzero shear forces.

As for the shape functions that interpolate the displacement s, since they only need to be differentiable once and there is only two essential boundary conditions the polynomial used to approximate s is linear yielding two linear shape functions which are the same used to interpolate the coordinates of the beam.

3.2.1 Chordwise motion

To derive the weak form for the chordwise motion of the Euler-Bernoulli beam, equations (2.4.17) and (2.4.18) are multiplied by the weighting functions $\bar{s}$ and $\bar{v}$ respectively, summed and integrated over the length L as follows

$$\begin{aligned}\int_0^L &\left\{\rho A\left(\frac{\partial^2 s}{\partial t^2} - 2\Omega\frac{\partial v}{\partial t} - \Omega^2 s\right) - \frac{\partial}{\partial x}\left(EA\frac{\partial s}{\partial x}\right) - \rho A\Omega^2(r+x) - f_s\right\}\bar{s} \\ &+\left\{\rho A\left(\frac{\partial^2 v}{\partial t^2} + 2\Omega\frac{\partial s}{\partial t} - \Omega^2 v\right) + \frac{\partial^2}{\partial x^2}\left(EI_z\frac{\partial^2 v}{\partial x^2}\right)\right. \\ &\left.- \frac{\partial}{\partial x}\left[\Omega^2\rho A\Big(r(L-x) + \frac{1}{2}(L^2-x^2)\Big)\frac{\partial v}{\partial x}\right] - f_v\right\}\bar{v}\,dx = 0\end{aligned} \tag{3.2.2}$$

after integrating by parts, considering the natural boundary conditions and knowing that the weighting functions satisfy the essential boundary conditions it follows that

$$\begin{aligned}\int_0^L &\left\{\rho A\left(\frac{\partial^2 s}{\partial t^2} - 2\Omega\frac{\partial v}{\partial t} - \Omega^2 s\right)\bar{s} + \rho A\left(\frac{\partial^2 v}{\partial t^2} + 2\Omega\frac{\partial s}{\partial t} - \Omega^2 v\right)\bar{v}\right. \\ &\left.+EA\frac{\partial s}{\partial x}\frac{\partial \bar{s}}{\partial x} + EI_z\frac{\partial^2 v}{\partial x^2}\frac{\partial^2 \bar{v}}{\partial x^2} + \Omega^2\rho A\Big(r(L-x) + \frac{1}{2}(L^2-x^2)\Big)\frac{\partial v}{\partial x}\frac{\partial \bar{v}}{\partial x}\right\}dx \\ &= \int_0^L (\rho A\Omega^2(r+x) + f_s)\bar{s} + f_v\bar{v}\,dx\end{aligned} \tag{3.2.3}$$

and after rewriting it

$$\begin{aligned}\int_0^L &\left\{\rho A\left(\bar{s}\frac{\partial^2 s}{\partial t^2} + \bar{v}\frac{\partial^2 v}{\partial t^2}\right) + 2\Omega\rho A\left(\bar{v}\frac{\partial s}{\partial t} - \bar{s}\frac{\partial v}{\partial t}\right) - \Omega^2\rho A(\bar{s}s + \bar{v}v)\right. \\ &\left.+EA\frac{\partial \bar{s}}{\partial x}\frac{\partial s}{\partial x} + EI_z\frac{\partial^2 \bar{v}}{\partial x^2}\frac{\partial^2 v}{\partial x^2} + \Omega^2\rho A\Big(r(L-x) + \frac{1}{2}(L^2-x^2)\Big)\frac{\partial \bar{v}}{\partial x}\frac{\partial v}{\partial x}\right\}dx \\ &= \int_0^L \bar{s}(\rho A\Omega^2(r+x) + f_s) + \bar{v}f_v\,dx\end{aligned} \tag{3.2.4}$$

The displacements and weighting functions are now approximated by the shape functions as

$$\bar{s} = (\bar{\mathbf{d}}_e^c)^T\mathbf{N}_s^T; \quad s = \mathbf{N}_s\mathbf{d}_e^c \tag{3.2.5a}$$

$$\bar{v} = (\bar{\mathbf{d}}_e^c)^T\mathbf{N}_v^T; \quad v = \mathbf{N}_v\mathbf{d}_e^c \tag{3.2.5b}$$

where $\mathbf{d}_e^c$ is the element displacement vector defined as

$$\mathbf{d}_e^c = \begin{Bmatrix} s_1 & v_1 & \psi_1 & s_2 & v_2 & \psi_2 \end{Bmatrix}^T \tag{3.2.6}$$

and $\bar{\mathbf{d}}_e^c$ is an arbitrary vector with the same dimensions of $\mathbf{d}_e^c$ and the matrix shape functions are

$$\mathbf{N}_s = \begin{bmatrix} N_1 & 0 & 0 & N_2 & 0 & 0 \end{bmatrix} \tag{3.2.7a}$$

$$\mathbf{N}_v = \begin{bmatrix} 0 & H_1 & H_2 & 0 & H_3 & H_4 \end{bmatrix} \tag{3.2.7b}$$

Introducing now these approximations from equations (3.2.5) in the weak form presented in equation (3.2.4), the weak form can also be written in a matricial form, yielding the discretized equation for the chordwise motion as

$$\sum_{e=1}^{N}(\bar{\mathbf{d}}_e^c)^T\{\mathbf{m}_e^c\ddot{\mathbf{d}}_e^c + 2\Omega\mathbf{g}_e^c\dot{\mathbf{d}}_e^c + [\mathbf{k}_e^c + \Omega^2(s_e^c - \mathbf{m}_e^c)]\mathbf{d}_e^c\} = \sum_{e=1}^{N}(\bar{\mathbf{d}}_e^c)^T\mathbf{f}_e^c \tag{3.2.8}$$

with the element matrices defined as

$$\mathbf{m}_e^c = \int_{-1}^{+1} \rho A(\mathbf{N}_s^T\mathbf{N}_s + \mathbf{N}_v^T\mathbf{N}_v)\, det(\mathbf{J})\, d\xi \tag{3.2.9a}$$

$$\mathbf{g}_e^c = \int_{-1}^{+1} \rho A(\mathbf{N}_v^T\mathbf{N}_s - \mathbf{N}_s^T\mathbf{N}_v)\, det(\mathbf{J})\, d\xi \tag{3.2.9b}$$

$$\mathbf{s}_e^c = \int_{-1}^{+1} \rho A\Big(r(L-x) + \frac{1}{2}(L^2 - x^2)\Big)\mathbf{N'}_v^T\mathbf{N'}_v\, det(\mathbf{J})\, d\xi \tag{3.2.9c}$$

$$\mathbf{k}_e^c = \int_{-1}^{+1} (EA\mathbf{N'}_s^T\mathbf{N'}_s + EI_z\mathbf{N''}_v^T\mathbf{N''}_v)\, det(\mathbf{J})\, d\xi \tag{3.2.9d}$$

$$\mathbf{f}_e^c = \int_{-1}^{+1} (\mathbf{N}_s^T(\Omega^2\rho A(r+x) + f_s) + \mathbf{N}_v^T f_v)\, det(\mathbf{J})\, d\xi \tag{3.2.9e}$$

where $\mathbf{m}_e^c$, $\mathbf{g}_e^c$, $\mathbf{s}_e^c$ and $\mathbf{k}_e^c$ are the mass, gyroscopic, centrifugal stiffness and stiffness element matrices respectively for the chordwise motion, and $\mathbf{f}_e^c$ is the element load vector.

Finally, since $\bar{\mathbf{d}}_e^c$ is an arbitrary vector, after assembling the element matrices and vectors equation (3.2.8) can be transformed into the global system of ordinary differential equations of motion defined as

$$\mathbf{M}_c\ddot{\mathbf{d}}_c + \underbrace{2\Omega\mathbf{G}_c}_{\mathbf{G}_{eq}}\dot{\mathbf{d}}_c + \underbrace{[\mathbf{K}_c + \Omega^2(\mathbf{S}_c - \mathbf{M}_c)]}_{\mathbf{K}_{eq}}\mathbf{d}_c = \mathbf{f}_c \tag{3.2.10}$$

3.2.2 Flapwise motion

Following the same procedure done for the chordwise motion, the weak form for the flapwise motion is derived as

$$\begin{aligned}\int_0^L \Bigg\{ &\rho A\frac{\partial^2 w}{\partial t^2} + \frac{\partial^2 w}{\partial x^2}\left(EI_y\frac{\partial^2 w}{\partial x^2}\right) \\ &- \frac{\partial}{\partial x}\left[\Omega^2\rho A\Big(r(L-x) + \frac{1}{2}(L^2 - x^2)\Big)\frac{\partial w}{\partial x}\right] - f_w\Bigg\}\bar{w}\, dx = 0\end{aligned} \tag{3.2.11}$$

$$\begin{aligned}\int_0^L \Bigg\{ &\rho A\frac{\partial^2 w}{\partial t^2}\bar{w} + EI_y\frac{\partial^2 w}{\partial x^2}\frac{\partial^2 \bar{w}}{\partial x^2} \\ &+ \Omega^2\rho A\Big(r(L-x) + \frac{1}{2}(L^2 - x^2)\Big)\frac{\partial w}{\partial x}\frac{\partial \bar{w}}{\partial x}\Bigg\}\, dx = \int_0^L f_w\bar{w}\, dx\end{aligned} \tag{3.2.12}$$

Introducing the element displacement vector as

$$\mathbf{d}_e^f = \begin{Bmatrix} w_1 & \theta_1 & w_2 & \theta_2 \end{Bmatrix} \tag{3.2.13}$$

and the flapwise matrix shape function as

$$\mathbf{N}_w = \begin{bmatrix} H_1 & H_2 & H_3 & H_4 \end{bmatrix} \tag{3.2.14}$$

approximations for the flapwise displacement and weighting functions through the shape functions are as follows

$$\bar{w} = (\bar{\mathbf{d}}_e^f)^T \mathbf{N}_w^T; \quad w = \mathbf{N}_w \mathbf{d}_e^f \tag{3.2.15}$$

Introducing the previous interpolations in the weak form, the discretized equation for the flapwise motion is given by

$$\sum_{e=1}^{N} (\bar{\mathbf{d}}_e^f)^T \{\mathbf{m}_e^f \ddot{\mathbf{d}}_e^f + [\mathbf{k}_e^f + \Omega^2 \mathbf{s}_e^f] \mathbf{d}_e^f\} = \sum_{e=1}^{N} (\bar{\mathbf{d}}_e^f)^T \mathbf{f}_e^f \tag{3.2.16}$$

with the element matrices defined as

$$\mathbf{m}_e^f = \int_{-1}^{+1} \rho A \mathbf{N}_w^T \mathbf{N}_w \, det(\mathbf{J}) \, d\xi \tag{3.2.17a}$$

$$\mathbf{s}_e^f = \int_{-1}^{+1} \rho A \Big(r(L-x) + \frac{1}{2}(L^2 - x^2) \Big) \mathbf{N'}_w^T \mathbf{N'}_w \, det(\mathbf{J}) \, d\xi \tag{3.2.17b}$$

$$\mathbf{k}_e^f = \int_{-1}^{+1} E I_y \mathbf{N''}_w^T \mathbf{N''}_w \, det(\mathbf{J}) \, d\xi \tag{3.2.17c}$$

$$\mathbf{f}_e^f = \int_{-1}^{+1} \mathbf{N}_w^T f_w \, det(\mathbf{J}) \, d\xi \tag{3.2.17d}$$

where $\mathbf{m}_e^f$, $\mathbf{s}_e^c$ and $\mathbf{k}_e^f$ are the mass, centrifugal stiffness and stiffness element matrices respectively for the flapwise motion, and $\mathbf{f}_e^f$ is the element load vector.

By assembling the element matrices and vectors and since $\bar{\mathbf{d}}_e^f$ is arbitrary, the global system of semi-discrete equations of motion is defined for the flapwise case as

$$\mathbf{M}_f \ddot{\mathbf{d}}_f + \underbrace{[\mathbf{K}_f + \Omega^2 \mathbf{S}_f]}_{\mathbf{K}_{eq}} \mathbf{d}_f = \mathbf{f}_f \tag{3.2.18}$$

3.3 Timoshenko element

In the Timoshenko beam theory, the cross sections rotations (θ and ψ) and bending deformations (w and v) are considered independent degrees of freedom resulting in only two essential boundary conditions for each deformation and rotation. As such the polynomial used to derive the shape functions needs only to be linear, which makes the shape functions used to interpolate the displacements also linear. The shape functions used are all the same for any degree of freedom and equal to those presented at the beginning of the chapter to interpolate the element geometry

3.3.1 Chordwise motion

Multiplying equations (2.5.14), (2.5.15) and (2.5.16) by the weighting functions $\bar{s}$, $\bar{v}$ and $\bar{\psi}$ respectively, summing an then integrating over the length of the beam leads to the following integral form

$$\begin{aligned}
\int_0^L & \left\{ \rho A \left(\frac{\partial^2 s}{\partial t^2} - 2\Omega \frac{\partial v}{\partial t} - \Omega^2 s \right) - \frac{\partial}{\partial x} \left(EA \frac{\partial s}{\partial x} \right) - \rho A \Omega^2 (r + x) - f_s \right\} \bar{s} \\
& + \left\{ \rho A \left(\frac{\partial^2 v}{\partial t^2} + 2\Omega \frac{\partial s}{\partial t} - \Omega^2 v \right) - \frac{\partial}{\partial x} \left[GA_y^* \left(\frac{\partial v}{\partial x} - \psi \right) \right] \right. \\
& \qquad \left. - \frac{\partial}{\partial x} \left[\Omega^2 \rho A \Big(r(L-x) + \frac{1}{2}(L^2 - x^2) \Big) \frac{\partial v}{\partial x} \right] - f_v \right\} \bar{v} \\
& \left\{ \rho I_z \left(\frac{\partial^2 \psi}{\partial t^2} - \Omega^2 \psi \right) - GA_y^* \left(\frac{\partial v}{\partial x} - \psi \right) - \frac{\partial}{\partial x} \left(EI_z \frac{\partial \psi}{\partial x} \right) - f_\psi \right\} \bar{\psi} = 0
\end{aligned} \tag{3.3.1}$$

and after integration by parts and considering the boundary conditions the weak form can be presented as

$$\begin{aligned}\int_0^L \Bigg\{ & \rho\Big(A\bar{s}\frac{\partial^2 s}{\partial t^2} + A\bar{v}\frac{\partial^2 v}{\partial t^2} + I_z\bar{\psi}\frac{\partial^2\psi}{\partial t^2}\Big) + 2\Omega\rho A\Big(\bar{v}\frac{\partial s}{\partial t} - \bar{s}\frac{\partial v}{\partial t}\Big) - \Omega^2\rho(A\bar{s}s + A\bar{v}v + I_z\bar{\psi}\psi) \\ & + EA\frac{\partial s}{\partial x}\frac{\partial \bar{s}}{\partial x} + EI_z\frac{\partial\psi}{\partial x}\frac{\partial\bar{\psi}}{\partial x} + GA_y^*\Big(\frac{\partial\bar{v}}{\partial x} - \bar{\psi}\Big)\Big(\frac{\partial v}{\partial x} - \psi\Big) \\ & \Omega^2\rho A\Big(r(L-x) + \frac{1}{2}(L^2 - x^2)\Big)\frac{\partial v}{\partial x}\frac{\partial\bar{v}}{\partial x}\Bigg\} dx \\ = & \int_0^L (\rho A\Omega^2(r+x) + f_s)\bar{s} + f_v\bar{v} + f_\psi\bar{\psi}\, dx\end{aligned} \tag{3.3.2}$$

The weighting functions and displacements are interpolated from the element displacement vector as follows

$$\bar{s} = (\bar{\mathbf{d}}_e^c)^T\mathbf{N}_s^T; \quad s = \mathbf{N}_s\mathbf{d}_e^c \tag{3.3.3a}$$
$$\bar{v} = (\bar{\mathbf{d}}_e^c)^T\mathbf{N}_v^T; \quad v = \mathbf{N}_v\mathbf{d}_e^c \tag{3.3.3b}$$
$$\bar{\psi} = (\bar{\mathbf{d}}_e^c)^T\mathbf{N}_\psi^T; \quad \psi = \mathbf{N}_\psi\mathbf{d}_e^c \tag{3.3.3c}$$

where the displacement vector for the Timoshenko chordwise motion is identical to that defined for the Euler-Bernoulli element and it is given by

$$\mathbf{d}_e^c = \begin{Bmatrix} s_1 & v_1 & \psi_1 & s_2 & v_2 & \psi_2 \end{Bmatrix}^T \tag{3.3.4}$$

and the shape functions matrices are now written as

$$\mathbf{N}_s = \begin{bmatrix} N_1 & 0 & 0 & N_2 & 0 & 0 \end{bmatrix} \tag{3.3.5a}$$
$$\mathbf{N}_v = \begin{bmatrix} 0 & N_1 & 0 & 0 & N_2 & 0 \end{bmatrix} \tag{3.3.5b}$$
$$\mathbf{N}_\psi = \begin{bmatrix} 0 & 0 & N_1 & 0 & 0 & N_2 \end{bmatrix} \tag{3.3.5c}$$

Introducing now the approximations made in equations (3.3.3) in the variational form (3.3.2), the discretized equation for the Timoshenko chordwise motion is

$$\sum_{e=1}^{N}(\bar{\mathbf{d}}_e^c)^T\{\mathbf{m}_e^c\ddot{\mathbf{d}}_e^c + 2\Omega\mathbf{g}_e^c\dot{\mathbf{d}}_e^c + [\mathbf{k}_e^c + \Omega^2(\mathbf{s}_e^c - \mathbf{m}_e^c)]\mathbf{d}_e^c\} = \sum_{e=1}^{N}(\bar{\mathbf{d}}_e^c)^T\mathbf{f}_e^c \tag{3.3.6}$$

which is quite identical to the one obtained for Euler-Bernoulli beam, although the element matrices and

vectors are defined differently as follows

$$\begin{aligned}\mathbf{m}_e^c &= \int_{-1}^{+1} \Big\{\rho A(\mathbf{N}_s^T\mathbf{N}_s + \mathbf{N}_v^T\mathbf{N}_v) + \rho I_z(\mathbf{N}_\psi^T\mathbf{N}_\psi)\Big\}\, det(\mathbf{J})d\xi \\ &= \sum_{i=1}^{m} w_i\Big\{\rho A(\mathbf{N}_s^T\mathbf{N}_s + \mathbf{N}_v^T\mathbf{N}_v) + \rho I_z(\mathbf{N}_\psi^T\mathbf{N}_\psi)\Big\}\, det(\mathbf{J})\end{aligned} \tag{3.3.7a}$$

$$\begin{aligned}\mathbf{g}_e^c &= \int_{-1}^{+1} \Big\{\rho A(\mathbf{N}_v^T\mathbf{N}_s - \mathbf{N}_s^T\mathbf{N}_v)\Big\}\, det(\mathbf{J})d\xi \\ &= \sum_{i=1}^{m} w_i\Big\{\rho A(\mathbf{N}_v^T\mathbf{N}_s - \mathbf{N}_s^T\mathbf{N}_v)\Big\}\, det(\mathbf{J})\end{aligned} \tag{3.3.7b}$$

$$\begin{aligned}\mathbf{k}_e^c &= \int_{-1}^{+1} \Big\{EA(\mathbf{N'}_s^T\mathbf{N'}_s) + EI_z(\mathbf{N'}_\psi^T\mathbf{N'}_\psi) + GA_y^*[(\mathbf{N'}_v - \mathbf{N}_\psi)^T(\mathbf{N'}_v - \mathbf{N}_\psi)]\Big\}\, det(\mathbf{J})d\xi \\ &= \sum_{i=1}^{m} w_i\Big\{EA(\mathbf{N'}_s^T\mathbf{N'}_s) + EI_z(\mathbf{N'}_\psi^T\mathbf{N'}_\psi) + GA_y^*[(\mathbf{N'}_v - \mathbf{N}_\psi)^T(\mathbf{N'}_v - \mathbf{N}_\psi)]\Big\}\, det(\mathbf{J})\end{aligned} \tag{3.3.7c}$$

$$\begin{aligned}\mathbf{s}_e^c &= \int_{-1}^{+1} \Big\{\rho A\Big(r(L-x) + \frac{1}{2}(L^2 - x^2)\Big)(\mathbf{N'}_v^T\mathbf{N'}_v)\Big\}\, det(\mathbf{J})d\xi \\ &= \sum_{i=1}^{m} w_i\Big\{\rho A\Big(r(L-x) + \frac{1}{2}(L^2 - x^2)\Big)(\mathbf{N'}_v^T\mathbf{N'}_v)\Big\}\, det(\mathbf{J})\end{aligned} \tag{3.3.7d}$$

$$\begin{aligned}\mathbf{f}_e^c &= \int_{-1}^{+1} \Big\{\Big(\rho A\Omega^2(r+x) + f_s\Big)\mathbf{N}_s^T + f_v\mathbf{N}_v^T + f_\psi\mathbf{N}_\psi^T\Big\}\, det(\mathbf{J})d\xi \\ &= \sum_{i=1}^{m} w_i\Big\{\Big(\rho A\Omega^2(r+x)\mathbf{N}_s^T + f_s\Big)\mathbf{N}_s^T + f_v\mathbf{N}_v^T + f_\psi\mathbf{N}_\psi^T\Big\}\, det(\mathbf{J})\end{aligned} \tag{3.3.7e}$$

where m is the number of Gauss points used for numeric integration.

By assembling the element matrices and vectors, the global matrices and vectors that define the spatial model are derived and the global system of equations for the chordwise motion is

$$\mathbf{M}_c\ddot{\mathbf{d}}_c + \underbrace{2\Omega\mathbf{G}_c}_{\mathbf{G}_{eq}}\dot{\mathbf{d}}_c + \underbrace{[\mathbf{K}_c + \Omega^2(\mathbf{S}_c - \mathbf{M}_c)]}_{\mathbf{K}_{eq}}\mathbf{d}_c = \mathbf{f}_c \tag{3.3.8}$$

3.3.2 Flapwise motion

The derivation of the flapwise variational form for the Timoshenko beam can be derived as

$$\begin{aligned}&\int_0^L \left\{\rho A\frac{\partial^2 w}{\partial t^2} - \frac{\partial}{\partial x}\left[GA^*\left(\frac{\partial w}{\partial x} + \theta\right)\right] - \frac{\partial}{\partial x}\left[\Omega^2\rho A\Big(r(L-x) + \frac{1}{2}(L^2-x^2)\Big)\frac{\partial w}{\partial x}\right] - f_w\right\}\bar{w} \\ &\left\{\rho I_y\left(\frac{\partial^2\theta}{\partial t^2} - \Omega^2\theta\right) + GA_z^*\left(\frac{\partial w}{\partial x} + \theta\right) - \frac{\partial}{\partial x}\left(EI_y\frac{\partial\theta}{\partial x}\right) - f_\theta\right\}\bar{\theta} = 0\end{aligned} \tag{3.3.9}$$

$$\begin{aligned}\int_0^L \Bigg\{&\rho A\bar{w}\frac{\partial^2 w}{\partial t^2} + \rho I_y\bar{\theta}\frac{\partial^2\theta}{\partial t^2} - \Omega^2\rho I_y\bar{\theta}\theta + EI_y\frac{\partial\bar{\theta}}{\partial x}\frac{\partial\theta}{\partial x} + GA_z^*\left(\frac{\partial w}{\partial x} + \theta\right)\left(\frac{\partial\bar{w}}{\partial x} + \bar{\theta}\right) \\ &\Omega^2\rho A\Big(r(L-x) + \frac{1}{2}(L^2-x^2)\Big)\frac{\partial w}{\partial x}\frac{\partial\bar{w}}{\partial x}\Bigg\}\, dx = \int_0^L \bar{w}f_w + \bar{\theta}f_\theta\, dx\end{aligned} \tag{3.3.10}$$

Introducing the beam displacement vector as well as the shape functions matrices

$$\mathbf{d}_e^f = \begin{Bmatrix} w_1 & \theta_1 & w_2 & \theta_2 \end{Bmatrix} \tag{3.3.11}$$

$$\mathbf{N}_w = \begin{bmatrix} N_1 & 0 & N_2 & 0 \end{bmatrix} \tag{3.3.12a}$$
$$\mathbf{N}_\theta = \begin{bmatrix} 0 & N_1 & 0 & N_2 \end{bmatrix} \tag{3.3.12b}$$

the weighting and displacement functions are approximated as follows

$$\bar{w} = \bar{\mathbf{d}}_e^f \mathbf{N}_w^T; \quad w = \mathbf{N}_w \mathbf{d}_e^f \tag{3.3.13a}$$
$$\bar{\theta} = \bar{\mathbf{d}}_e^f \mathbf{N}_\theta^T; \quad \theta = \mathbf{N}_\theta \mathbf{d}_e^f \tag{3.3.13b}$$

Introducing these approximations in the weak form yields the discretized equation for the flapwise motion using the Timoshenko finite element

$$\sum_{e=1}^{N} (\bar{\mathbf{d}}_e^f)^T \{\mathbf{m}_e^f \ddot{\mathbf{d}}_e^f + [\mathbf{k}_e^f + \Omega^2(\mathbf{s}_e^f - \boldsymbol{\theta}_e^f)]\mathbf{d}_e^f\} = \sum_{e=1}^{N} (\bar{\mathbf{d}}_e^f)^T \mathbf{f}_e^f \tag{3.3.14}$$

Note that now there is a difference in the expression due to taking into account the rotary inertia of the beam originating the $\boldsymbol{\theta}_e^f$ element matrix. Element matrices of the previous equation are defined as

$$\begin{aligned} \mathbf{m}_e^f &= \int_{-1}^{+1} \Big\{ \rho A \mathbf{N}_w^T \mathbf{N}_w + \rho I_y \mathbf{N}_\theta^T \mathbf{N}_\theta \Big\} det(\mathbf{J}) d\xi \\ &= \sum_{i=1}^{m} w_i \Big\{ \rho A \mathbf{N}_w^T \mathbf{N}_w + \rho I_y \mathbf{N}_\theta^T \mathbf{N}_\theta \Big\} det(\mathbf{J}) \end{aligned} \tag{3.3.15a}$$

$$\begin{aligned} \mathbf{k}_e^f &= \int_{-1}^{+1} \Big\{ E I_y \mathbf{N'}_\theta^T \mathbf{N'}_\theta + G A_z^* (\mathbf{N'}_w + \mathbf{N}_\theta)^T (\mathbf{N'}_w + \mathbf{N}_\theta) \Big\} det(\mathbf{J}) d\xi \\ &= \sum_{i=1}^{m} w_i \Big\{ E I_y \mathbf{N'}_\theta^T \mathbf{N'}_\theta + G A_z^* (\mathbf{N'}_w + \mathbf{N}_\theta)^T (\mathbf{N'}_w + \mathbf{N}_\theta) \Big\} det(\mathbf{J}) \end{aligned} \tag{3.3.15b}$$

$$\begin{aligned} \mathbf{s}_e^f &= \int_{-1}^{+1} \Big\{ \rho A \Big(r(L-x) + \frac{1}{2}(L^2 - x^2) \Big) \mathbf{N'}_w^T \mathbf{N'}_w \Big\} det(\mathbf{J}) d\xi \\ &= \sum_{i=1}^{m} w_i \Big\{ \rho A \Big(r(L-x) + \frac{1}{2}(L^2 - x^2) \Big) \mathbf{N'}_w^T \mathbf{N'_w} \Big\} det(\mathbf{J}) \end{aligned} \tag{3.3.15c}$$

$$\begin{aligned} \boldsymbol{\theta}_e^f &= \int_{-1}^{+1} \Big\{ \rho I_y \mathbf{N}_\theta^T \mathbf{N}_\theta \Big\} det(\mathbf{J}) d\xi \\ &= \sum_{i=1}^{m} w_i \Big\{ \rho I_y \mathbf{N}_\theta^T \mathbf{N}_\theta \Big\} det(\mathbf{J}) \end{aligned} \tag{3.3.15d}$$

$$\begin{aligned} \mathbf{f}_e^f &= \int_{-1}^{+1} \Big\{ f_w \mathbf{N}_w + f_\theta \mathbf{N}_\theta \Big\} det(\mathbf{J}) d\xi \\ &= \sum_{i=1}^{m} w_i \Big\{ f_w \mathbf{N}_w + f_\theta \mathbf{N}_\theta \Big\} det(\mathbf{J}) \end{aligned} \tag{3.3.15e}$$

with m as the number of Gauss points.
After assembling the element matrices and vectors and since $\bar{\mathbf{d}}_e^f$ is arbitrary, the global system of equations for the flapwise motion becomes

$$\mathbf{M}_f \ddot{\mathbf{d}}_f + \underbrace{[\mathbf{K}_f + \Omega^2(\mathbf{S}_f - \boldsymbol{\Theta}_f)]}_{\mathbf{K}_{eq}} \mathbf{d}_f = \mathbf{f}_f \tag{3.3.16}$$

3.4 Pre-twisted Timoshenko element

Following the same procedure presented in the previous sections the integral form for the pre-twisted Timoshenko rotating beam can be presented as

$$
\begin{aligned}
&\int_0^L \left\{ \rho A\left(\frac{\partial^2 s}{\partial t^2} - 2\Omega\frac{\partial v}{\partial t} - \Omega^2 s\right) - \frac{\partial}{\partial x}\left(EA\frac{\partial s}{\partial x}\right) - \rho A\Omega^2(r+x) - f_s \right\}\bar{s} \\
&+\left\{ \rho A\left(\frac{\partial^2 v}{\partial t^2} + 2\Omega\frac{\partial s}{\partial t} - \Omega^2 v\right) - \frac{\partial}{\partial x}\left[GA_y^*\left(\frac{\partial v}{\partial x} - \psi\right)\right] \right. \\
&\qquad \left. - \frac{\partial}{\partial x}\left[\Omega^2\rho A\Big(r(L-x) + \frac{1}{2}(L^2 - x^2)\Big)\frac{\partial v}{\partial x}\right] - f_v \right\}\bar{v} \\
&+\left\{ \rho I_z\left(\frac{\partial^2 \psi}{\partial t^2} - \Omega^2\psi\right) - \rho I_{yz}\left(\frac{\partial^2 \theta}{\partial t^2} - \Omega^2\theta\right) \right. \\
&\qquad \left. - GA_y^*\left(\frac{\partial v}{\partial x} - \psi\right) - \frac{\partial}{\partial x}\left(EI_z\frac{\partial \psi}{\partial x}\right) + \frac{\partial}{\partial x}\left(EI_{yz}\frac{\partial \theta}{\partial x}\right) - f_\psi \right\}\bar{\psi} \\
&+\left\{ \rho A\frac{\partial^2 w}{\partial t^2} - \frac{\partial}{\partial x}\left[GA_z^*\left(\frac{\partial w}{\partial x} + \theta\right)\right] - \frac{\partial}{\partial x}\left[\Omega^2\rho A\Big(r(L-x) + \frac{1}{2}(L^2 - x^2)\Big)\frac{\partial w}{\partial x}\right] - f_w \right\}\bar{w} \\
&+\left\{ \rho I_y\left(\frac{\partial^2 \theta}{\partial t^2} - \Omega^2\theta\right) - \rho I_{yz}\left(\frac{\partial^2 \psi}{\partial t^2} - \Omega^2\psi\right) \right. \\
&\qquad \left. + GA_z^*\left(\frac{\partial w}{\partial x} + \theta\right) - \frac{\partial}{\partial x}\left(EI_y\frac{\partial \theta}{\partial x}\right) + \frac{\partial}{\partial x}\left(EI_{yz}\frac{\partial \psi}{\partial x}\right) - f_\theta \right\}\bar{\theta}\, dx = 0
\end{aligned}
\tag{3.4.1}
$$

and after integrating the previous equation by parts, considering the natural boundary conditions and keeping in mind that the weighting functions meet the geometric boundary conditions, the weak form for the pre-twisted beam can be derived as

$$
\begin{aligned}
&\int_0^L \left\{ \rho\left(A\bar{s}\frac{\partial^2 s}{\partial t^2} + A\bar{v}\frac{\partial^2 v}{\partial t^2} + A\bar{w}\frac{\partial^2 w}{\partial t^2} + I_y\bar{\theta}\frac{\partial^2 \theta}{\partial t^2} + I_z\bar{\psi}\frac{\partial^2 \psi}{\partial t^2} - I_{yz}\bar{\psi}\frac{\partial^2 \theta}{\partial t^2} - I_{yz}\bar{\theta}\frac{\partial^2 \psi}{\partial t^2}\right) \right. \\
&\quad + 2\Omega\rho A\left(\bar{v}\frac{\partial s}{\partial t} - \bar{s}\frac{\partial v}{\partial t}\right) - \Omega^2\rho(A\bar{s}s + A\bar{v}v + I_z\bar{\psi}\psi + I_y\bar{\theta}\theta + I_{yz}\bar{\psi}\theta + I_{yz}\bar{\theta}\psi) \\
&\quad + EA\frac{\partial s}{\partial x}\frac{\partial \bar{s}}{\partial x} + EI_y\frac{\partial \bar{\theta}}{\partial x}\frac{\partial \theta}{\partial x} + EI_z\frac{\partial \psi}{\partial x}\frac{\partial \bar{\psi}}{\partial x} + EI_{yz}\frac{\partial \bar{\psi}}{\partial x}\frac{\partial \theta}{\partial x} + EI_{yz}\frac{\partial \bar{\theta}}{\partial x}\frac{\partial \psi}{\partial x} \\
&\quad + GA_y^*\left(\frac{\partial \bar{v}}{\partial x} - \bar{\psi}\right)\left(\frac{\partial v}{\partial x} - \psi\right) + GA_z^*\left(\frac{\partial w}{\partial x} + \theta\right)\left(\frac{\partial \bar{w}}{\partial x} + \bar{\theta}\right) \\
&\quad \left. \Omega^2\rho A\Big(r(L-x) + \frac{1}{2}(L^2 - x^2)\Big)\left(\frac{\partial \bar{v}}{\partial x}\frac{\partial v}{\partial x} + \frac{\partial \bar{w}}{\partial x}\frac{\partial w}{\partial x}\right) \right\} dx \\
&= \int_0^L (\rho A\Omega^2(r+x) + f_s)\bar{s} + f_v\bar{v} + \bar{w}f_w + \bar{\theta}f_\theta + f_\psi\bar{\psi}\, dx
\end{aligned}
\tag{3.4.2}
$$

Since the flapwise and chordwise motions are coupled the element displacement vector is now given by

$$
\mathbf{d}_e = \begin{Bmatrix} s_1 & v_1 & w_1 & \theta_1 & \psi_1 & s_2 & v_2 & w_2 & \theta_2 & \psi_2 \end{Bmatrix}^T \tag{3.4.3}
$$

It is worth to mention that the shape functions and the approximations of the displacements and weighting functions are still the same as those defined for the Timoshenko simple beam, only now the shape functions matrices need to have a number of columns equal to the size of vector $\mathbf{d}_e$ and each shape function N_1 and N_2 placed at the adequate location. Introducing these approximations into the variational form yields the finite element discretized equation

$$\sum_{e=1}^{N}(\bar{\mathbf{d}}_e)^T\{\mathbf{m}_e\ddot{\mathbf{d}}_e + 2\Omega\mathbf{g}_e\dot{\mathbf{d}}_e + [\mathbf{k}_e + \Omega^2(\mathbf{ks}_e - \mathbf{ms}_e)]\mathbf{d}_e\} = \sum_{e=1}^{N}(\bar{\mathbf{d}}_e)^T\mathbf{f}_e \tag{3.4.4}$$

and the element matrices are computed using the Gauss integration technique using m Gauss points for the numeric integration as

$$\mathbf{m}_e = \sum_{i=1}^{m} w_i \begin{bmatrix}\mathbf{N}_s\\ \mathbf{N}_v\\ \mathbf{N}_w\\ \mathbf{N}_\theta\\ \mathbf{N}_\psi\end{bmatrix}^T \rho \begin{bmatrix}A & 0 & 0 & 0 & 0\\ 0 & A & 0 & 0 & 0\\ 0 & 0 & A & 0 & 0\\ 0 & 0 & 0 & I_y & -I_{yz}\\ 0 & 0 & 0 & -I_{yz} & I_z\end{bmatrix} \begin{bmatrix}\mathbf{N}_s\\ \mathbf{N}_v\\ \mathbf{N}_w\\ \mathbf{N}_\theta\\ \mathbf{N}_\psi\end{bmatrix} det(\mathbf{J}) \tag{3.4.5}$$

$$\mathbf{g}_e = \sum_{i=1}^{m} w_i \begin{bmatrix}\mathbf{N}_s\\ \mathbf{N}_v\end{bmatrix}^T \rho A \begin{bmatrix}0 & -1\\ 1 & 0\end{bmatrix} \begin{bmatrix}\mathbf{N}_s\\ \mathbf{N}_v\end{bmatrix} det(\mathbf{J}) \tag{3.4.6}$$

$$\begin{aligned}\mathbf{k}_e = \sum_{i=1}^{m} w_i \Bigg\{ &\begin{bmatrix}\mathbf{N}_s\\ \mathbf{N}_\theta\\ \mathbf{N}_\psi\end{bmatrix}^T E \begin{bmatrix}A & 0 & 0\\ 0 & I_y & -I_{yz}\\ 0 & -I_{yz} & I_z\end{bmatrix} \begin{bmatrix}\mathbf{N}_s\\ \mathbf{N}_\theta\\ \mathbf{N}_\psi\end{bmatrix}\\ &+ \begin{bmatrix}\mathbf{N'}_v - \mathbf{N}_\psi\\ \mathbf{N'}_w + \mathbf{N}_\theta\end{bmatrix}^T G \begin{bmatrix}A_y^* & 0\\ 0 & A_z^*\end{bmatrix} \begin{bmatrix}\mathbf{N'}_v - \mathbf{N}_\psi\\ \mathbf{N'}_w + \mathbf{N}_\theta\end{bmatrix} \Bigg\} det(\mathbf{J})\end{aligned} \tag{3.4.7}$$

$$\mathbf{ks}_e = \sum_{i=1}^{m} w_i \begin{bmatrix}\mathbf{N'}_v\\ \mathbf{N'}_w\end{bmatrix}^T \rho A \left[r(L-x) + \frac{1}{2}(L^2 - x^2)\right] \begin{bmatrix}1 & 0\\ 0 & 1\end{bmatrix} \begin{bmatrix}\mathbf{N'}_v\\ \mathbf{N'}_w\end{bmatrix} det(\mathbf{J}) \tag{3.4.8}$$

$$\mathbf{ms}_e = \sum_{i=1}^{m} w_i \begin{bmatrix}\mathbf{N}_s\\ \mathbf{N}_v\\ \mathbf{N}_\theta\\ \mathbf{N}_\psi\end{bmatrix} \rho \begin{bmatrix}A & 0 & 0 & 0\\ 0 & A & 0 & 0\\ 0 & 0 & I_y & -I_{yz}\\ 0 & 0 & -I_{yz} & I_z\end{bmatrix} \begin{bmatrix}\mathbf{N}_s\\ \mathbf{N}_v\\ \mathbf{N}_\theta\\ \mathbf{N}_\psi\end{bmatrix} det(\mathbf{J}) \tag{3.4.9}$$

The global spatial model for the pre-twisted beam is then defined by assembling the element matrices and vectors as

$$\mathbf{M}\ddot{\mathbf{d}} + \underbrace{2\Omega\mathbf{G}}_{\mathbf{G}_{eq}}\dot{\mathbf{d}} + \underbrace{[\mathbf{K} + \Omega^2(\mathbf{Ks} - \mathbf{Ms})]}_{\mathbf{K}_{eq}}\mathbf{d} = \mathbf{f} \tag{3.4.10}$$

3.5 Natural frequencies: Eigenvalue problem

From the semi-discrete global equations of motion, the eigenvalue problems are derived from which the natural frequencies can be computed, by neglecting the external forces and assuming the steady state solution as

$$\mathbf{d} = \mathbf{X}e^{j\omega t}, \quad \dot{\mathbf{d}} = j\omega\mathbf{X}e^{j\omega t}, \quad \ddot{\mathbf{d}} = -\omega^2\mathbf{X}e^{j\omega t} \tag{3.5.1}$$

where $j = \sqrt{-1}$, ω is the natural frequency and $\mathbf{X}$ is the amplitude of vibration.

3.5.1 Flapwise motion

Introducing the steady state solution in equations (3.2.18) and (3.3.16), leads to[1]

$$\{\mathbf{K}_{eq} - \omega^2\mathbf{M}_{eq}\}\mathbf{X}e^{j\omega t} = \mathbf{0} \tag{3.5.2}$$

and since $e^{j\omega t} \neq 0$ it yields the linear generalized eigenvalue problem as follows

[1] $\mathbf{M}_{eq}$ refers to any generic global mass matrix defined for any of the beam types analyzed in previous sections (M_f,M_c and M)

$$\mathbf{K}_{eq}\mathbf{X} = \omega^2\mathbf{M}_{eq}\mathbf{X} \tag{3.5.3}$$

whose real eigenvalues are the squares of the natural frequencies and the real eigenvectors represent the flapwise mode shapes for the rotating beam.

3.5.2 Chordwise motion

Introducing now the steady state solutions in equations (3.2.10), (3.3.8) and (3.4.10) on the other hand, leads to a quadratic eigenvalue problem as follows

$$\{\mathbf{K}_{eq} + j\omega\mathbf{G}_{eq} - \omega^2\mathbf{M}_{eq}\}\mathbf{X}e^{j\omega t} = \mathbf{0} \tag{3.5.4}$$

To solve this quadratic eigenvalue problem, one needs to linearize it which can be done by introducing the state vector $\mathbf{z}$

$$\mathbf{z} = \begin{Bmatrix}\mathbf{d}\\ \dot{\mathbf{d}}\end{Bmatrix} = \begin{Bmatrix}1\\ j\omega\end{Bmatrix}\mathbf{X}e^{j\omega t}, \quad \dot{\mathbf{z}} = \begin{Bmatrix}\dot{\mathbf{d}}\\ \ddot{\mathbf{d}}\end{Bmatrix} = j\omega\begin{Bmatrix}1\\ j\omega\end{Bmatrix}\mathbf{X}e^{j\omega t} \tag{3.5.5}$$

and an identity defined as

$$\mathbf{K}_{eq}\dot{\mathbf{d}} - \mathbf{K}_{eq}\dot{\mathbf{d}} = \mathbf{0} \tag{3.5.6}$$

It's important to note that the matrix involved in the identity has to be positive-definite, and since the beam is fixed at the hub the stiffness matrix can and will be used.

The state vector (3.5.5) and its time derivative can be introduced in equation (3.5.4) and in the identity (3.5.6) yielding

$$\begin{bmatrix}\mathbf{K}_{eq} & \mathbf{0}\end{bmatrix}\dot{\mathbf{z}} + \begin{bmatrix}\mathbf{0} & -\mathbf{K}_{eq}\end{bmatrix}\mathbf{z} = \mathbf{0} \tag{3.5.7a}$$

$$\begin{bmatrix}\mathbf{0} & \mathbf{M}_{eq}\end{bmatrix}\dot{\mathbf{z}} + \begin{bmatrix}\mathbf{K}_{eq} & \mathbf{G}_{eq}\end{bmatrix}\mathbf{z} = \mathbf{0} \tag{3.5.7b}$$

and after grouping both equations one gets

$$\left\{\underbrace{\begin{bmatrix}\mathbf{0} & -\mathbf{K}_{eq}\\ \mathbf{K}_{eq} & \mathbf{G}_{eq}\end{bmatrix}}_{\mathbf{K}_{ss}} + j\omega\underbrace{\begin{bmatrix}\mathbf{K}_{eq} & \mathbf{0}\\ \mathbf{0} & \mathbf{M}_{eq}\end{bmatrix}}_{\mathbf{M}_{ss}}\right\}\begin{Bmatrix}1\\ j\omega\end{Bmatrix}\mathbf{X}e^{j\omega t} = \mathbf{0} \tag{3.5.8}$$

Again since $e^{j\omega t} \neq 0$ it follows that

$$\underbrace{\begin{bmatrix}\mathbf{0} & -\mathbf{K}_{eq}\\ \mathbf{K}_{eq} & \mathbf{G}_{eq}\end{bmatrix}}_{\mathbf{K}_{ss}}\begin{Bmatrix}1\\ j\omega\end{Bmatrix}\mathbf{X} = -j\omega\underbrace{\begin{bmatrix}\mathbf{K}_{eq} & \mathbf{0}\\ \mathbf{0} & \mathbf{M}_{eq}\end{bmatrix}}_{\mathbf{M}_{ss}}\begin{Bmatrix}1\\ j\omega\end{Bmatrix}\mathbf{X} \tag{3.5.9}$$

which is now a linearized complex eigenvalue problem whose imaginary parts of the purely imaginary complex conjugate eigenvalues are the natural frequencies. Were the gyroscopic matrix any other damping matrix, the resultant eigenvalues would be complex numbers. The gyroscopic matrix is actually a particular damping matrix because the system is still conservative, hence the purely imaginary eigenvalues.

Note that other linearizations could easily be obtained following the same process, needing only to change the matrix involved in the identity introduced, which must still be definite positive, and/or changing the state vector. The linearization obtained here was chosen because it was the one that proved more stable and provided better results in a numerical implementation.

Chapter 4

Numerical results

In this chapter numerical results will be obtained from the finite element models derived in the previuos chapter. For convenience of discussion and for the sake of comparison with results from the literature, the following dimensionless quantities will be introduced

$$\xi = \frac{x}{L}, \quad \delta = \frac{r}{L}, \quad \alpha = \sqrt{\frac{AL^2}{I_z}}, \quad \vartheta = \frac{I_y}{I_z} \tag{4.0.1a}$$

$$T = \sqrt{\frac{\rho A L^4}{E I_z}}, \quad \gamma = T\Omega, \quad \bar{\omega} = T\omega, \quad \mu = \frac{\kappa G}{E} \tag{4.0.1b}$$

where γ, $\bar{\omega}$, δ, ϑ, μ and α represent the angular speed ratio, the natural frequency ratio, the hub radius ratio, the principal moment of inertia ratio, the effective shear to tensile stiffness ratio and the slenderness ratio. Note that the shear correction factors κ_y and κ_z are different for shear in the xy and xz planes and they may not be constant along the length of the beam [6], although in this study it is assumed that the shear correction factors are constant and equal for both shear planes. Also, the following results are obtained assuming that $E/G \approx 2.66$, or in other words, that $\nu \approx 0.33$, in order to obtain closer results with those found in the literature. Furthermore, unless stated otherwise, the results obtained using the Timoshenko element are obtained using selective integration which means that the terms in the stiffness matrix regarding shear stiffness are computed with one less Gauss point than what it would need for complete integration in order to prevent shear locking phenomena. All other matrices are determined using full integration and the number of elements used is 100.

4.1 Simple rotating beam

4.1.1 Chordwise motion

In table 4.1 one can see how the first six natural frequencies for a stationary beam using Timoshenko and Euler-Bernoulli elements converge as the number of elements increase. It is clear that the use of selective integration (T. s.i.) provides better results which is more noticeable when the number of elements is low. As the number of elements increase the difference between Timoshenko results using complete or selective integration is not very high. Considering a rotating beam, as it is shown in table 4.2, one can see that the natural frequencies also converge as the number of elements increase. In figure 4.1 are shown the first eight mode shapes, bending and stretching, for the chordwise motion of a stationary beam. This figure serves only to show that the first two stretching modes correspond to the fourth and eighth modes of the chordwise motion and since the first stretch mode is far separated from the first bending modes it is sometimes neglected in the literature.

Comparing the results obtained in tables 4.1 and 4.2 and also considering figure 4.2, it is noticeable that the differences between the Euler-Bernoulli and Timoshenko theories are small. This is because the slenderness ratio α is high enough so that the Euler-Bernoulli beam theory is valid. Also, from these same results one can conclude that even if the beam is slender the Timoshenko theory provides accurate

Table 4.1: Convergence of the first six chordwise natural frequencies for a non-rotating beam ($\gamma = 0$, $\alpha = 70$, $\vartheta = 1$, $\kappa = 5/6$)

No. of elements	Element type	1	2	3	4	5	6
5	E.B.	3.5161	22.0455	61.9188	110.4085	122.3197	203.0202
	T.	8.6524	55.9227	110.4085	167.0225	342.1695	349.4495
	T. s.i.	3.5254	23.9357	78.7906	110.4085	199.5564	342.1695
10	E.B.	3.5160	22.0352	61.7129	110.0688	121.0171	200.3633
	T.	5.2938	33.1683	93.5296	110.0688	185.7555	312.5871
	T. s.i.	3.5133	22.2664	63.9636	110.0688	130.5429	227.6545
20	E.B.	3.5160	22.0345	61.6982	109.9840	120.9095	199.8934
	T.	4.0306	25.0387	69.2999	109.9840	133.7980	217.4676
	T. s.i.	3.5101	21.8670	60.7831	109.9840	118.0444	193.1981
40	E.B.	3.5160	22.0345	61.6973	109.9628	120.9024	199.8617
	T.	3.6465	22.6032	62.2544	109.9628	119.2780	191.9331
	T. s.i.	3.5093	21.7683	60.0184	109.9628	115.1561	185.6018
60	E.B.	3.5160	22.0345	61.6972	109.9589	120.9020	199.8600
	T.	3.5708	22.1251	60.8819	109.9589	116.4804	187.0756
	T. s.i.	3.5092	21.7501	59.8781	109.9589	114.6312	184.2371
80	E.B.	3.5160	22.0345	61.6972	109.9575	120.9019	199.8597
	T.	3.5439	21.9555	60.3957	109.9575	115.4919	185.3641
	T. s.i.	3.5091	21.7437	59.8291	109.9575	114.4482	183.7625
100	E.B.	3.5160	22.0345	61.6972	109.9569	120.9019	199.8596
	T.	3.5314	21.8765	60.1697	109.9569	115.0326	184.5699
	T. s.i.	3.5091	21.7408	59.8064	109.9569	114.3636	183.5433

Table 4.2: Convergence of the first six chordwise natural frequencies for a rotating beam ($\gamma = 50$, $\alpha = 90$, $\delta = 0.2$, $\vartheta = 1$, $\kappa = 5/6$)

Element type	No. of elements	1st	2nd	3rd	4th	5th	6th
10	E.B.	23.3841	127.7347	167.8763	225.7464	336.5344	438.3731
	T.	22.9044	127.8050	167.7918	229.0700	349.6593	438.4626
40	E.B.	23.2641	127.5142	167.7394	225.3023	335.7715	434.8271
	T.	22.8983	126.7553	167.6423	222.9776	330.6099	434.7228
70	E.B.	23.2627	127.5096	167.7341	225.2931	335.7566	434.6684
	T.	22.8980	126.7072	167.6356	222.6909	329.7105	434.5376
100	E.B.	23.2624	127.5086	167.7328	225.2913	335.7536	434.6291
	T.	22.8980	126.6953	167.6339	222.6198	329.4872	434.4908

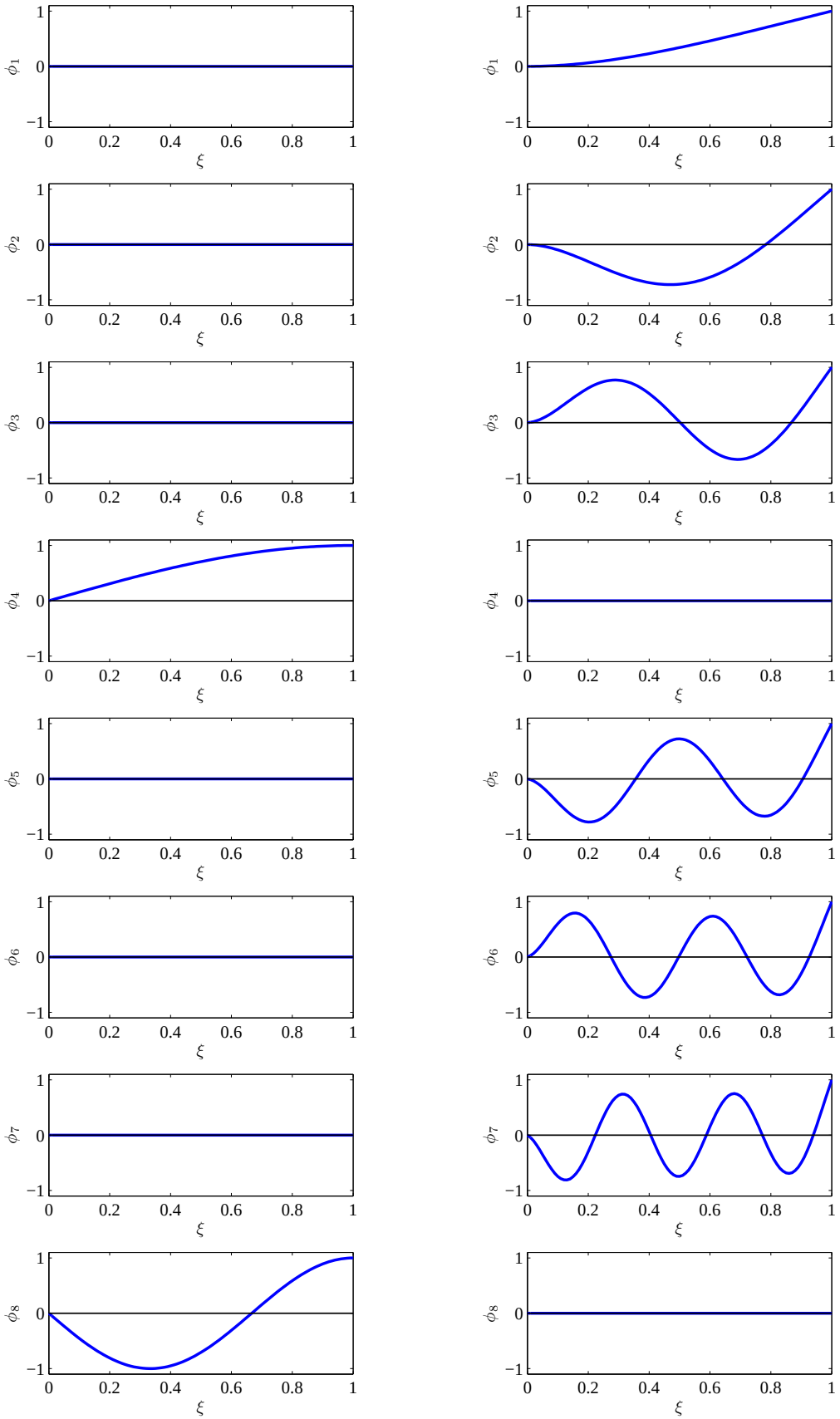

Figure 4.1: First eight Chordwise stretching (left) and bending (right) mode shapes for a non-rotating Timoshenko finite element beam ($\vartheta = 1$, $\alpha = 70$)

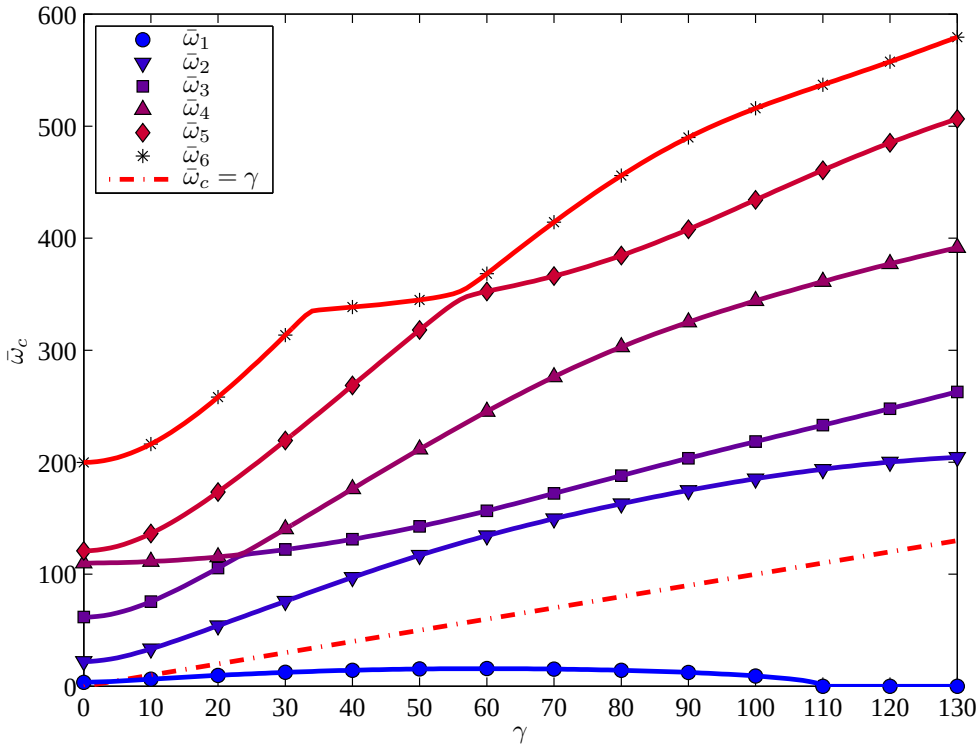

(a) Euler-Bernoulli finite element beam

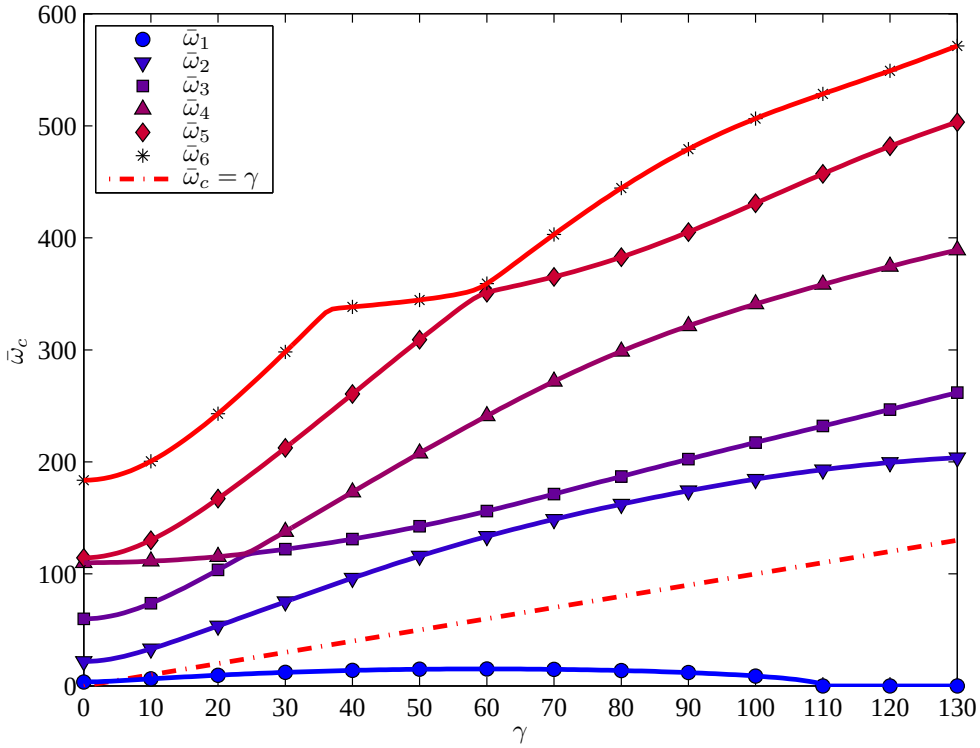

(b) Timoshenko finite element beam ($\kappa = 5/6$)

Figure 4.2: Variation of the first six dimensionless chordwise natural frequencies ($\delta = 0.1$, $\alpha = 70$, $\vartheta = 1$)

results differing only more significantly for higher modes. On the other hand considering figure 4.3, when the slenderness ratio becomes lower and the beam is thick, results from the Euler-Bernoulli theory differ from those obtained using Timoshenko theory because the assumption of negligible shear stresses and strains is no longer valid, although judging from the figure results are only with significant difference after the first two natural frequencies.

Also interesting is the variation of the natural frequencies with the rotating speed. One can see the presence of the gyroscopic coupling effect between bending and stretching modes caused by rotating motion, which results in the veering phenomena of the natural frequencies. For instance, at around $\gamma \approx 22$ the third and fourth natural frequencies veer together while the fifth and sixth natural frequencies veer at around $\gamma \approx 58$.

Another discernible fact is the presence of instability as well as tuned angular speed. As it can be seen from figures 4.2 there is a point at which the first chordwise natural frequency becomes null. The critical rotating speed (or buckling speed) at which the beam turns unstable depends only on the slenderness ratio as it will be shown. As for the tuned angular speed, it can also be seen from figures 4.2 that there is certain rotating speed at which the line representing $\bar{\omega} = \gamma$ intersects the first natural frequency leading to resonance.

Analyzing figures 4.5, it is clear the effects that the slenderness ratio has on the beam. As the beam becomes more slender (bigger values of α) the buckling speed occurs at higher values of the rotating speed and likewise so do the veering regions. As the beam becomes thicker the veering regions occur earlier on at lower rotating speeds and the beam becomes unstable also for lower rotating speeds. All this might sound contradictory as one would think that since the beam becomes more fragile as it becomes slender, the opposite should happen. However, the centrifugal inertia force (mass matrix $\mathbf{M}_c$ in the equivalent stiffness matrix $\mathbf{K}_{eq}$) which has an important contribution to buckle the beam, also decreases when the beam becomes more slender. Even though it is not so evident, the slenderness ratio also has an effect on the tuned angular speed. As it can be seen in figures 4.4 as the slenderness ratio increases so does the tuned angular speed, although for the same change in the slenderness ratio the effect is greater if the hub radius ratio is higher.

Analyzing the results from tables 4.3 and 4.4 it can be seen that the assumption of negligible gyroscopic coupling can or not be reasonable depending on the value of the hub radius and greatly on the value of the slenderness ratio. It is noted that the natural frequencies obtained by including or neglecting the gyroscopic effect deviate from each other as the rotating speed increases aggravating with the increase of the hub radius. It can also be seen that for thick beams (lower values of α) the maximum rotating speed, after which the gyroscopic effect is no longer negligible, is low ($\gamma < 10$). On the contrary, as the beam becomes more slender it is noted that even for higher rotating speeds the results obtained neglecting the gyroscopic coupling are fairly approximated. This effect is also shown in figure 4.6 where it can be seen that for $\alpha = 70$ the results differ allot for higher rotating speeds whereas for $\alpha = 220$ the results are very close with or without the gyroscopic matrix. It is also interesting to note that whether the gyroscopic effect is included or neglected the beam buckles at exactly the same speed. In the case of neglecting the gyroscopic effect however, it's the fourth natural frequency at $\gamma = 0$ (first stretching mode) that drops until it's nil intersecting every other natural frequency, while in the case of including the gyroscopic effect its the first natural frequency (first bending mode).

Considering now figure 4.7, it can be seen how the hub radius ratio influences the changing in the natural frequencies. As the hub radius ratio increase the natural frequencies also increase and the veering regions not only increase in number but also become more prominent as well. Since the increase in the hub radius ratio has the effect of increasing the natural frequencies, by increasing the first natural frequency it pushes the tuned angular speed forward and so, has the hub radius increase relatively to the beam the tuned angular speed occurs at higher rotating speeds. Also interesting in the effect of this ratio is the fact that the buckling speed has nothing to do with it, as it can be seen from figures 4.7 no matter what value δ has all the plots have the buckling speed occuring at the same dimensionless rotating speed.

As it was noted in Yoo and Shin [2] the natural mode shapes undergo an abrupt change as the angular speed increases around the veering region. This is shown in figures 4.8 and 4.9. Since the hub radius ratio, the slenderness ratio as well as using the Euler-Bernoulli or the Timoshenko beam theory can change the rotating speeds at which the veering regions occur, these effects can automatically change in an abrupt

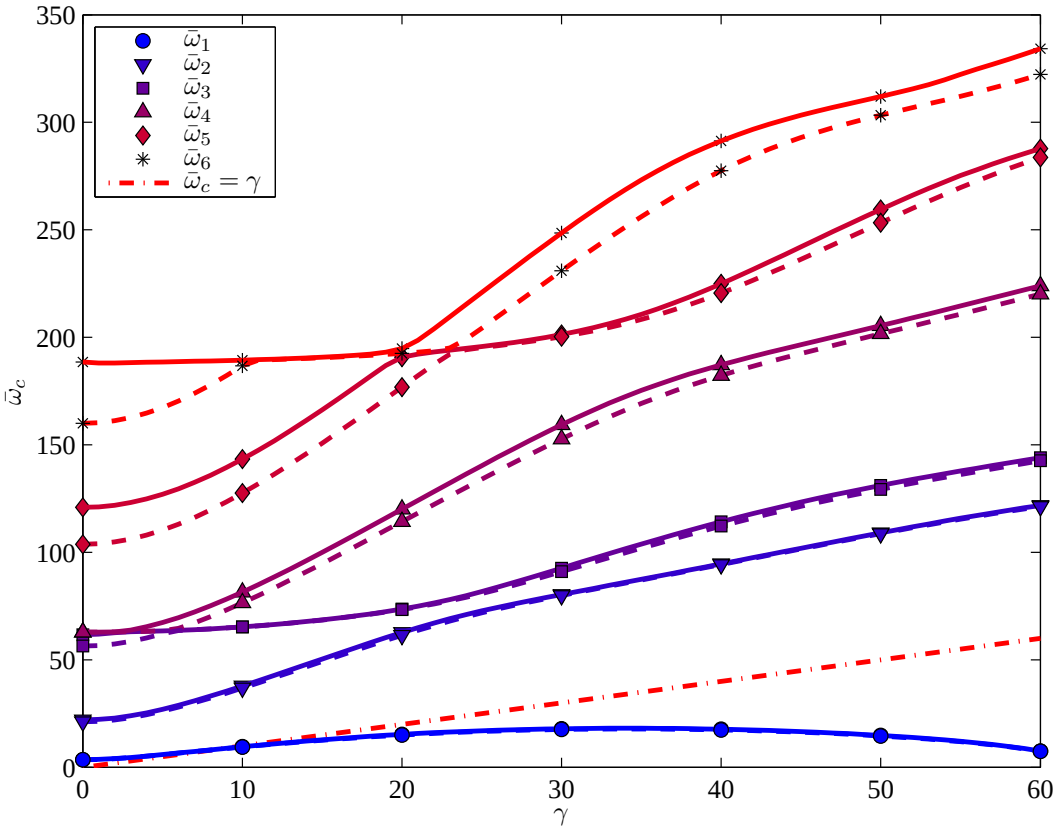

Figure 4.3: Comparison of the first six chordwise natural frequencies for the Euler-Bernoulli(-) and Timoshenko(- -) beams ($\delta = 0.5$, $\alpha = 40$, $\vartheta = 1$, $\kappa = 5/6$)

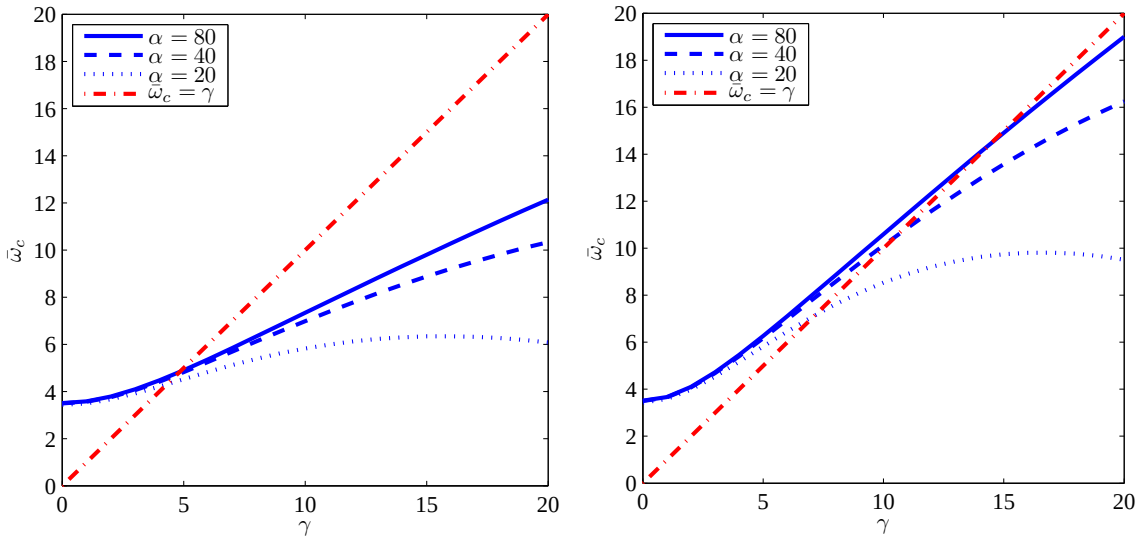

(a) $\delta = 0.2$ (b) $\delta = 0.6$

Figure 4.4: Effect of α and δ on the first tuned dimensionless natural frequency for a Timoshenko finite element beam ($\kappa = 5/6$, $\vartheta = 1$)

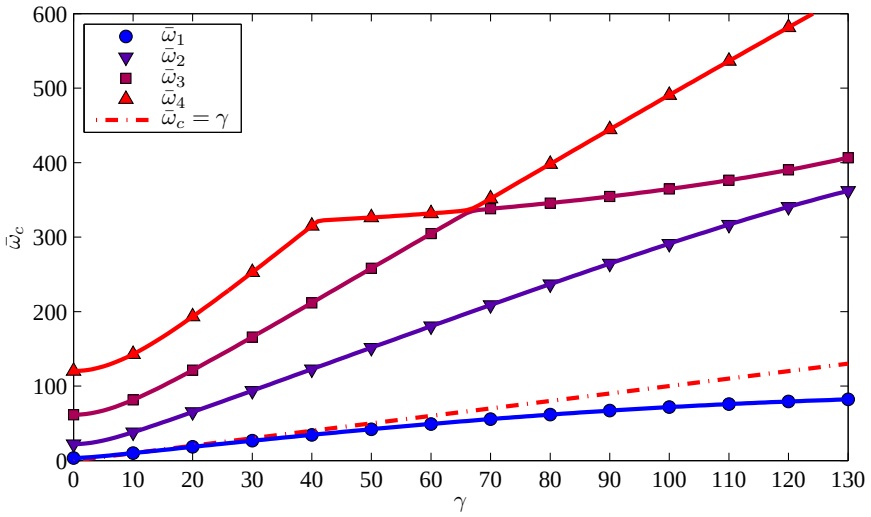

(a) $\alpha = 200$

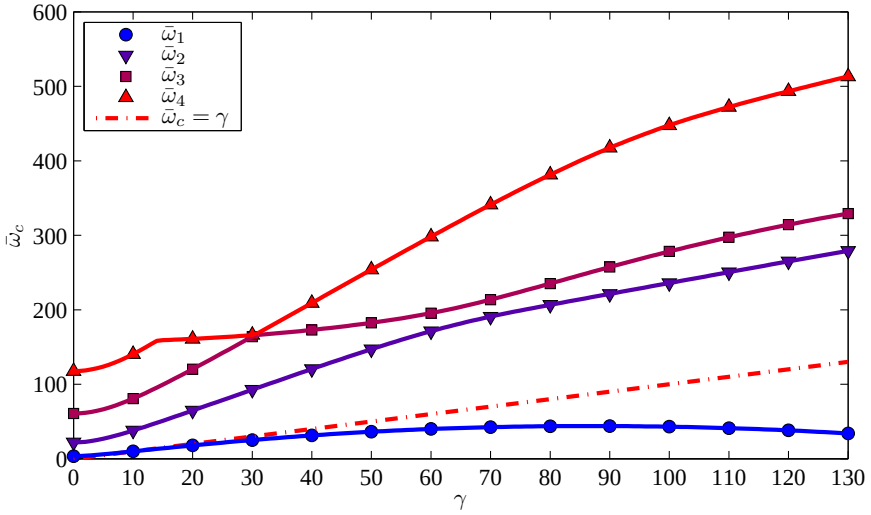

(b) $\alpha = 100$

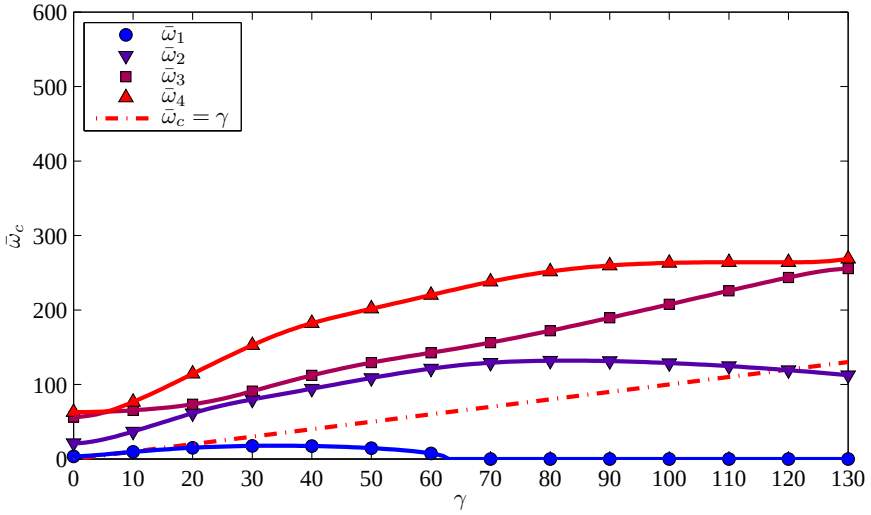

(c) $\alpha = 40$

Figure 4.5: Effect of α on the first four chordwise dimensionless natural frequencies for a Timoshenko finite element beam ($\delta = 0.5$, $\kappa = 5/6$, $\vartheta = 1$)

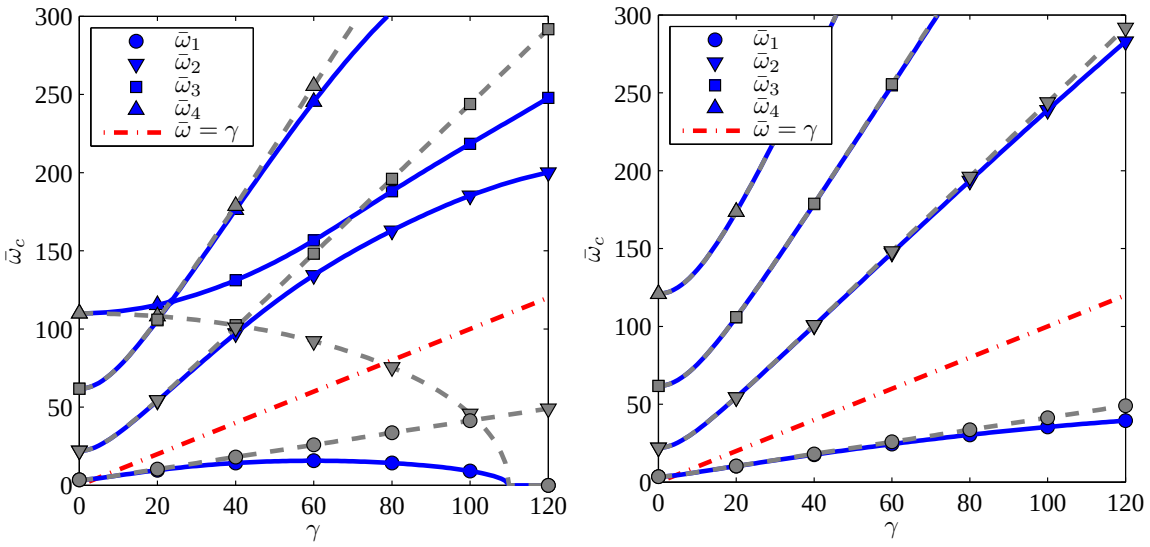

(a) ($\alpha = 70$) (b) ($\alpha = 220$)

Figure 4.6: Effect of the gyroscopic coupling matrix (-with, - -without) for different values of α (Euler-Bernoulli finite element beam, $\vartheta = 1$, $\delta = 0.1$)

way the natural mode shapes or, in the case of using the Euler-Bernoulli theory if the slenderness ratio is somewhat low, then the mode shapes can be wrongly predicted. These effects are shown in figures 4.10.

Table 4.3: Comparison of the first bending natural frequency for the chordwise motion ($\alpha = 70$, $\kappa = 5/6$, $\vartheta = 1$)

		Gyroscopic coupling included				Gyroscopic coupling neglected		
δ	γ	T.	E.B.	Ref.[4]	Ref.[2]	T.	E.B.	Ref.[2]
0	2	3.6113	3.6196	3.6196	3.62	3.6135	3.6218	3.62
	10	4.9151	4.9700	4.9700	4.97	4.9932	5.0490	5.05
	50	6.2358	7.3337	7.3337	7.55	8.8817	10.4474	10.5
1	2	4.3894	4.3978	4.3978	4.40	4.3921	4.4005	4.40
	10	12.9948	13.0482	13.0482	13.1	13.2037	13.2579	13.3
	50	40.9263	41.2275	41.2275	41.4	61.1016	61.5899	61.6
5	2	6.6322	6.6430	6.6430	6.64	6.6363	6.6471	6.65
	10	27.1565	27.2658	27.2660	27.3	27.6152	27.7262	27.7
	50	73.8532	74.0094	74.0031	74.2	134.9205	135.4485	136

Table 4.4: Effect of α on the first two bending natural frequencies and on the gyroscopic coupling (Timoshenko finite element, $\vartheta = 1$, $\delta = 0.5$)

α	Gyroscopic coupling	γ			
		2	10	50	100
First mode					
50	Including	4.0092	9.6467	21.6470	-
	Neglecting	4.0141	9.9512	43.5596	86.1723
100	Including	4.0250	9.9406	36.2660	43.0103
	Neglecting	4.0262	10.0181	43.9365	86.5490
200	Including	4.0290	10.0166	42.0447	71.7268
	Neglecting	4.0293	10.0361	44.1621	86.9020
Second mode					
50	Including	22.3366	37.2859	117.9094	164.9836
	Neglecting	22.3415	37.4622	150.2987	296.5021
100	Including	22.7634	37.9060	147.0811	235.8916
	Neglecting	22.7646	37.9483	151.9041	299.2665
200	Including	22.8744	38.0680	151.5709	291.1570
	Neglecting	22.8747	38.0785	152.5293	300.3405

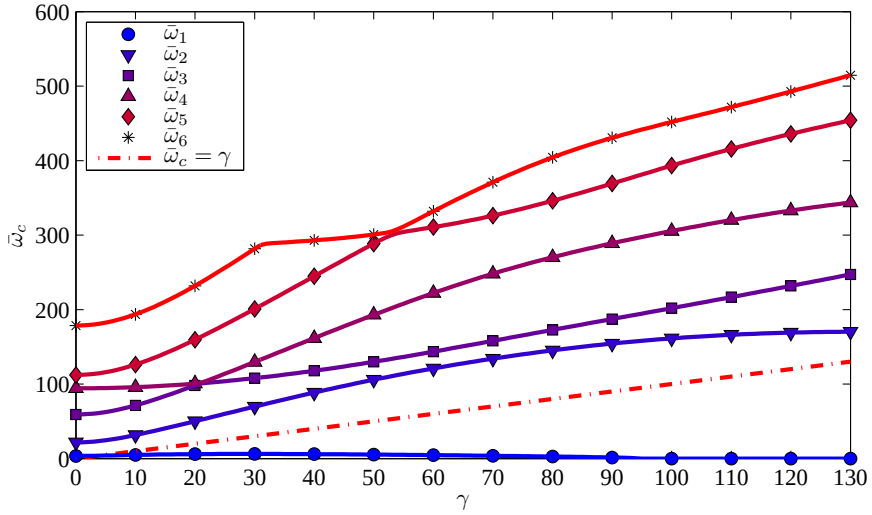

(a) $\delta = 0$

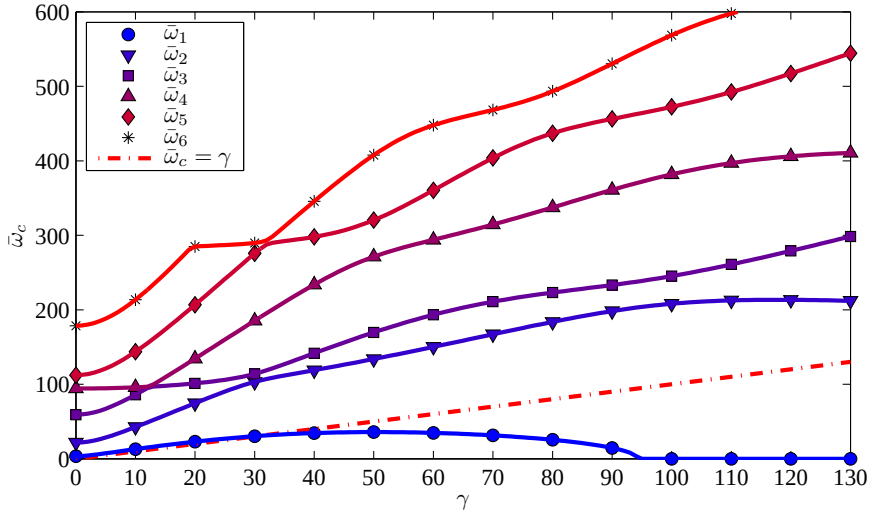

(b) $\delta = 1$

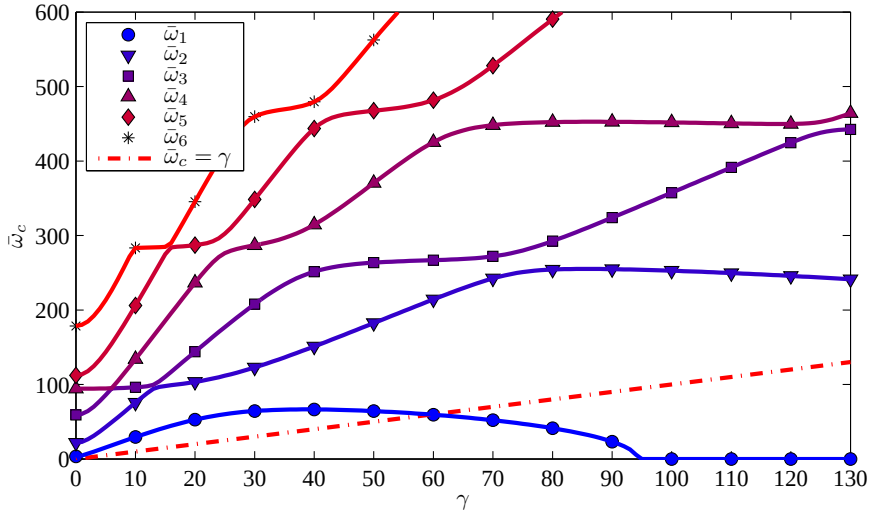

(c) $\delta = 6$

Figure 4.7: Effect of δ on the first six chordwise dimensionless natural frequencies for a Timoshenko beam element ($\alpha = 60$, $\kappa = 5/6$, $\vartheta = 1$)

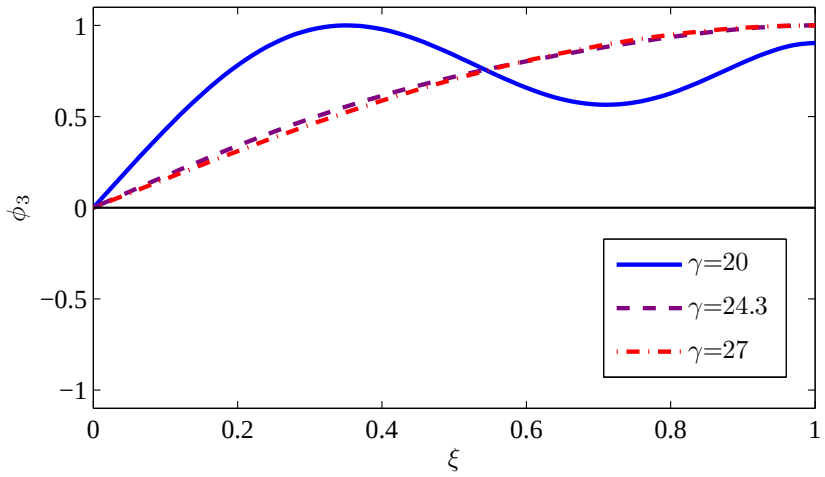

(a) Third stretching mode shape

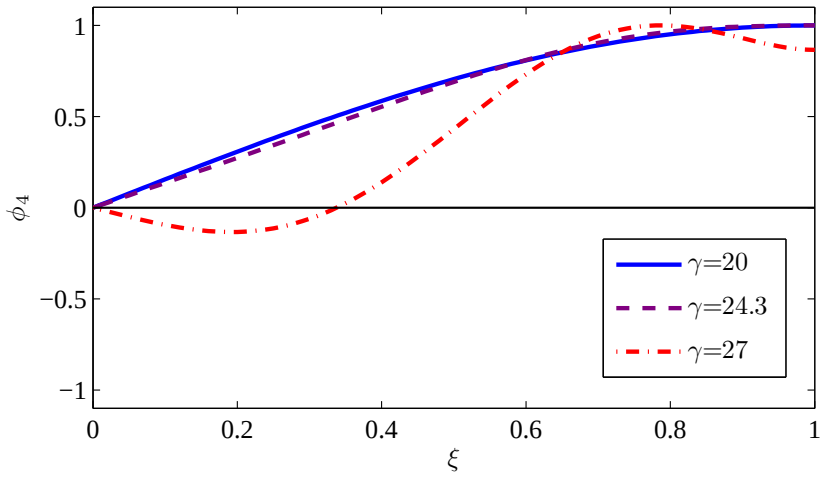

(b) Fourth stretching mode shape

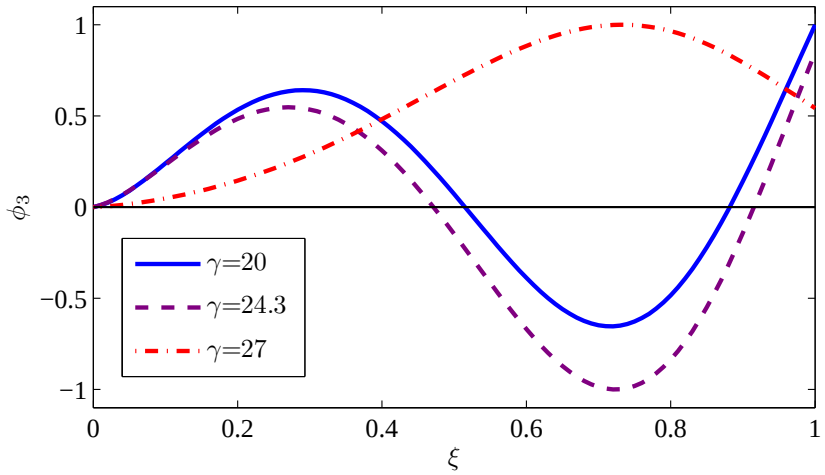

(c) Third bending mode shape

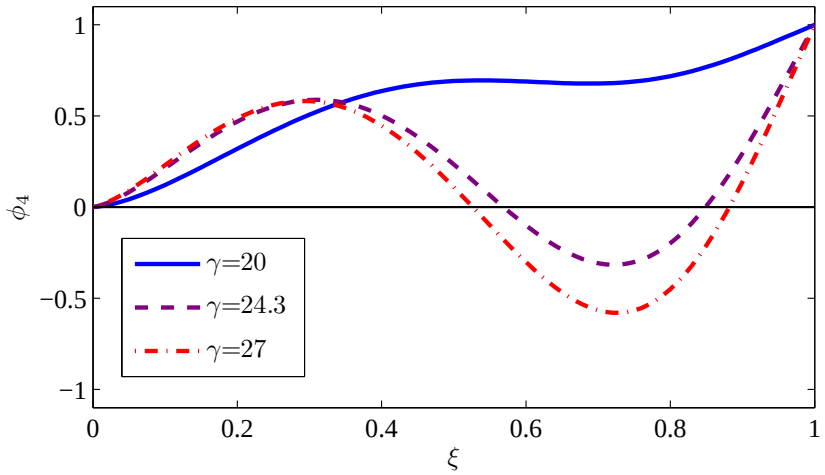

(d) Fourth bending mode shape

Figure 4.8: Mode shape variations along the abrupt veering region (Timoshenko beam, $\delta = 0.1$, $\alpha = 70$, $\vartheta = 1$, $\kappa = 5/6$)

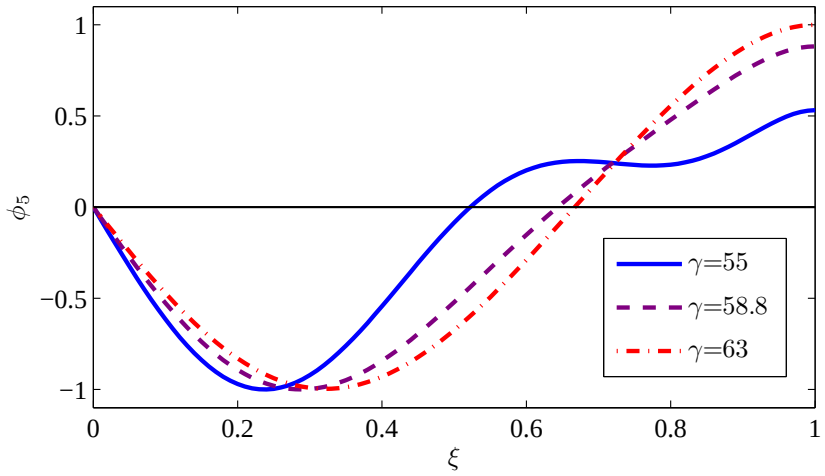

(a) Fifth stretching mode shape

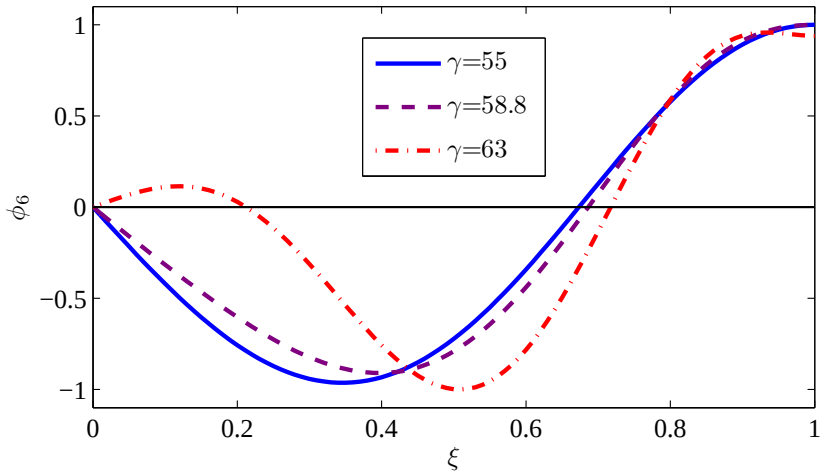

(b) Sixth stretching mode shape

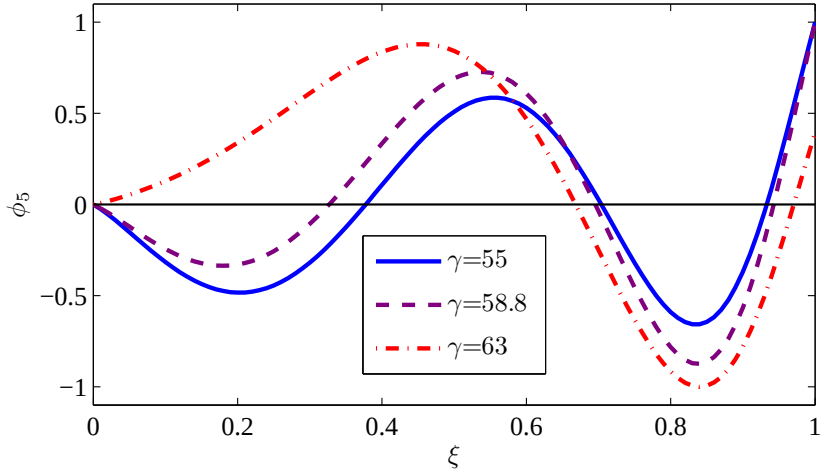

(c) Fifth bending mode shape

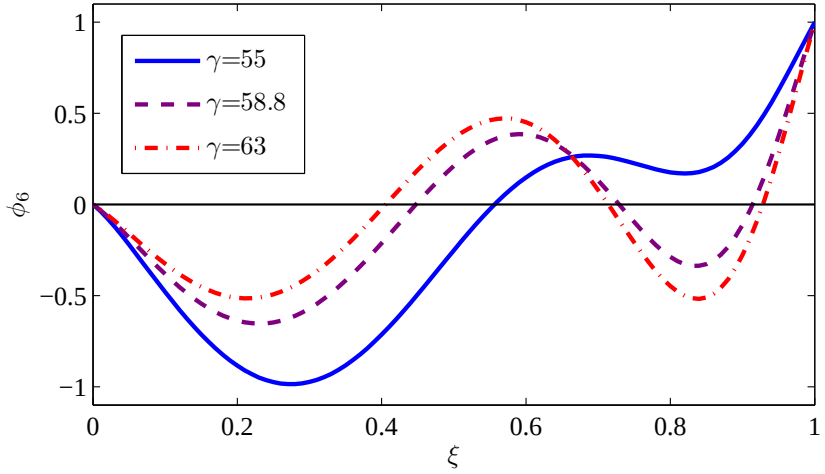

(d) Sixth bending mode shape

Figure 4.9: Mode shape variations along the abrupt veering region (Timoshenko beam, $\delta = 0.1$, $\alpha = 70$, $\vartheta = 1$, $\kappa = 5/6$)

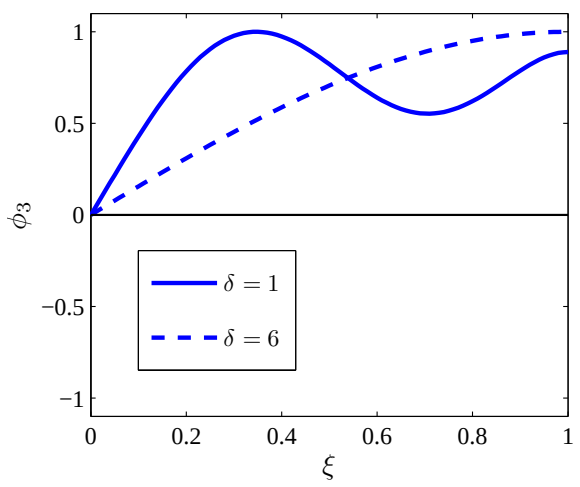

(a) Third stretching mode shape ($\gamma = 8$, $\alpha = 60$, Timoshenko beam)

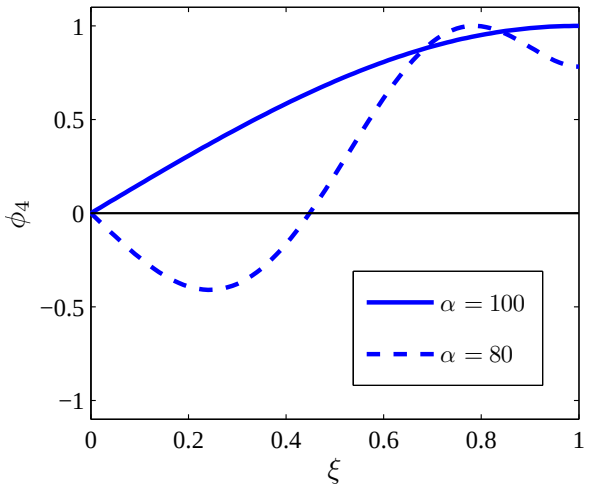

(b) Fourth stretching mode shape ($\gamma = 28$, $\delta = 0.5$, Timoshenko beam)

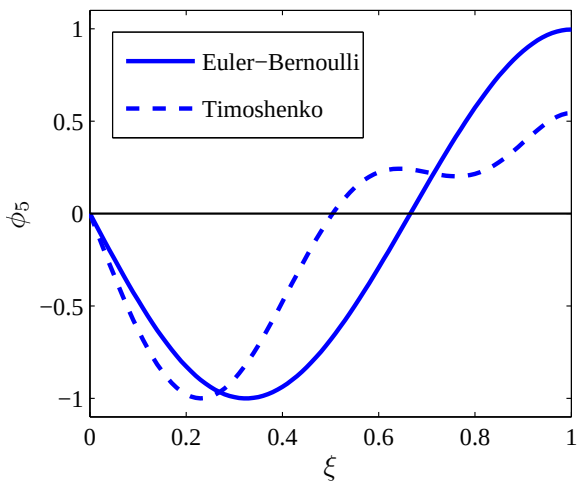

(c) Fifth stretching mode shape ($\gamma = 21$, $\delta = 0.5$)

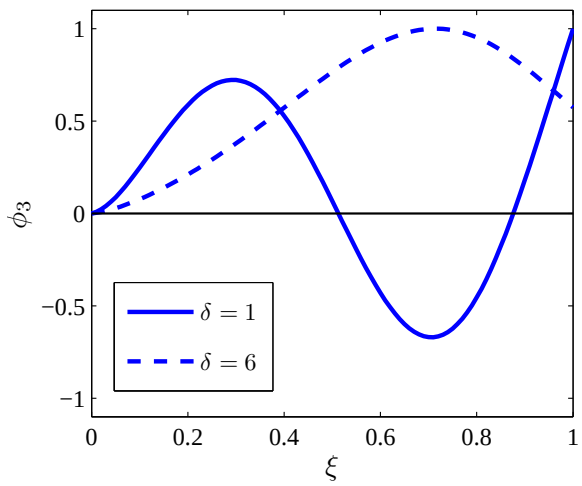

(d) Third bending mode shape ($\gamma = 8$, $\alpha = 60$, Timoshenko beam)

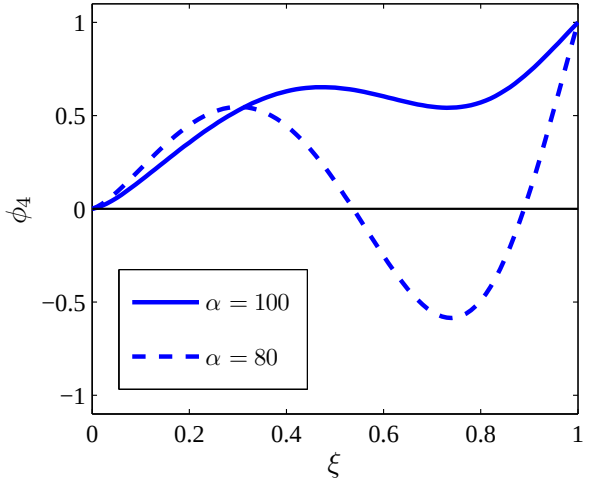

(e) Fourth bending mode shape ($\gamma = 28$, $\delta = 0.5$, Timoshenko beam)

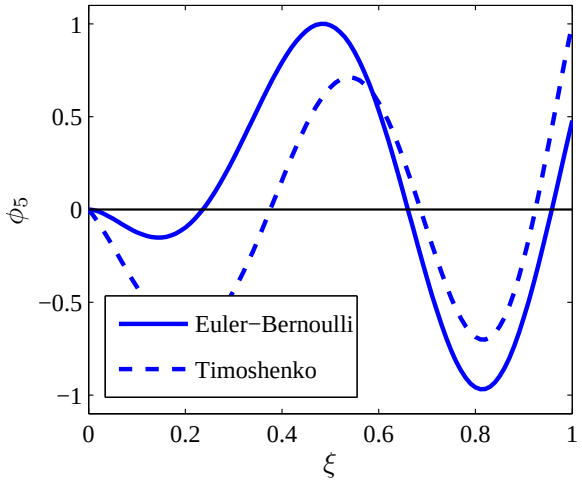

(f) Fifth bending mode shape ($\gamma = 21$, $\delta = 0.5$)

Figure 4.10: Mode shape variations due to δ, α and beam element theories ($\kappa = 5/6$, $\vartheta = 1$)

4.1.2 Flapwise motion

In table 4.5 it is shown the convergence of the first six flapwise natural frequencies for a stationary beam, and in tables 4.6 and 4.7 it is shown the convergence of the first three flapwise natural frequencies for a rotating Euler-Bernoulli and Timoshenko beams respectively, where it can be seen that results converge. Note that for a non-rotating beam the first four flapwise natural frequencies are equal to the first three and fifth chordwise natural frequencies, which makes sense seeing that for a non-rotating beam chordwise bending and stretching motions are uncoupled and also that the inertia moments of the cross section are considered the equal for both axes. Once again one sees that the use of selective integration provides better results especially when the number of elements is low, preventing shear locking. Also, even for slender beams the Timoshenko element provided close results to those from the Euler-Bernoulli element, diverging more significantly only for higher natural frequencies (fifth and sixth modes).

In tables 4.8 and 4.9 results from the present method are compared with those found in the literature, obtaining similar results. In table 4.8 it can be seen that as the angular speed increases the natural frequencies also increase due to centrifugal stiffening of the beam. This can also be observed from figure 4.11 noting that the natural frequencies for the flapwise motion monotonically increase with the angular speed, opposed to what happened for the chordwise motion. From table 4.9 one can see that as the slenderness ratio increases, the flap wise natural frequencies also increase using the Timoshenko beam theory. On the other hand, using the Euler-Bernoulli beam theory the slenderness ratio makes no difference whatsoever as it is demonstrated in table 4.10, proving the lack of accuracy that the Euler-Bernoulli beam has for non-slender beams.

In figure 4.12b it is analyzed the effect of the hub radius ratio on the first three flapwise natural frequencies. The main effect is that with the increase in the hub radius ratio there is an increase in the flapwise natural frequencies of the beam which makes sense since the centrifugal stiffness matrix increase with δ and thus it stiffens the beam.

Considering figure 4.12a it can be seen that no tuned angular speed occurs, whether the beam is slender or thick . It is observable that the effect of α only makes a difference after the first natural frequency, and since δ only pushes the natural frequencies away from the line $\bar{\omega} = \gamma$, one can conclude that no tuned angular speed can occur for the flapwise motion, opposed to what happens for the chordwise motion.

From figure 4.12c one can see that for a non-slender beam the Euler-Bernoulli and Timoshenko theories differ from each other , although the first natural frequency remains roughly the same for both theories even for a thick beam.

Finally the mode shapes are analyzed in figures 4.13, 4.14 and 4.15. It can be observed that main effect of the rotation speed is that it pushes the vibration nodes forward, whereas for the hub radius ratio δ, as it increases the effect is identical. In figure 4.15 one can see that as the beam becomes thicker, the nodes are also pushed forward, although only the third and fourth mode shapes are plotted since the effect for the first two was almost negligible.

Table 4.5: Convergence of the first six flapwise natural frequencies ($\gamma = 0$, $\delta = 0$, $\vartheta = 1$, $\kappa = 5/6$, $\alpha = 70$)

No. of elements	Element type	1st	2nd	3rd	4th	5th	6th
5	E.B.	3.5161	22.0455	61.9188	122.3197	203.0202	337.2727
	T.	8.6524	55.9227	167.0225	349.4495	567.9314	2751.2059
	T. s.i.	3.5254	23.9357	78.7906	199.5564	461.0860	1408.8197
10	E.B.	3.5160	22.0352	61.7129	121.0171	200.3633	300.1671
	T.	5.2938	33.1683	93.5296	185.7555	312.5871	475.9287
	T. s.i.	3.5133	22.2664	63.9636	130.5429	227.6545	362.3362
20	E.B.	3.5160	22.0345	61.6982	120.9095	199.8934	298.6674
	T.	4.0306	25.0387	69.2999	133.7980	217.4676	319.0138
	T. s.i.	3.5101	21.8670	60.7831	118.0444	193.1981	285.5989
40	E.B.	3.5160	22.0345	61.6973	120.9024	199.8617	298.5627
	T.	3.6465	22.6032	62.2544	119.2780	191.9331	278.1668
	T. s.i.	3.5093	21.7683	60.0184	115.1561	185.6018	269.4609
60	E.B.	3.5160	22.0345	61.6972	120.9020	199.8600	298.5570
	T.	3.5708	22.1251	60.8819	116.4804	187.0756	270.4994
	T. s.i.	3.5092	21.7501	59.8781	114.6312	184.2371	266.5982
80	E.B.	3.5160	22.0345	61.6972	120.9019	199.8597	298.5560
	T.	3.5439	21.9555	60.3957	115.4919	185.3641	267.8062
	T. s.i.	3.5091	21.7437	59.8291	114.4482	183.7625	265.6054
100	E.B.	3.5160	22.0345	61.6972	120.9019	199.8596	298.5557
	T.	3.5314	21.8765	60.1697	115.0326	184.5699	266.5579
	T. s.i.	3.5091	21.7408	59.8064	114.3636	183.5433	265.1474

Table 4.6: Convergence of the first three dimensionless natural frequencies using the Euler-Bernoulli beam element ($\gamma = 100$, $\delta = 0$, $\alpha = 70$, $\vartheta = 1$)

No. of elements	1st	2nd	3rd
10	101.3464	248.7626	400.7600
40	101.0753	248.1707	399.7508
70	101.0704	248.1600	399.7326
100	101.0699	248.1589	399.7306
Ref[2]	101.17	248.38	400.15

Table 4.7: Convergence of the first three dimensionless natural frequencies using the Timoshenko beam element ($\gamma = 8$, $\alpha = 50$, $\delta = 0$, $\vartheta = 1$, $\mu = 0.25$)

No. of elements	1st	2nd	3rd
10	9.2087	29.7521	69.8057
40	9.2095	29.3482	66.4885
70	9.2096	29.3302	66.3445
100	9.2096	29.3257	66.3089
Ref.[6]	9.2132	29.3501	66.4010

Table 4.8: Comparison of the first two flapwise natural frequencies for a Timoshenko and a Euler-Bernoulli rotating beam ($\delta = 0$, $\alpha = 70$, $\kappa = 5/6$, $\vartheta = 1$)

	First natural frequency				Second natural frequency			
γ	T.	E.B.	Ref[4]	Ref[2]	T.	E.B.	Ref[4]	Ref[2]
0	3.5091	3.5160	3.5160	3.5160	21.7408	22.0345	22.0345	22.035
1	3.6745	3.6816	3.6816	3.6816	21.8876	22.1810	22.1810	22.181
2	4.1296	4.1373	4.1373	4.1373	22.3222	22.6149	22.6149	22.615
3	4.7885	4.7973	4.7973	4.7973	23.0284	23.3203	23.3203	23.320
4	5.5746	5.5850	5.5850	5.5850	23.9819	24.2733	24.2733	24.273
5	6.4371	6.4495	6.4495	6.4495	25.1542	25.4461	25.4461	25.446
6	7.3455	7.3604	7.3604	7.3604	26.5156	26.8091	26.8091	26.809
7	8.2819	8.2996	8.2996	8.2996	28.0374	28.3341	28.3341	28.334
8	9.2359	9.2568	9.2568	9.2568	29.6938	29.9954	29.9954	29.995
9	10.2011	10.2257	10.2257	10.226	31.4623	31.7705	31.7705	31.771
10	11.1739	11.2023	11.2023	11.202	33.3237	33.6404	33.6404	33.640

Table 4.9: Comparison of the first four flapwise natural frequencies for a Timoshenko rotating beam and analysis of the slenderness ratio ($\delta = 0$, $\vartheta = 1$, $\mu = 0.25$)

	γ											
	0			4			8			10		
α	T.	Ref.[6]	Ref.[5]	T.	Ref.[6]	Ref.[5]	T.	Ref.[6]	Ref.[5]	T.	Ref.[6]	Ref.[5]
1000	3.5160	3.5059	3.5160	5.5849	5.5850	5.5850	9.2567	9.2568	9.2568	11.2021	13.1704	13.1702
	22.0381	22.0296	22.0345	24.2767	24.2726	24.2733	29.9982	29.9950	29.9954	33.6430	37.6037	37.6031
	61.7288	61.8502	61.6971	63.9975	63.9627	63.9666	70.3220	70.2896	70.2929	74.6775	79.6136	79.6144
	121.0304	120.2983	120.9010	123.3886	123.2354	123.2610	130.1725	130.0251	130.0490	135.0055	140.5155	140.5340
50	3.4998	3.5000	3.4998	5.5616	5.5623	5.5616	9.2096	9.2132	9.2096	11.1383	13.0972	13.0870
	21.3597	21.3692	21.3547	23.6108	23.6240	23.6061	29.3257	29.3501	29.3215	32.9461	36.9140	36.8659
	57.5071	57.5636	57.4705	59.8475	59.9130	59.8117	66.3089	66.4010	66.2748	70.7149	75.8382	75.6698
	107.0554	107.2812	106.9260	109.5866	109.8286	9.4590	116.7893	117.0778	116.6650	121.8577	128.0863	127.6040
25	3.4527	3.4534	3.4527	5.4951	5.4980	5.4951	9.0854	9.0975	9.0854	10.9794	12.9229	12.8934
	19.6538	19.6965	19.6497	21.9596	22.0126	21.9557	27.7118	27.7933	27.7082	31.3092	35.3077	35.1811
	48.9145	49.1256	48.8891	51.5069	51.7372	51.4822	58.4746	58.7562	58.4507	63.1043	68.6107	68.2339
	84.1906	84.8053	84.1133	87.2602	87.9002	87.1836	95.7181	96.4247	95.6423	101.4698	108.7570	107.8870
12.5	3.2837	3.2863	3.2837	5.2749	5.2840	5.2749	8.7455	8.7746	8.7456	10.5872	12.5134	12.4581
	15.4908	15.5873	15.4883	18.0651	18.1781	18.0628	24.0502	24.1961	24.0479	27.5939	31.4634	31.2846
	34.3128	34.6138	34.3005	37.7439	38.0639	37.7317	45.9810	46.3420	45.9683	50.9045	56.3909	55.9744
	53.6846	54.2503	53.6516	57.9819	58.5494	57.9491	67.8523	68.3629	67.8215	72.9827	77.4992	77.1047
10	3.1738	3.1774	3.1738	5.1448	5.1570	5.1448	8.5735	8.6077	8.5735	10.3963	12.3066	12.2467
	13.6625	13.7694	13.6607	16.3964	16.5184	16.3946	22.3524	22.4979	22.3506	25.6606	29.0691	28.9100
	29.3707	29.6487	29.3614	33.1886	33.4810	33.1793	41.4726	41.7829	41.4632	45.8120	49.9746	49.6484
	43.9311	44.3234	43.9102	47.8275	48.1460	47.8101	53.2924	53.5041	53.2833	55.0746	56.9137	56.6750

Table 4.10: Analysis of the effect of the slenderness ratio on the first four flapwise natural frequencies for an Euler-Bernoulli rotating beam element ($\delta = 0$, $\vartheta = 1$)

	γ			
α	0	4	8	10
1000	3.5160	5.5850	9.2568	11.2023
	22.0345	24.2733	29.9954	33.6404
	61.6972	63.9668	70.2930	74.6493
	120.9019	123.2615	130.0490	134.8841
10	3.5160	5.5850	9.2568	11.2023
	22.0345	24.2733	29.9954	33.6404
	61.6972	63.9668	70.2930	74.6493
	120.9019	123.2615	130.0490	134.8841

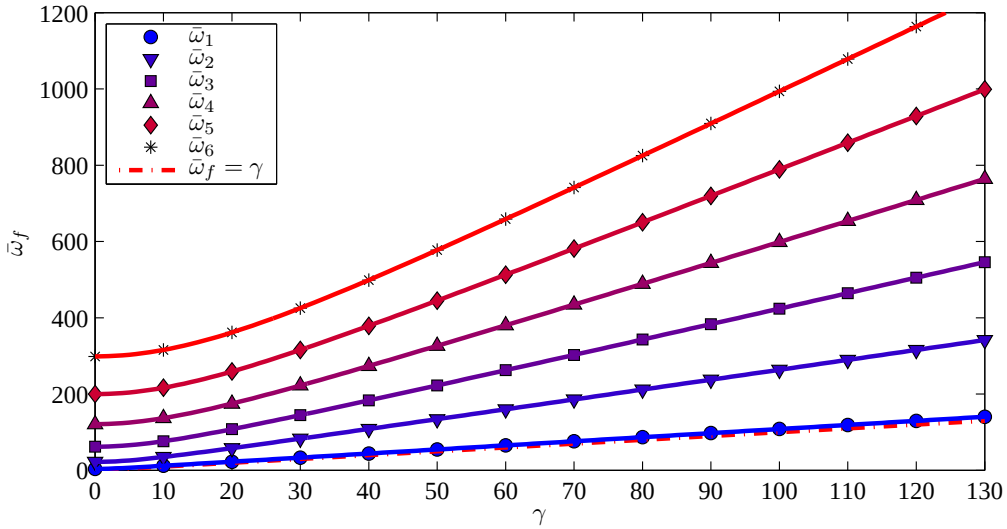

(a) Euler-Bernoulli beam

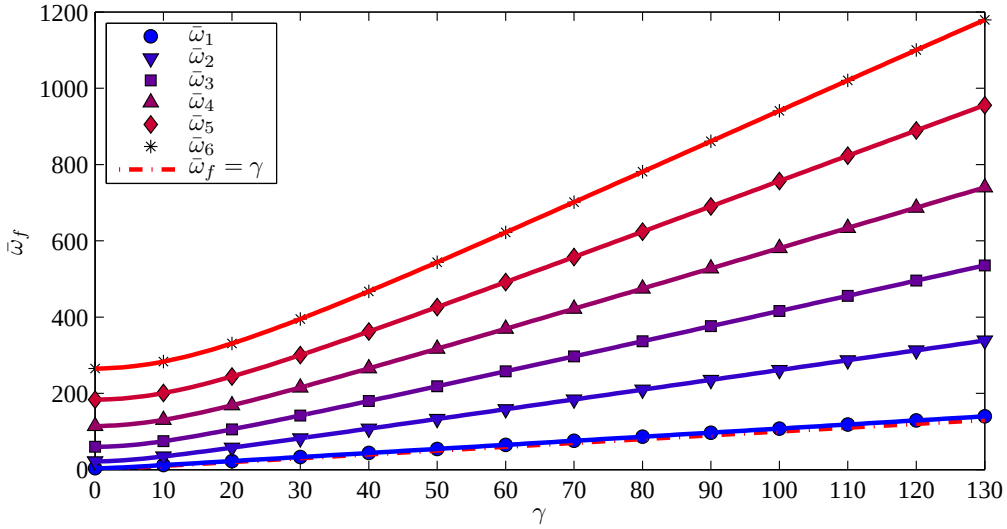

(b) Timoshenko beam ($\kappa = 5/6$)

Figure 4.11: Variation of the first six flapwise dimensionless natural frequencies ($\delta = 0.1$, $\alpha = 70$, $\vartheta = 1$)

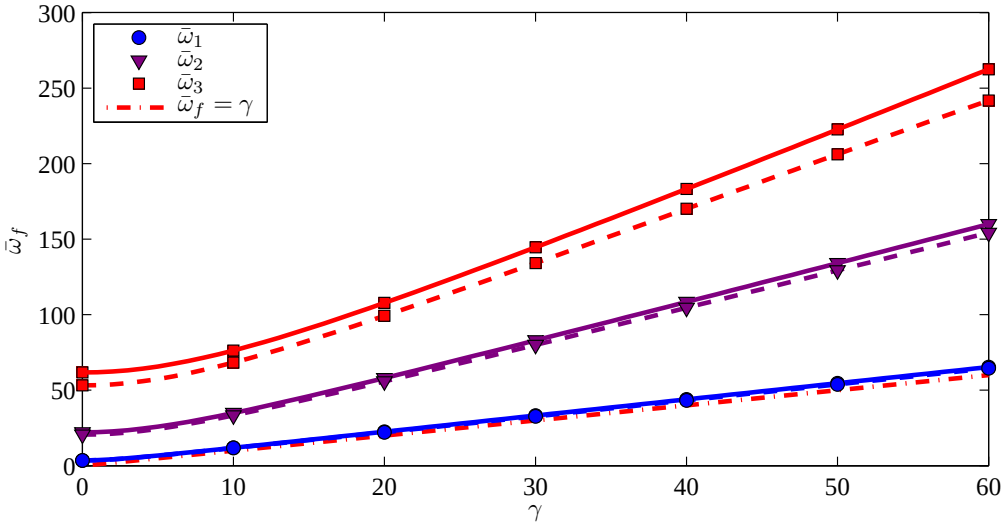

(a) Effect of α (Timoshenko beam, $\vartheta = 1$, $\delta = 0.1$, $\kappa = 5/6$, -$\alpha = 800$, - -$\alpha = 30$)

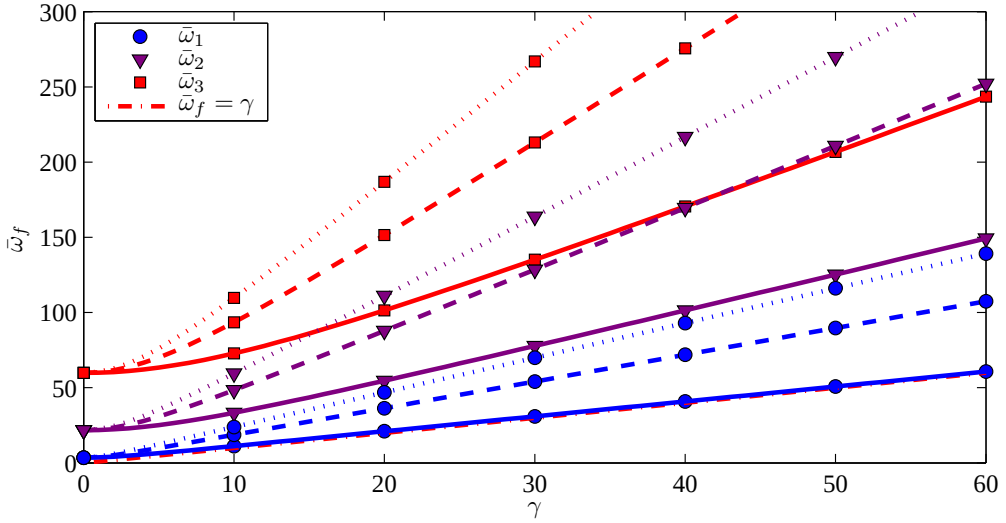

(b) Effect of δ (Timoshenko beam, $\alpha = 70$, $\vartheta = 1$, $\kappa = 5/6$, -$\delta = 0$, - -$\delta = 1.5$, : $\delta = 3$)

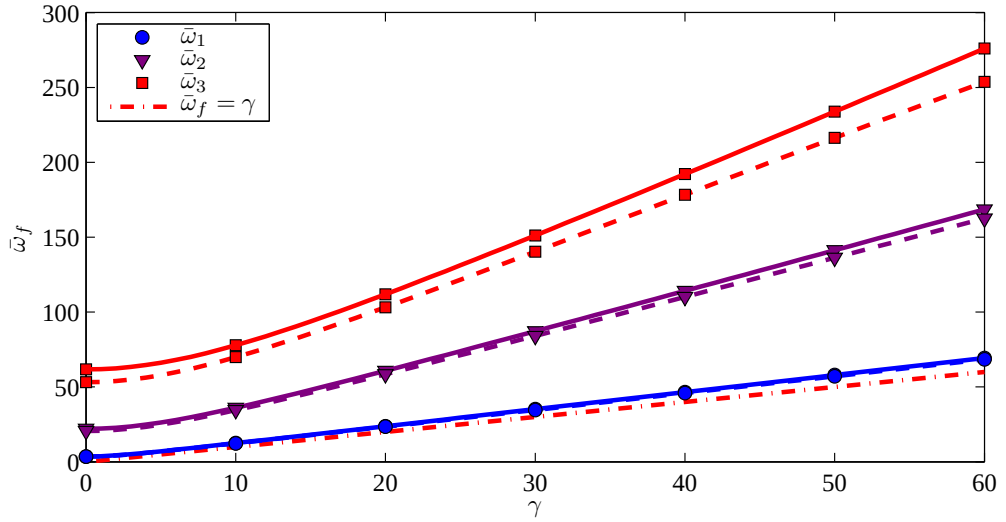

(c) Effect of beam element theories ($\delta = 0.2$, $\alpha = 30$, $\vartheta = 1$, Euler-Bernoulli(-), Timoshenko(- -), $\kappa = 5/6$)

Figure 4.12: Effect of α, δ and beam element theories on the first three flapwise dimensionless natural frequencies

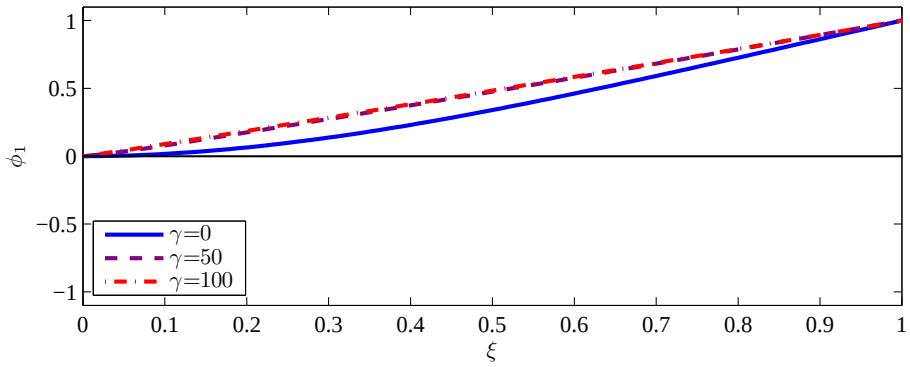

(a) First mode shape

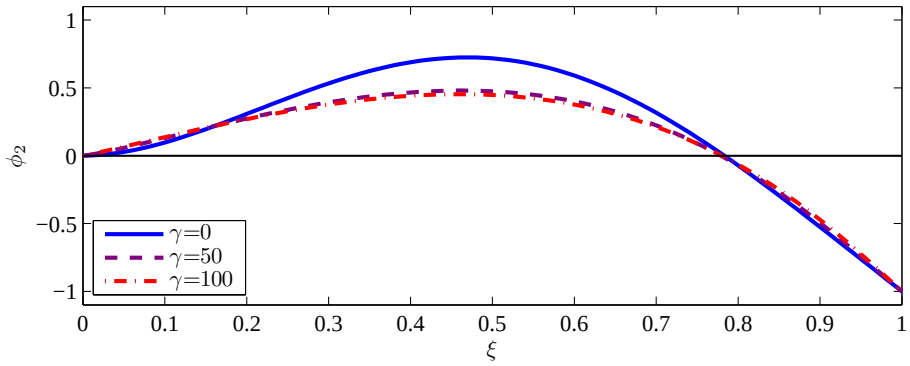

(b) Second mode shape

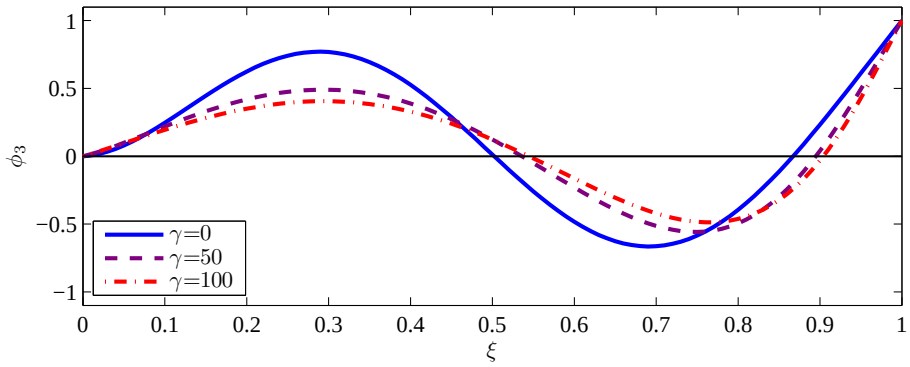

(c) Third mode shape

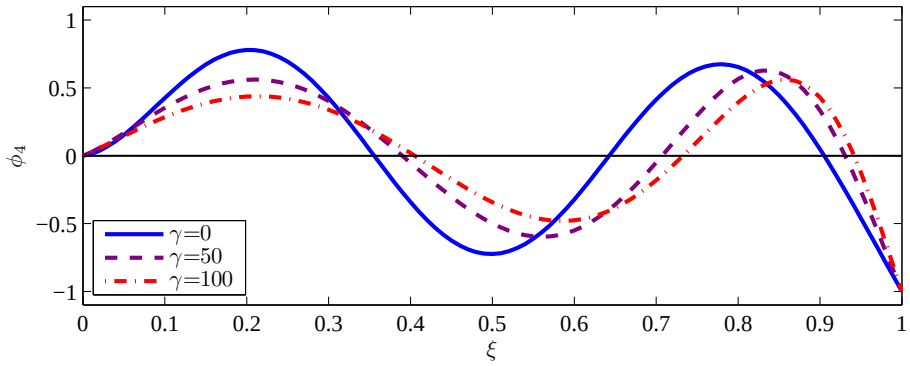

(d) Fourth mode shape

Figure 4.13: First four flapwise mode shapes for a rotating Timoshenko beam ($\kappa = 5/6$, $\alpha = 70$, $\vartheta = 1$, $\delta = 0.1$)

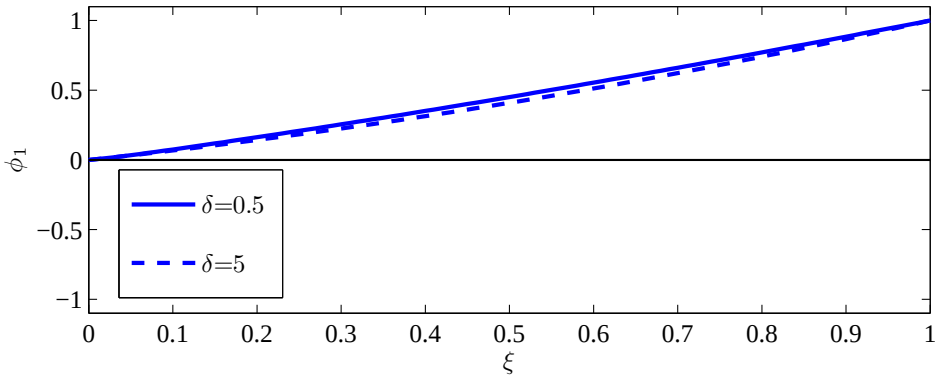

(a) First mode shape

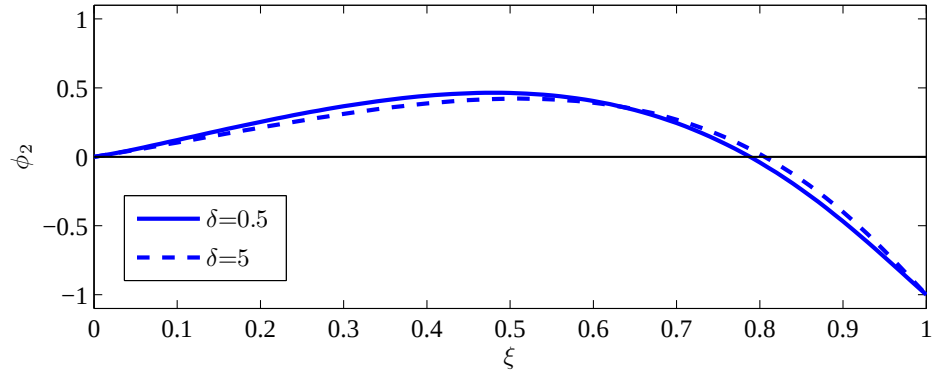

(b) Second mode shape

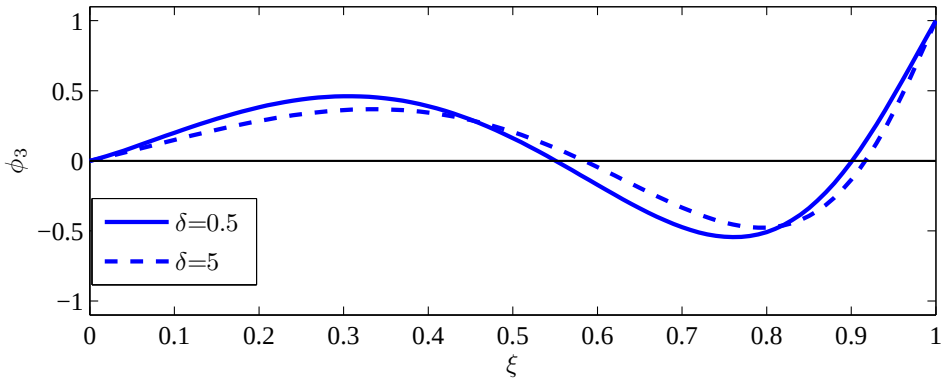

(c) Third mode shape

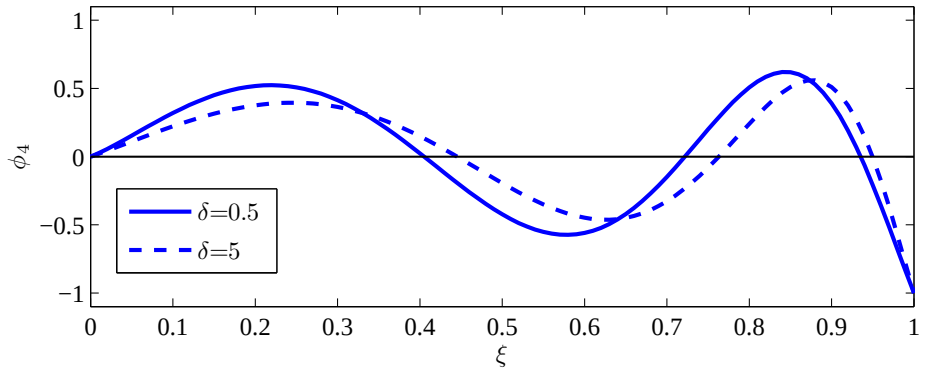

(d) Fourth mode shape

Figure 4.14: Effect of δ on the first four flapwise mode shapes for a rotating Timoshenko beam ($\kappa = 5/6$, $\alpha = 70$, $\vartheta = 1$, $\gamma = 50$)

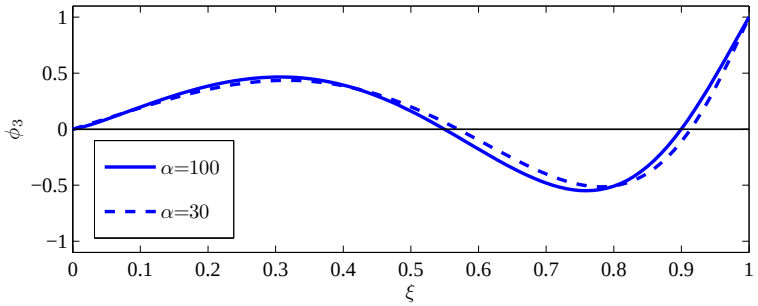

(a) Third mode shape

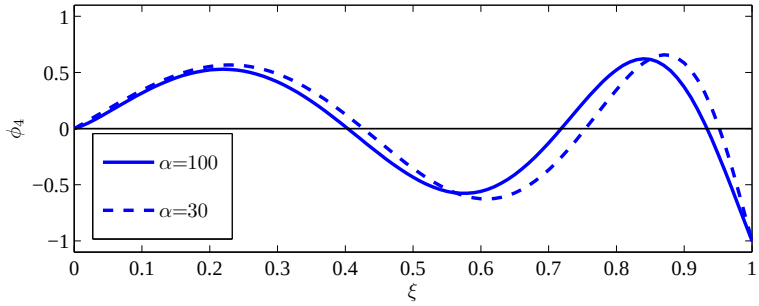

(b) Fourth mode shape

Figure 4.15: Effect of α on the third and fourth flapwise mode shapes for a rotating Timoshenko beam ($\kappa = 5/6$, $\delta = 0.5$, $\vartheta = 1$, $\gamma = 50$)

4.2 Pre-twisted rotating beam

In the present section it is analyzed the pre-twisted Timoshenko element. Mostly, the interest will fall over the effect of the pre-twist angle, as the other effects are similar to those analyzed in the previous section. Note that ideally the pre-twist angle would be determined continuously for each cross section but, the element matrices need to be determined for each element and as such the pre-twist angle is approximated as

$$\beta_{x_e} \approx \frac{(x_{e+1} + x_e)/2}{L}\beta_L \tag{4.2.1}$$

The natural frequencies from the present method are compared to those found in the literature in tables 4.11 and 4.12 and results obtained are similar. In a general way the effect that the pre-twist angle introduces in the natural frequencies is small as it can be seen in tables 4.12 and 4.13, and comparing both tables it can also be observed that whether the slenderness ratio is high or low the effect of the pre-twist angle over the natural frequencies still remains quite small. It is also noticeable that the differences in the natural frequencies introduced by the pre-twist angle become even smaller as the rotating speed of the beam increases.

It is interesting that for a stationary beam, as the pre-twist angle increases the natural frequencies obtained for the first and third modes also increase, but on the other hand the natural frequencies obtained for the second and fourth modes decrease. This is also shown in figure 4.16b, but around the veering regions the effect is the opposite and as the pre-twist angle increases the veering region becomes more gradual, separating the natural frequencies. Comparing figures 4.16 one sees that the natural frequencies for a rotating pre-twisted beam are composed of flapwise and chordwise natural frequencies. Note that the first two (bending) natural frequencies aren't equal because $\vartheta = 0.25$ and hence $I_y < I_z$ which makes the first flapwise frequency lower than the first chordwise frequency, intersecting with each other afterwards. When the pre-twist angle is introduced, the intersections between chordwise and flapwise natural frequencies become veering regions and as the pre-twist angle approaches zero degrees the more abrupt the veering regions become. Note that the third flapwise natural frequency does not intervene in the first four pre-twisted natural frequencies. The first natural frequency is composed of flapwise natural frequencies for low rotating speeds and around the veering becomes composed of chordwise natural frequencies, and the opposite can be said for the second natural frequency. A similar explanation can describe the third natural frequency. However, the fourth natural frequency has initially the contribution of the first chordwise frequencies then it changes to the second flapwise frequencies ($\gamma \approx 11$) and finally it is composed of the third chordwise frequencies. These effects are also shown in figures 4.17 where it can be seen that the introduction of a pre-twist angle pushes the intersections/veering regions forward specially for higher values of δ. The pre-twist angle also showed to have effect on the value of the tuned rotating speed although the influence is very small.

In figure 4.18 the effect that the centrifugal mass matrix has over the natural frequencies is analyzed by determining the frequencies with and without this matrix. It can be seen as it would be expected, that the $\mathbf{M}_s$ matrix lowers the natural frequencies since it lowers the overall stiffness ($\mathbf{K}_{eq}$) of the beam. It is also quite noticeable how much of a contribution this matrix has to the buckling of the beam and that without it the limit of instability would not exist. However this matrix has negligible effect over the flapwise bending frequencies and has a very important effect on the chordwise frequencies. This fact can be explained by noting in the element formulation that the centrifugal mass matrix doesn't involve the flapwise bending deformation w and the only flapwise degree of freedom is the rotation θ which involves the rotary inertia of the beam which in turn doesn't have much effect over the natural frequencies. As the slenderness ratio increases the effect of the centrifugal mass matrix also becomes negligible for higher chordwise modes.

Table 4.11: Comparison of the first two natural frequencies for a pre-twisted rotating beam ($\delta = 2$, $\beta_L = 30°$, $\alpha = 1000$, $\vartheta = 1/400$, $\kappa = 5/6$)

	First natural frequency		Second natural frequency	
γ	Present	Ref.[7]	Present	Ref.[7]
0.0000	0.1764	0.1763	0.9826	0.9825
0.0882	0.2290	0.2200	1.0292	1.0203
0.1763	0.3401	0.3157	1.1569	1.1254
0.2645	0.4685	0.4288	1.3402	1.2796

Table 4.12: Comparison of the first four dimensionless natural frequencies for a non-rotating pre-twisted Timoshenko beam and effect of the pre-twist angle for a slender beam ($\alpha = 1000$, $\delta = 0.1$, $\vartheta = 0.25$, $\mu = 0.25$)

	γ						
	0			5	10	50	100
$\beta_L(°)$	Present	Ref.[7]	Ref.[6]				
First							
30	1.7623	1.7623	1.7622	4.2860	5.7442	17.1613	30.7434
60	1.7748	1.7748	1.7748	4.2369	5.7319	17.1608	30.7434
90	1.7950	1.7950	1.7950	4.1651	5.7126	17.1601	30.7433
Second							
30	3.4793	3.4793	3.4793	5.7723	10.9078	52.3499	104.1798
60	3.3799	3.3799	3.3798	5.7854	10.9099	52.3500	104.1798
90	3.2426	3.2425	3.2426	5.8032	10.9131	52.3501	104.1797
Third							
30	11.1718	11.1693	11.1690	17.2066	28.2712	120.1755	235.3134
60	11.6071	11.6046	11.6040	17.4188	28.2151	119.7515	235.0759
90	12.2673	12.2649	12.2644	17.7572	28.1675	119.3585	234.8542
Fourth							
30	21.4530	21.4489	21.4470	24.8062	32.6470	128.1613	254.2857
60	20.1591	20.1545	20.1531	23.9274	32.3188	128.5290	254.4976
90	18.7351	18.7307	18.7301	22.8911	31.9158	128.8638	254.6948

Table 4.13: Effect of the pre-twist angle on the first four dimensionless for a thick beam ($\alpha = 50$, $\delta = 0.1$, $\vartheta = 0.25$, $\mu = 0.25$)

	γ				
β_L	0	5	10	50	100
First					
30	1.7602	4.2164	5.4559	8.1020	-
60	1.7725	4.1702	5.4470	8.1100	-
90	1.7923	4.1012	5.4310	8.1176	-
Second					
30	3.4638	5.7629	10.8807	52.1048	103.7987
60	3.3662	5.7742	10.8804	52.0949	103.7788
90	3.2309	5.7903	10.8812	52.0852	103.7592
Third					
30	11.0772	17.1052	28.1042	103.8946	144.2324
60	11.4932	17.2908	27.9778	103.8697	144.3031
90	12.1230	17.5875	27.8393	103.7907	144.3457
Fourth					
30	20.8449	24.1603	31.8425	121.0578	195.6655
60	19.6761	23.3991	31.6508	121.0222	195.6704
90	18.3590	22.4827	31.4063	120.9775	195.6772

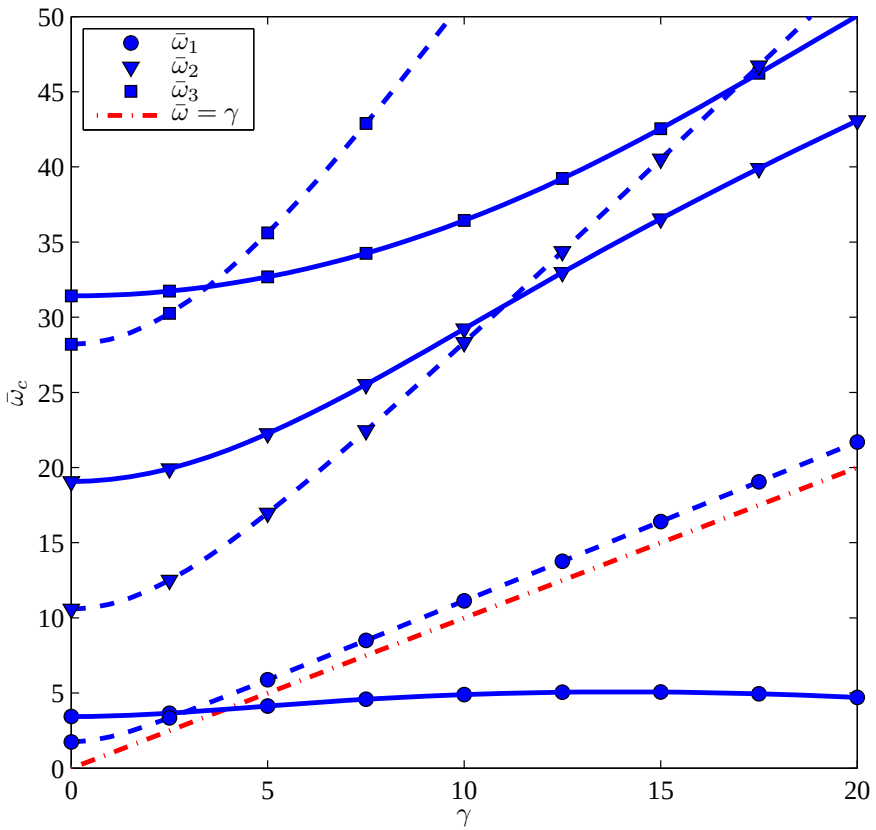

(a) $\beta_L = 0°$ (-chordwise, - -flapwise)

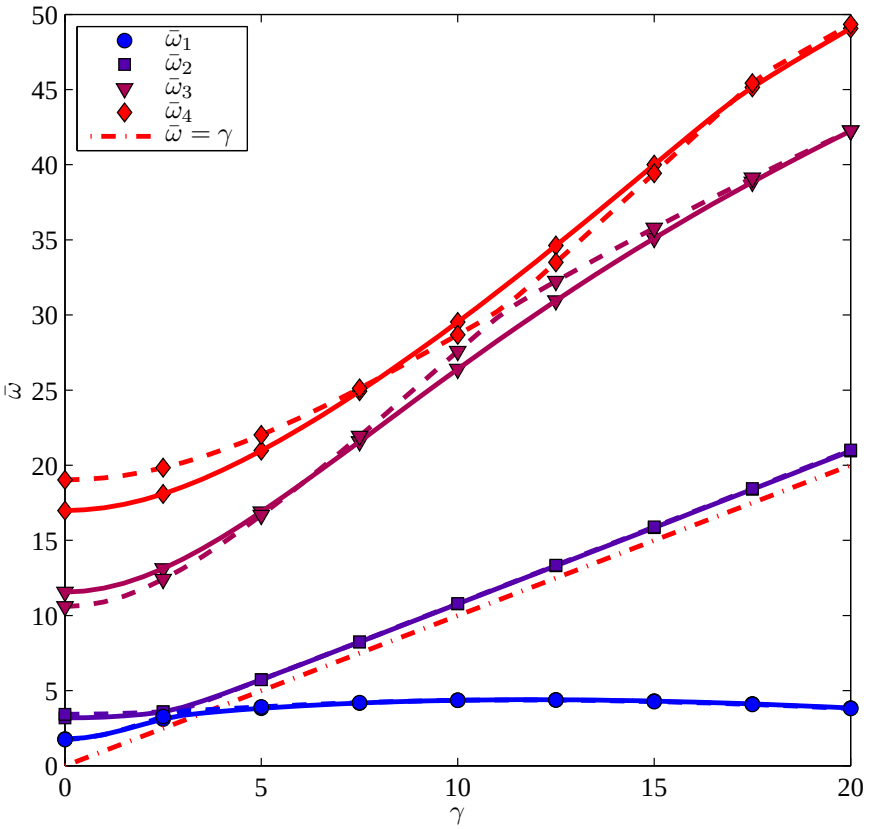

(b) - -$\beta_L = 10°$, -$\beta_L = 90°$

Figure 4.16: Effect of β_L on the first six dimensionless natural frequencies of a rotating pre-twisted Timoshenko beam ($\alpha = 20$, $\vartheta = 0.25$, $\delta = 0.1$, $\kappa = 5/6$

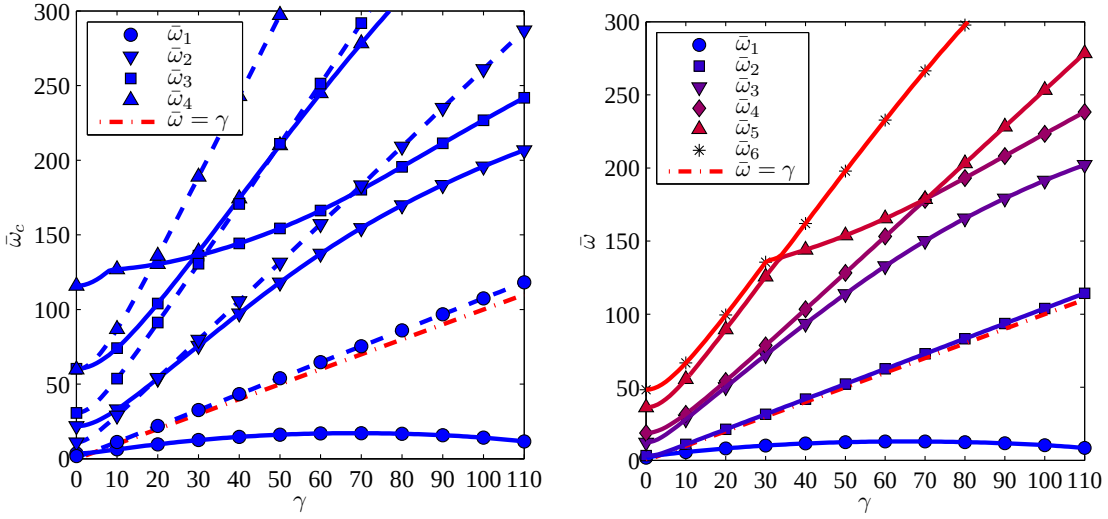

(a) $\delta = 0.1$, $\alpha = 80$, $\beta_L = 0°$

(b) $\delta = 0.1$, $\alpha = 80$, $\beta_L = 90°$

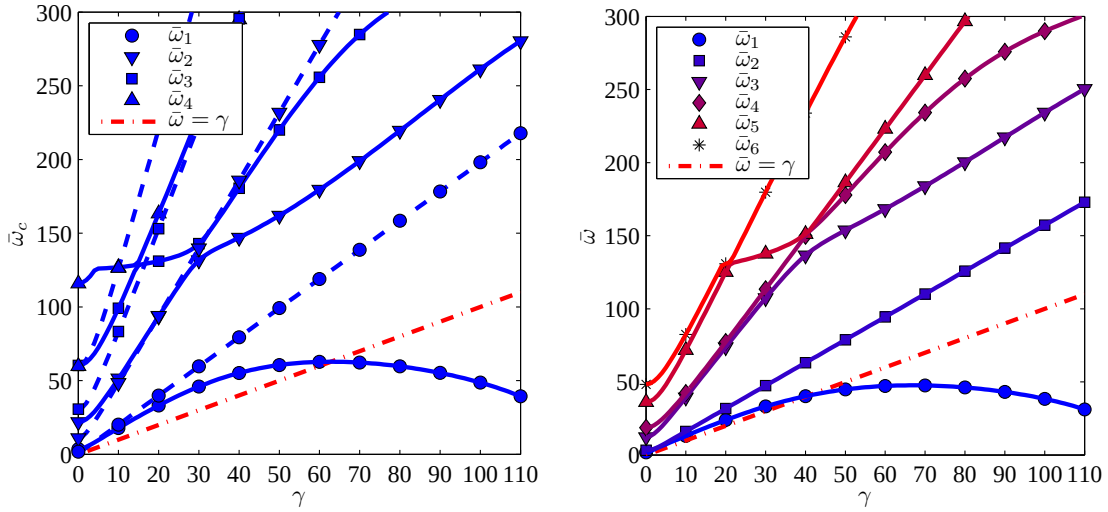

(c) $\delta = 2$, $\alpha = 80$, $\beta_L = 0°$

(d) $\delta = 2$, $\alpha = 80$, $\beta_L = 90°$

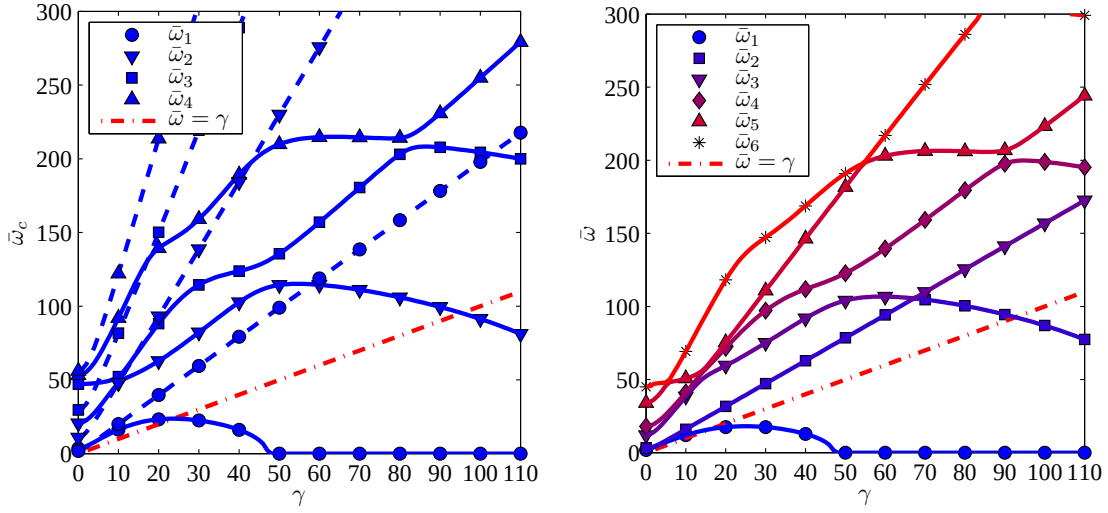

(e) $\delta = 2$, $\alpha = 30$, $\beta_L = 0°$

(f) $\delta = 2$, $\alpha = 30$, $\beta_L = 90°$

Figure 4.17: Comparison of the first six dimensionless frequencies between a pre-twisted and a simple (-chordwise, - -flapwise) Timoshenko beam ($\vartheta = 0.25$, $\kappa = 5/6$)

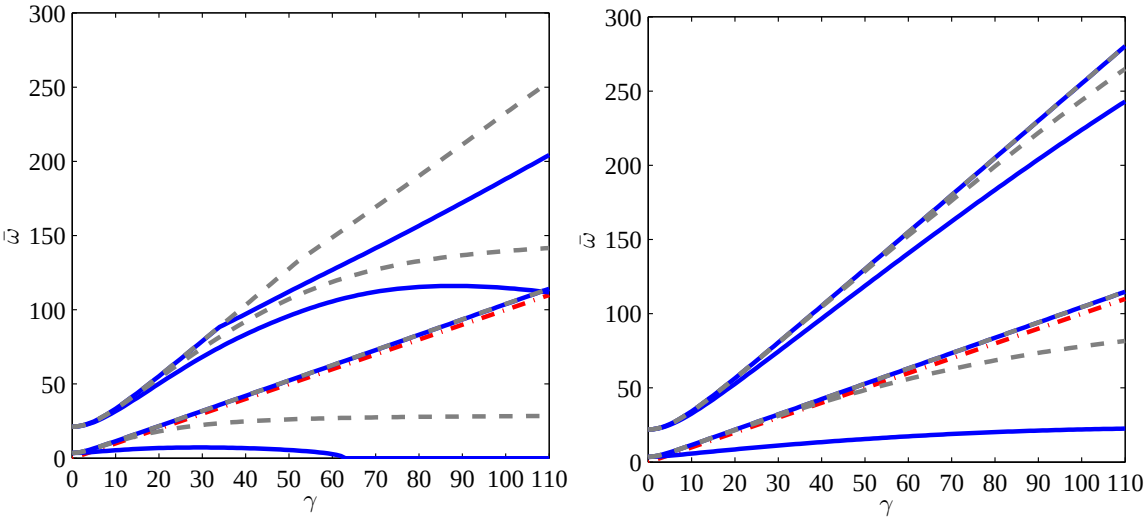

(a) $\alpha = 40$ (b) $\alpha = 150$

Figure 4.18: Effect of the centrifugal mass matrix $\mathbf{M}_s$ (-with, - -without) on the first four dimensionless natural frequencies ($\vartheta = 1$, $\beta_L = 0°$, $\delta = 0.1$, $\kappa = 5/6$)

Chapter 5

Pre-Twisted layerwise model

In the present chapter, a finite element model for a pre-twisted beam composed of several layers will be developed using a layerwise theory and Hamilton's principle. In figure 5.1a it's presented a generic cross section for a pre-twisted multi-layered beam and in figure 5.1b it's presented a detail of the axes for a generic layer. The displacements will be determined for each layer considering the axial displacement u of the first base layer and the rotations θ_j of the cross section of each layer about an horizontal axis that passes through the middle of length h_k. One can see that with these displacements the first moment of area (static moments) for any generic layer are no longer null since the rotations are about two axes that do not pass through the center of the cross-section of the layer, and likewise also the moments of inertia need to be determined for each layer taking into account these horizontal and vertical distances (D_h and D_v, respectively) using the parallel axis theorem otherwise known as *Steiner's theorem*. These area moments are derived with detail in appendix A.

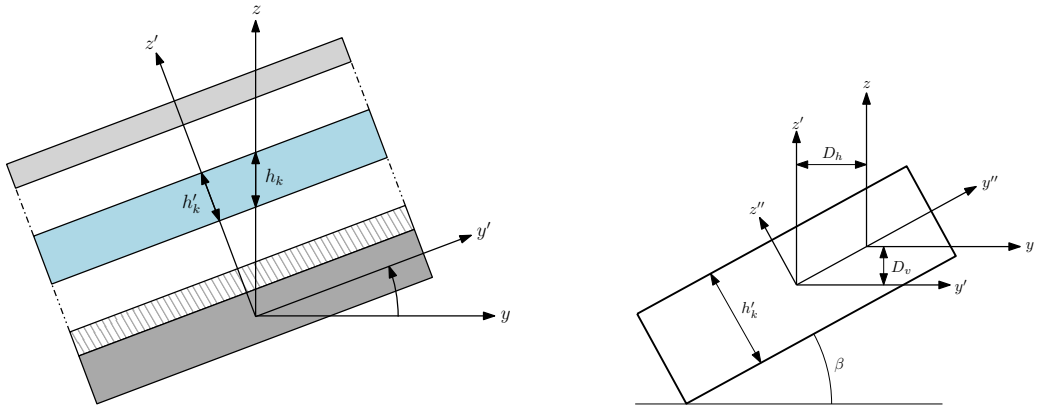

(a) Scheme of a layerwise pre-twisted beam (b) Axes detail for a generic layer

Figure 5.1: Generic cross section of a pre-twisted multilayer beam

In the following sections the process of derivation of the weak form for the pre-twisted layerwise beam will be presented using Hamilton's principle and under the following assumptions: flapwise and chordwise bending displacements w and v are assumed equal for all the layers as well as the rotation about the z axis.

5.1 Displacement and velocity fields

For a generic layer k of the beam the displacement field can be described by the following vector

$$\mathbf{u} = \begin{Bmatrix} u_x^k \\ u_y^k \\ u_z^k \end{Bmatrix} = \begin{Bmatrix} u + \frac{h_1}{2}\theta_1 + \sum_{j=2}^{k-1} h_j\theta_j + \frac{h_k}{2}\theta_k + z_k\theta_k - y\psi \\ v \\ w \end{Bmatrix} \tag{5.1.1}$$

and hence by using (2.2.6) the velocity field can be given by

$$\overrightarrow{\mathbf{v}}_P = \begin{Bmatrix} \dot{u}_x^k \\ \dot{u}_y^k \\ \dot{u}_z^k \end{Bmatrix} + \begin{Bmatrix} -\Omega u_y^k \\ \Omega(r + x + u_x^k) \\ 0 \end{Bmatrix} \tag{5.1.2}$$

5.2 Kinetic energy

Replacing 5.1.1 in 5.1.2 and also replacing the relation between u and s it follows that the velocity field vector can be given as

$$\mathbf{v}_P = \begin{Bmatrix} \dot{s} - (\dot{h}_v + \dot{h}_w) + \frac{h_1}{2}\dot{\theta}_1 + \sum_{j=2}^{k-1} h_j\dot{\theta}_j + \frac{h_k}{2}\dot{\theta}_k + z_k\dot{\theta}_k - y\dot{\psi} - \Omega v \\ \dot{v} + \Omega[(r + x) + s - (h_v + h_w) + \frac{h_1}{2}\theta_1 + \sum_{j=2}^{k-1} h_j\theta_j + \frac{h_k}{2}\theta_k + z_k\theta_k - y\psi] \\ \dot{w} \end{Bmatrix} \tag{5.2.1}$$

and the kinetic energy for a generic layer k becomes

$$\begin{aligned} T_k = \frac{1}{2}\int_V \rho_k \Bigg\{ & \left[\dot{s} + \frac{h_1}{2}\dot{\theta}_1 + \sum_{j=2}^{k-1} h_j\dot{\theta}_j + \frac{h_k}{2}\dot{\theta}_k - \Omega v + z_k\dot{\theta}_k - y\dot{\psi}\right]^2 \\ & + \left[\dot{v} + \Omega\left((r + x) + s + \frac{h_1}{2}\theta_1 + \sum_{j=2}^{k-1} h_j\theta_j + \frac{h_k}{2}\theta_k + z_k\theta_k - y\psi\right)\right]^2 \\ & - 2\Omega^2(r + x)(h_v + h_w) + \dot{w}^2 \Bigg\} dV \end{aligned} \tag{5.2.2}$$

As it was already said in the introduction of this chapter, for any generic layer not only the pre-twist angle but also the distances to the center of the beam's section need to be accounted for. As such, when integrating over the cross sectional area of the layer the kinetic energy is written as follows

$$\begin{aligned} T_k = \frac{1}{2}\int_0^L \rho_k \Bigg\{ & A_k\left[\dot{s} + \frac{h_1}{2}\dot{\theta}_1 + \sum_{j=2}^{k-1} h_j\dot{\theta}_j + \frac{h_k}{2}\dot{\theta}_k - \Omega v\right]^2 + I_y^k\dot{\theta}_k^2 - 2I_{yz}^k\dot{\theta}_k\dot{\psi} + I_z^k\dot{\psi}^2 \\ & + 2\left(\dot{s} + \frac{h_1}{2}\dot{\theta}_1 + \sum_{j=2}^{k-1} h_j\dot{\theta}_j + \frac{h_k}{2}\dot{\theta}_k - \Omega v\right)\left(S_y^k\dot{\theta}_k - S_z^k\dot{\psi}\right) \\ & + A_k\left[\dot{v} + \Omega\left(r + x + s + \frac{h_1}{2}\theta_1 + \sum_{j=2}^{k-1} h_j\theta_j + \frac{h_k}{2}\theta_k\right)\right]^2 \\ & + 2\Omega\left(S_y^k\theta_k - S_z^k\psi\right)\left[\dot{v} + \Omega\left((r + x) + s + \frac{h_1}{2}\theta_1 + \sum_{j=2}^{k-1} h_j\theta_j + \frac{h_k}{2}\theta_k\right)\right] \\ & + \Omega^2(I_y^k\theta_k^2 - 2I_{yz}^k\theta_k\psi + I_z^k\psi^2) - 2\Omega^2 A_k(r + x)(h_v + h_w) + A_k\dot{w}^2 \Bigg\} dx \end{aligned} \tag{5.2.3}$$

Applying the variational to the kinetic energy 5.2.3, integrating it by parts and taking into account that by definition the displacements are null at t_i and t_f, the following result arrives

$$
\begin{aligned}
&\int_{t_i}^{t_f} \delta T_k \, dt = \\
&= \int_0^L \int_{t_i}^{t_f} \rho_k \Bigg\{ A_k \left[\Omega^2 v - \Omega \left(\dot{s} + \frac{h_1}{2}\dot{\theta}_1 + \sum_{j=2}^{k-1} h_j \dot{\theta}_j + \frac{h_k}{2}\dot{\theta}_k \right) \right] \delta v \\
&\quad - A_k \left(\ddot{s} + \frac{h_1}{2}\ddot{\theta}_1 + \sum_{j=2}^{k-1} h_j \ddot{\theta}_j + \frac{h_k}{2}\ddot{\theta}_k - \Omega \dot{v} \right) \delta \left(s + \frac{h_1}{2}\theta_1 + \sum_{j=2}^{k-1} h_j \theta_j + \frac{h_k}{2}\theta_k \right) \\
&\quad - \left(\ddot{s} + \frac{h_1}{2}\ddot{\theta}_1 + \sum_{j=2}^{k-1} h_j \ddot{\theta}_j + \frac{h_k}{2}\ddot{\theta}_k - \Omega \dot{v} \right) \delta \left(S_y^k \theta_k - S_z^k \psi \right) \\
&\quad - \left(S_y^k \ddot{\theta}_k - S_z^k \ddot{\psi} \right) \delta \left(s + \frac{h_1}{2}\theta_1 + \sum_{j=2}^{k-1} h_j \theta_j + \frac{h_k}{2}\theta_k \right) \\
&\quad - \Omega (S_y^k \dot{\theta}_k - S_z^k \dot{\psi}) \delta v - \rho_k (I_y^k \ddot{\theta}_k \delta\theta_k - I_{yz}^k \ddot{\psi} \delta\theta_k - I_{yz}^k \ddot{\theta}_k \delta\psi + I_z^k \ddot{\psi} \delta\psi) \\
&\quad - A_k \left[\ddot{v} + \Omega \left(\dot{s} + \frac{h_1}{2}\dot{\theta}_1 + \sum_{j=2}^{k-1} h_j \dot{\theta}_j + \frac{h_k}{2}\dot{\theta}_k \right) \right] \delta v \\
&\quad + A_k \left[\Omega \dot{v} + \Omega^2 \left((r+x) + s + \frac{h_1}{2}\theta_1 + \sum_{j=2}^{k-1} h_j \theta_j + \frac{h_k}{2}\theta_k \right) \right] \\
&\qquad\qquad \delta \left(s + \frac{h_1}{2}\theta_1 + \sum_{j=2}^{k-1} h_j \theta_j + \frac{h_k}{2}\theta_k \right) \\
&\quad + \left[\Omega \dot{v} + \Omega^2 \left((r+x) + s + \frac{h_1}{2}\theta_1 + \sum_{j=2}^{k-1} h_j \theta_j + \frac{h_k}{2}\theta_k \right) \right] \delta \left(S_y^k \theta_k - S_z^k \psi \right) \\
&\quad + \Omega^2 \left(S_y^k \theta_k - S_z^k \psi \right) \delta \left(s + \frac{h_1}{2}\theta_1 + \sum_{j=2}^{k-1} h_j \theta_j + \frac{h_k}{2}\theta_k \right) \\
&\quad - \Omega \left(S_y^k \dot{\theta}_k - S_z^k \dot{\psi} \right) \delta v + \Omega^2 \rho (I_y^k \theta_k \delta\theta_k - I_{yz}^k \psi \delta\theta_k - I_{yz}^k \theta_k \delta\psi + I_z^k \psi \delta\psi) \\
&\quad - \Omega^2 A_k \left(r(L-x) + \frac{1}{2}(L^2 - x^2) \right) v' \delta v' \\
&\quad - \Omega^2 A_k \left(r(L-x) + \frac{1}{2}(L^2 - x^2) \right) w' \delta w' - A_k \ddot{w} \delta w \Bigg\} \, dx
\end{aligned}
\tag{5.2.4}
$$

By introducing the following displacement vector

$$
\Delta = \begin{Bmatrix} s & v & w & \psi & \theta_1 & \cdots & \theta_j & \cdots & \theta_k & \theta_{k+1} & \cdots & \theta_n \end{Bmatrix}^T \tag{5.2.5}
$$

the variation of the kinetic energy can be written in a compact matricial form as

$$
\int_{t_i}^{t_f} \delta T \, dt = \int_{t_i}^{t_f} \int_0^L -\delta\Delta^T \{ \mathbf{J}\ddot{\Delta} + 2\Omega \mathbf{J_g} \dot{\Delta} - \Omega^2 \mathbf{J_s} \Delta \} - \Omega^2 \{ (\mathcal{L}_s \delta\Delta)^T \mathbf{D_s} \mathcal{L}_s \Delta + \Omega^2 \delta\Delta^T \mathbf{f_s} \} \, dx \, dt \tag{5.2.6}
$$

and the matrices and vector present in the previous equation are defined as

$$\mathbf{J}^k = \rho_k \begin{bmatrix} A_k & 0 & 0 & -S_z^k & A_k\frac{h_1}{2} & \cdots & A_k h_j & \cdots & S_y + A_k\frac{h_k}{2} & 0 & \cdots & 0 \\ & A_k & 0 & 0 & 0 & \cdots & 0 & \cdots & 0 & 0 & \cdots & 0 \\ & & A_k & 0 & 0 & \cdots & 0 & \cdots & 0 & 0 & \cdots & 0 \\ & & & I_z^k & -S_z\frac{h_1}{2} & \cdots & -S_z^k h_j & \cdots & -I_{yz}^k - S_z^k\frac{h_k}{2} & 0 & \cdots & 0 \\ & & & & A_k\frac{h_1^2}{4} & \cdots & A_k\frac{h_1 h_j}{2} & \cdots & S_y^k\frac{h_1}{2} + A_k\frac{h_1 h_k}{4} & 0 & \cdots & 0 \\ & & & & & \ddots & \vdots & \ddots & \vdots & \vdots & \ddots & \vdots \\ & & & & & & A_k h_j^2 & \cdots & S_y^k h_j + A_k\frac{h_j h_k}{2} & 0 & \cdots & 0 \\ & & & & & & & \ddots & \vdots & \vdots & \ddots & \vdots \\ & & & & & & & & I_y^k + S_y^k h_k + A_k\frac{h_k^2}{4} & 0 & \cdots & 0 \\ & & & & & & & & & 0 & \cdots & 0 \\ & & & & & & & & & & \ddots & \vdots \\ \text{sym.} & & & & & & & & & & & 0 \end{bmatrix} \tag{5.2.7}$$

$$\mathbf{J}_g^k = \rho_k \begin{bmatrix} 0 & -A_k & 0 & 0 & 0 & \cdots & 0 & \cdots & 0 & 0 & \cdots & 0 \\ & 0 & 0 & -S_z^k & A_k\frac{h_1}{2} & \dots & A_k h_j & \dots & S_y^k + A_k\frac{h_k}{2} & 0 & \cdots & 0 \\ & & 0 & 0 & 0 & \cdots & 0 & \cdots & 0 & 0 & \cdots & 0 \\ & & & 0 & 0 & \cdots & 0 & \cdots & 0 & 0 & \cdots & 0 \\ & & & & 0 & \cdots & 0 & \cdots & 0 & 0 & \cdots & 0 \\ & & & & & \ddots & \vdots & \ddots & \vdots & \vdots & \ddots & \vdots \\ & & & & & & 0 & \cdots & 0 & 0 & \cdots & 0 \\ & & & & & & & \ddots & \vdots & \vdots & \ddots & \vdots \\ & & & & & & & & 0 & 0 & \cdots & 0 \\ & & & & & & & & & 0 & \cdots & 0 \\ & & & & & & & & & & \ddots & \vdots \\ \text{skew-sym.} & & & & & & & & & & & 0 \end{bmatrix} \tag{5.2.8}$$

$$\mathbf{J}_s^k = \rho_k \begin{bmatrix} A_k & 0 & 0 & -S_z^k & A_k\frac{h_1}{2} & \cdots & A_k h_j & \cdots & S_y^k + A_k\frac{h_k}{2} & 0 & \cdots & 0 \\ & A_k & 0 & 0 & 0 & \cdots & 0 & \cdots & 0 & 0 & \cdots & 0 \\ & & 0 & 0 & 0 & \cdots & 0 & \cdots & 0 & 0 & \cdots & 0 \\ & & & I_z^k & -S_z^k\frac{h_1}{2} & \cdots & -S_z^k h_j & \cdots & -I_{yz}^k - S_z^k\frac{h_k}{2} & 0 & \cdots & 0 \\ & & & & A_k\frac{h_1^2}{4} & \cdots & A_k\frac{h_1 h_j}{2} & \cdots & S_y^k\frac{h_1}{2} + A_k\frac{h_1 h_k}{4} & 0 & \cdots & 0 \\ & & & & & \ddots & \vdots & \ddots & \vdots & \vdots & \ddots & \vdots \\ & & & & & & A_k h_j^2 & \cdots & S_y^k h_j + A_k\frac{h_j h_k}{2} & 0 & \cdots & 0 \\ & & & & & & & \ddots & \vdots & \vdots & \ddots & \vdots \\ & & & & & & & & I_y^k + S_y^k h_k + A_k\frac{h_k^2}{4} & 0 & \cdots & 0 \\ & & & & & & & & & 0 & \cdots & 0 \\ & & & & & & & & & & \ddots & \vdots \\ \text{sym.} & & & & & & & & & & & 0 \end{bmatrix} \tag{5.2.9}$$

$$\mathbf{D}_s^k = \rho_k A_k \left(r(L-x) + \frac{1}{2}(L^2 - x^2) \right) \begin{bmatrix} 0 & 0 & 0 & 0 & 0 & \cdots & 0 & \cdots & 0 & 0 & \cdots & 0 \\ & 1 & 0 & 0 & 0 & \cdots & 0 & \cdots & 0 & 0 & \cdots & 0 \\ & & 1 & 0 & 0 & \cdots & 0 & \cdots & 0 & 0 & \cdots & 0 \\ & & & 0 & 0 & \cdots & 0 & \cdots & 0 & 0 & \cdots & 0 \\ & & & & 0 & \cdots & 0 & \cdots & 0 & 0 & \cdots & 0 \\ & & & & & \ddots & \vdots & \ddots & \vdots & \vdots & \ddots & \vdots \\ & & & & & & 0 & \cdots & 0 & 0 & \cdots & 0 \\ & & & & & & & \ddots & \vdots & \vdots & \ddots & \vdots \\ & & & & & & & & 0 & 0 & \cdots & 0 \\ & & & & & & & & & 0 & \cdots & 0 \\ & & & & & & & & & & \ddots & \vdots \\ \text{sym.} & & & & & & & & & & & 0 \end{bmatrix} \tag{5.2.10}$$

$$\mathcal{L}_s = \operatorname{diag} \begin{bmatrix} 1 & \dfrac{\partial}{\partial x} & \dfrac{\partial}{\partial x} & 1 & 1 & \cdots & 1 & \cdots & 1 & 1 & \cdots & 1 \end{bmatrix} \tag{5.2.11}$$

$$\mathbf{f}_s^k = (r+x)\rho_k A_k \begin{bmatrix} 1 & 0 & 0 & -S_z & \dfrac{h_1}{2} & \cdots & h_j & \cdots & \dfrac{h_k}{2} + S_y & 0 & \cdots & 0 \end{bmatrix}^T \tag{5.2.12}$$

5.3 Potential energy

From the displacement field for a generic layer k and taking into account the stretch strain defined in equation (2.3.14), the strain field can be expressed for a generic layer k as

$$\varepsilon_{xx}^k = s' + \frac{h_1}{2}\theta_1' + \sum_{j=2}^{k-1} h_j \theta_j' + \frac{h_k}{2}\theta_k' + z_k \theta_k' - y\psi' \tag{5.3.1a}$$

$$\gamma_{xy}^k = v' - \psi \tag{5.3.1b}$$

$$\gamma_{zx}^k = w' + \theta \tag{5.3.1c}$$

and using the elasticity relations for an isotropic material the stress field can be defined as

$$\sigma_{xx}^k = E_k \varepsilon_{xx}^k \tag{5.3.2a}$$

$$\tau_{xy}^k = G_k \gamma_{xy}^k \tag{5.3.2b}$$

$$\tau_{zx}^k = G_k \gamma_{zx}^k \tag{5.3.2c}$$

Having the strain and stress fields defined the potential energy for a generic layer k can be written as

$$\begin{aligned} \Pi_k = \frac{1}{2} \int_V \Bigg\{ & E_k \left(s' + \frac{h_1}{2}\theta_1' + \sum_{j=2}^{k-1} h_j \theta_j' + \frac{h_k}{2}\theta_k' + z_k \theta_k' - y\psi' \right)^2 \\ & + G_k [(v' - \psi)^2 + (w' + \theta)^2] \Bigg\} dV \end{aligned} \tag{5.3.3}$$

which after integrating over the cross section of the layer and considering the distances to the centroid of the cross section becomes

$$\begin{aligned}\Pi_k = \frac{1}{2}\int_0^L \Bigg\{ & E_k A_k \Bigg(s' + \frac{h_1}{2}\theta_1' + \sum_{j=2}^{k-1} h_j \theta_j' + \frac{h_k}{2}\theta_k' \Bigg)^2 \\ & + 2E_k \Bigg(s' + \frac{h_1}{2}\theta_1' + \sum_{j=2}^{k-1} h_j \theta_j' + \frac{h_k}{2}\theta_k' \Bigg) \Big(S_y^k \theta_k' - S_z^k \psi' \Big) \\ & + E_k \Big(I_y^k {\theta_k'}^2 - 2 I_{yz}^k \theta_k' \psi' + I_z^k {\psi'}^2 \Big) \\ & + G_k A_k^* [(v' - \psi)^2 + (w' + \theta)^2] \Bigg\} dx \end{aligned} \tag{5.3.4}$$

Applying the variational to the potential energy leads to the following result

$$\begin{aligned}\int_{t_i}^{t_f} \delta\Pi_k \, dt = \int_{t_i}^{t_f} \int_0^L \Bigg\{ & E_k A_k \Bigg(s' + \frac{h_1}{2}\theta_1' + \sum_{j=2}^{k-1} h_j \theta_j' + \frac{h_k}{2}\theta_k' \Bigg) \\ & \qquad \delta \Bigg(s' + \frac{h_1}{2}\theta_1' + \sum_{j=2}^{k-1} h_j \theta_j' + \frac{h_k}{2}\theta_k' \Bigg) \\ & + E_k \Bigg(s' + \frac{h_1}{2}\theta_1' + \sum_{j=2}^{k-1} h_j \theta_j' + \frac{h_k}{2}\theta_k' \Bigg) \delta \Big(S_y^k \theta_k' - S_z^k \psi' \Big) \\ & + E_k \Big(S_y^k \theta_k' - S_z^k \psi' \Big) \delta \Bigg(s' + \frac{h_1}{2}\theta_1' + \sum_{j=2}^{k-1} h_j \theta_j' + \frac{h_k}{2}\theta_k' \Bigg) \\ & + E_k (I_y^k \theta_k' \delta\theta_k' - I_{yz}^k \psi' \delta\theta_k' - I_{yz}^k \theta_k' \delta\psi' + I_z^k \psi' \delta\psi') \\ & + G_k A_k^* [(v' - \psi)\delta v' - (v' - \psi)\delta\psi] \\ & + G_k A_k^* [(w' + \theta_k)\delta w' + (w' + \theta_k)\delta\theta_k] \Bigg\} dx \, dt \end{aligned} \tag{5.3.5}$$

After introducing the displacement vector Δ defined in section 5.2 the previous equation can be written in the following compact matricial form

$$\int_{t_i}^{t_f} \delta\Pi_k \, dt = \int_{t_i}^{t_f} \int_0^L (\mathcal{L}_\varepsilon \delta\Delta)^T \mathbf{D}_\varepsilon \mathcal{L}_\varepsilon \Delta + (\mathcal{L}_\gamma \delta\Delta)^T \mathbf{D}_\gamma \mathcal{L}_\gamma \Delta \, dx \, dt \tag{5.3.6}$$

with the matrices defined as

$$\mathbf{D}_{\varepsilon}^{k} = E_k \begin{bmatrix} A_k & 0 & 0 & -S_z^k & A_k\frac{h_1}{2} & \cdots & A_k h_j & \cdots & S_y^k + A_k\frac{h_k}{2} & 0 & \cdots & 0 \\ & 0 & 0 & 0 & 0 & \cdots & 0 & \cdots & 0 & 0 & \cdots & 0 \\ & & 0 & 0 & 0 & \cdots & 0 & \cdots & 0 & 0 & \cdots & 0 \\ & & & I_z^k & -S_z^k\frac{h_1}{2} & \cdots & -S_z^k h_j & \cdots & -I_{yz}^k - S_z^k\frac{h_k}{2} & 0 & \cdots & 0 \\ & & & & A_k\frac{h_1^2}{4} & \cdots & A_k\frac{h_1 h_j}{2} & \cdots & S_y\frac{h_1}{2} + A_k\frac{h_1 h_k}{4} & 0 & \cdots & 0 \\ & & & & & \ddots & \vdots & \ddots & \vdots & \vdots & \ddots & \vdots \\ & & & & & & A_k h_j^2 & \cdots & S_y^k h_j + A_k\frac{h_j h_k}{2} & 0 & \cdots & 0 \\ & & & & & & & \ddots & \vdots & \vdots & \ddots & \vdots \\ & & & & & & & & I_y^k + S_y^k h_k + A_k\frac{h_k^2}{4} & 0 & \cdots & 0 \\ & & & & & & & & & 0 & \cdots & 0 \\ & & & & & & & & & & \ddots & \vdots \\ \text{sym.} & & & & & & & & & & & 0 \end{bmatrix} \tag{5.3.7}$$

$$\mathcal{L}_{\varepsilon} = \operatorname{diag}\begin{bmatrix} \frac{\partial}{\partial x} & 1 & 1 & \frac{\partial}{\partial x} & \frac{\partial}{\partial x} & \cdots & \frac{\partial}{\partial x} & \cdots & \frac{\partial}{\partial x} & 1 & \cdots & 1 \end{bmatrix} \tag{5.3.8}$$

$$\mathbf{D}_{\gamma}^{k} = G_k A_k^* \begin{bmatrix} 0 & 0 & 0 & 0 & 0 & \cdots & 0 & \cdots & 0 & 0 & \cdots & 0 \\ & 1 & 0 & -1 & 0 & \cdots & 0 & \cdots & 0 & 0 & \cdots & 0 \\ & & 1 & 0 & 0 & \cdots & 0 & \cdots & 1 & 0 & \cdots & 0 \\ & & & 1 & 0 & \cdots & 0 & \cdots & 0 & 0 & \cdots & 0 \\ & & & & 0 & \cdots & 0 & \cdots & 0 & 0 & \cdots & 0 \\ & & & & & \ddots & \vdots & \ddots & \vdots & \vdots & \ddots & \vdots \\ & & & & & & 0 & \cdots & 0 & 0 & \cdots & 0 \\ & & & & & & & \ddots & \vdots & \vdots & \ddots & \vdots \\ & & & & & & & & 1 & 0 & \cdots & 0 \\ & & & & & & & & & 0 & \cdots & 0 \\ & & & & & & & & & & \ddots & \vdots \\ \text{sym.} & & & & & & & & & & & 0 \end{bmatrix} \tag{5.3.9}$$

$$\mathcal{L}_{\gamma} = \operatorname{diag}\begin{bmatrix} 1 & \frac{\partial}{\partial x} & \frac{\partial}{\partial x} & 1 & 1 & \cdots & 1 & \cdots & 1 & 1 & \cdots & 1 \end{bmatrix} \tag{5.3.10}$$

5.4 Layerwise Weak Form

Note that up until now we have been dealing with only one generic layer of the multilayer beam. To consider all of the layers in the kinetic and potential energies of the beam, one needs only to sum the kinetic and potential energies of each layer and so it follows that

$$\Pi = \sum_{k=1}^{n} \Pi_k \text{ and } T = \sum_{k=1}^{n} T_k \tag{5.4.1}$$

which after applying the variational and knowing that the variational and sum are interchangeable becomes

$$\delta\Pi = \sum_{k=1}^{n} \delta\Pi_k \text{ and } \delta T = \sum_{k=1}^{n} \delta T_k \tag{5.4.2}$$

By introducing equations (5.2.6) and (5.3.6) into equations (5.4.2) an then introducing these in Hamilton's principle one gets

$$\sum_{k=1}^{n}\int_0^L \delta\Delta^T\mathbf{J}^k\ddot{\Delta} + 2\Omega\delta\Delta^T\mathbf{J}_g^k\dot{\Delta} + \Omega^2(\mathcal{L}_s\delta\Delta)^T\mathbf{D}_s^k\mathcal{L}_s\Delta - \Omega^2\delta\Delta^T\mathbf{J}_s^k\Delta + (\mathcal{L}_\varepsilon\delta\Delta)^T\mathbf{D}_\varepsilon^k(\mathcal{L}_\varepsilon\Delta) + (\mathcal{L}_\gamma\delta\Delta)^T\mathbf{D}_\gamma^k(\mathcal{L}_\gamma\Delta)\,dx = \sum_{k=1}^{n}\int_0^L \Omega^2\delta\Delta^T\mathbf{f}_s^k\,dx \tag{5.4.3}$$

The displacement vector Δ can now be interpolated from the element displacement vector, that can be written as

$$\mathbf{d}_e = \{\{\mathbf{d}\}_\mathbf{1}\{\mathbf{d}\}_\mathbf{2}\}^\mathbf{T} \tag{5.4.4}$$

and by using the shape functions matrix defined as

$$\mathbf{N} = \begin{bmatrix} \ddots & & \ddots & \\ & N_1 & & N_2 \\ & \ddots & & \ddots \end{bmatrix} \tag{5.4.5}$$

$\mathbf{d}_1$ and $\mathbf{d}_2$ represent the node displacements of the element at the first and second nodes respectively and are defined as

$$\mathbf{d}_i = \begin{Bmatrix} s & v & w & \psi & \theta_1 & \cdots & \theta_j & \cdots & \theta_k & \theta_{k+1} & \cdots & \theta_n \end{Bmatrix}_i \tag{5.4.6}$$

The displacement vector Δ can then be approximated through the element displacements using the shape functions matrix as

$$\Delta = \mathbf{N}\mathbf{d}_e \tag{5.4.7}$$

By introducing the previous equation into equation (5.4.3) the same can be written in a discretized form as follows

$$\sum_{e=1}^{N}\delta\mathbf{d}_e^T\{\mathbf{m}_e\ddot{\mathbf{d}}_e + 2\Omega\mathbf{g}_e\dot{\mathbf{d}}_e + [\Omega^2(\mathbf{ks}_e - \mathbf{ms}_e) + \mathbf{k}_e]\mathbf{d}_e\}\,dx = \sum_{e=1}^{N}\Omega^2\Delta^T\mathbf{f}_s \tag{5.4.8}$$

with the previous element matrices defined as

$$\mathbf{m}_e = \sum_{k=1}^{n}\int_{-1}^{+1}\mathbf{N}^T\mathbf{J}^k\mathbf{N}det(\mathbf{J})\,d\xi = \sum_{k=1}^{n}\sum_{i=1}^{m}w_i\{\mathbf{N}^T\mathbf{J}^k\mathbf{N}\}det(\mathbf{J}) \tag{5.4.9a}$$

$$\mathbf{g}_e = \sum_{k=1}^{n}\int_{-1}^{+1}\mathbf{N}^T\mathbf{J}_g^k\mathbf{N}det(\mathbf{J})\,d\xi = \sum_{k=1}^{n}\sum_{i=1}^{m}w_i\{\mathbf{N}^T\mathbf{J}_g^k\mathbf{N}\}det(\mathbf{J}) \tag{5.4.9b}$$

$$\mathbf{ms}_e = \sum_{k=1}^{n}\int_{-1}^{+1}\mathbf{N}^T\mathbf{J}_s^k\mathbf{N}det(\mathbf{J})\,d\xi = \sum_{k=1}^{n}\sum_{i=1}^{m}w_i\{\mathbf{N}^T\mathbf{J}_s^k\mathbf{N}\}det(\mathbf{J}) \tag{5.4.9c}$$

$$\mathbf{ks}_e = \sum_{k=1}^{n}\int_{-1}^{+1}\mathbf{B}_s^T\mathbf{D}_s^k\mathbf{B}_s det(\mathbf{J})\,d\xi = \sum_{k=1}^{n}\sum_{i=1}^{m}w_i\{\mathbf{B}_s^T\mathbf{D}_s^k\mathbf{B}_s\}det(\mathbf{J}) \tag{5.4.9d}$$

$$\mathbf{k}_e = \sum_{k=1}^{n}\int_{-1}^{+1}(\mathbf{B}_\varepsilon^T\mathbf{D}_\varepsilon^k\mathbf{B}_\varepsilon + \mathbf{B}_\gamma^T\mathbf{D}_\gamma^k\mathbf{B}_\gamma)det(\mathbf{J})\,d\xi = \sum_{k=1}^{n}\sum_{i=1}^{m}w_i\{\mathbf{B}_\varepsilon^T\mathbf{D}_\varepsilon^k\mathbf{B}_\varepsilon + \mathbf{B}_\gamma^T\mathbf{D}_\gamma^k\mathbf{B}_\gamma\}det(\mathbf{J}) \tag{5.4.9e}$$

where m represents the number of Gauss points used. The previous deformation matrices are defined as

$$\mathbf{B}_s = \mathcal{L}_s\mathbf{N}; \quad \mathbf{B}_\varepsilon = \mathcal{L}_\varepsilon\mathbf{N}; \quad \mathbf{B}_\gamma = \mathcal{L}_\gamma\mathbf{N} \tag{5.4.10}$$

By assembling the multilayer element matrices and vectors and since $\delta\mathbf{d}_e$ are arbitrary, the global system of equations is written as

$$\mathbf{M}\ddot{\mathbf{d}} + \mathbf{G}\dot{\mathbf{d}} + [\mathbf{K} + \Omega^2(\mathbf{Ks} - \mathbf{Ms})]\mathbf{d} = \mathbf{f} \tag{5.4.11}$$

5.5 Numerical results

The results are obtained here using the same dimensionless quantities as used in chapter 4. From the dimensionless quantities α and ϑ both height and width of the cross section of the beam can be obtained and from the number of layers the height of each layer can be determined, assuming that all of the layers have the same height.

In table 5.1 it is shown the results obtained for the first four natural frequencies of a rotating beam and they are compared with the results obtained for a simple beam. The results obtained for a simple beam are presented between parenthesis. It can be seen that the layerwise model developed provides accurate results, close to those obtained for a simple beam. Also it can be seen that as the number of layers increase the natural frequencies converge.

On the other hand results obtained for the pre-twisted multilayer beam could not be validated. The effect of the distances D_v and D_h creates a stiffening of beam leading to natural frequencies higher than what it would be expected, specially when the number of layers increase. As it can be observed from table 5.2, including the effects of the distances, the natural frequencies obtained are quite different from those determined from the simple beam. Although, under the assumption of small pre-twist angles, the distances D_v and D_h can become quite small and as such negligible. So, by neglecting the effect of the distances it can be seen from table 5.2 that results obtained are closer to those obtained from a simple pre-twisted beam. In figure 5.2 a comparison of the first five dimensionless natural frequencies is made between a simple beam and a multilayered model with five layers. It can be seen that the development of the frequencies with the rotating speed is similar in both cases although some differences are noted specially for higher rotating speeds like the increase in the second natural frequency and the decrease in the fifth that occurs from the simple beam to the multilayer beam.

Other effects from other parameters such as the hub radius ratio δ and the slenderness ratio α were found out to have similar effects as those seen in chapter 4 as it would be expected.

Table 5.1: Comparison of the first four dimensionless natural frequencies for a multi-layered rotating beam without pre-twist ($\delta = 0$, $\beta_L = 0°$, $\alpha = 50$, $\vartheta = 1$)

No. of layers	γ			
	0	10	50	100
First	(3.5025)	(4.7921)	(4.1651)	(-)
2	3.5025	4.7921	4.1651	-
3	3.5015	4.7921	4.1651	-
5	3.5008	4.7921	4.1651	-
10	3.5005	4.7921	4.1651	-
Second	(3.5025)	(11.1477)	(50.6067)	(100.2752)
2	3.5025	11.1477	50.6067	100.2752
3	3.5025	11.1446	50.5947	100.2662
5	3.5025	11.1425	50.5864	100.2600
10	3.5025	11.1415	50.5817	100.2564
Third	(21.4654)	(31.3589)	(101.0709)	(140.8544)
2	21.4654	31.3589	101.0709	140.8544
3	21.4256	31.3589	101.0709	140.8544
5	21.4002	31.3589	101.0709	140.8544
10	21.3883	31.3589	101.0709	140.8544
Fourth	(21.4654)	(33.0329)	(119.7703)	(193.2080)
2	21.4654	33.0329	119.7703	193.2080
3	21.4654	33.0021	119.7703	193.2080
5	21.4654	32.9822	119.7703	193.2080
10	21.4654	32.9726	119.7703	193.2080

Table 5.2: Comparison of the first three natural frequencies for a rotating beam with pre-twist and effects of the distances D_h and D_v ($\delta = 0.2$, $\alpha = 50$, $\vartheta = 0.5$, $\beta_L = 30°$)

γ	0		10	
No. of layers	Including	Neglecting	Including	Neglecting
First mode	(2.4826)		(5.9341)	
2	2.1501	2.4791	7.0022	6.9813
3	2.6091	2.4758	7.0131	6.9811
5	3.2446	2.4738	7.0202	6.9809
10	3.4788	2.4728	6.3777	6.9809
Second mode	(3.4835)		(11.4314)	
2	3.7307	3.4787	12.0769	12.0633
3	4.0231	3.4779	12.1186	12.0600
5	4.6250	3.4775	12.3219	12.0579
10	5.1046	3.4773	13.3535	12.0568
Third mode	(15.3440)		(30.6097)	
2	27.9339	15.2526	40.0725	31.6123
3	33.5035	15.1685	41.6646	31.5259
5	36.8146	15.1180	42.1186	31.4787
10	37.7870	15.0952	40.4713	31.4579

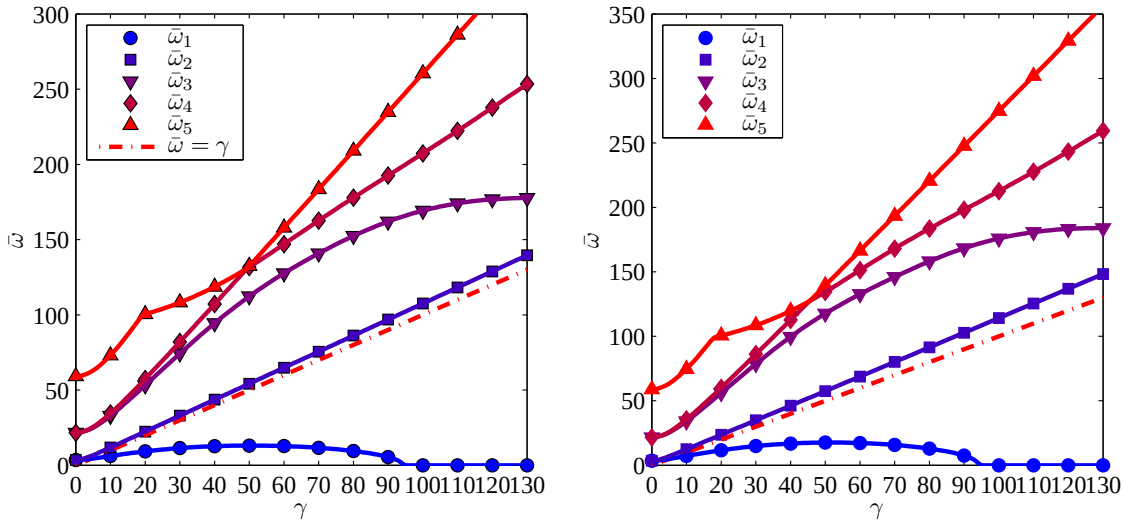

(a) ($\vartheta = 1$, $\beta_L = 0°$)

(b) five layers($\vartheta = 1$, $\beta_L = 0°$)

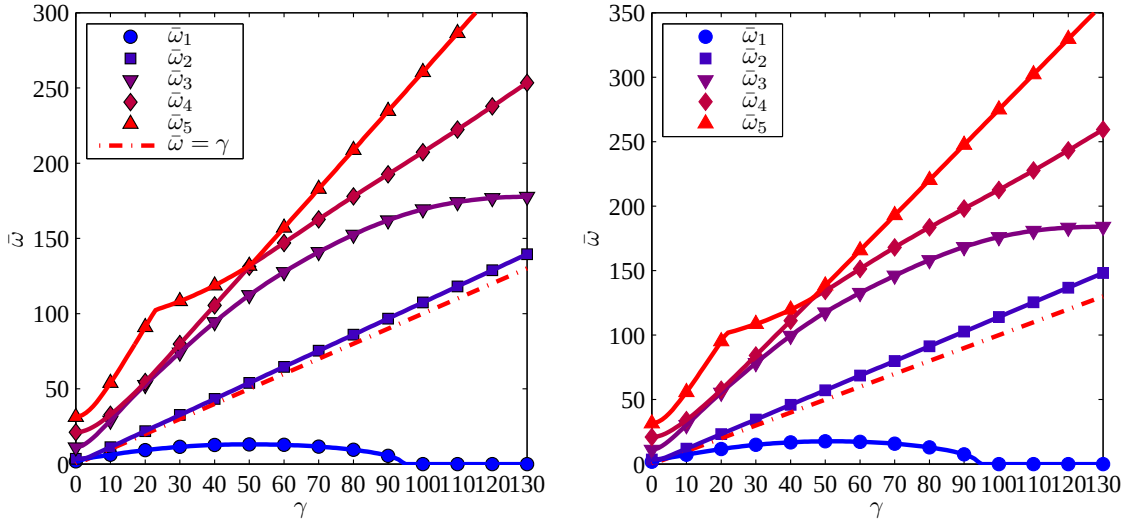

(c) ($\vartheta = 0.25$, $\beta_L = 30°$)

(d) five layers($\vartheta = 0.25$, $\beta_L = 30°$)

Figure 5.2: Comparison of the first five dimensionless natural frequencies for the simple and multilayer beam ($\alpha = 60$, $\delta = 0.2$, $\vartheta = 1$)

Chapter 6

Viscoelastic damping

To determine the effect that a viscoelastic damping treatment has over a rotating cantilever beam the frequency response function (FRF) will be used which will be obtained by the direct frequency analysis procedure.

For a rotating multi-layered cantilever beam the global system of equations of motion system was already defined as

$$\mathbf{M}\ddot{\mathbf{d}} + 2\Omega\mathbf{G}\dot{\mathbf{d}} + \{\mathbf{K} + \Omega^2[\mathbf{K}_s - \mathbf{M}_s]\}\mathbf{d} = \mathbf{f} \tag{6.0.1}$$

In deriving equation (6.0.1) it was assumed in the finite element model that all of the layers have an elastic behaviour, but should it occur that one or more of the layers of the beam possesses viscoelastic behaviour, and the stiffness matrix needs to be divided into two different stiffness matrices, one regarding the elastic layers ($\mathbf{K}^e$), and another one ($\mathbf{K}^v(j\omega)$) regarding the viscoelastic ones.

Rewriting the global system of equations including the effect of viscoelastic layers one gets

$$\mathbf{M}\ddot{\mathbf{d}} + 2\Omega\mathbf{G}\dot{\mathbf{d}} + \{[\mathbf{K}^e + \mathbf{K}^v(j\omega)] + \Omega^2[\mathbf{K}_s - \mathbf{M}_s]\}\mathbf{d} = \mathbf{f} \tag{6.0.2}$$

Assuming now an harmonic excitation of the system as

$$\mathbf{f} = \mathbf{F}e^{j\omega t}, \tag{6.0.3}$$

and also a steady state response as

$$\mathbf{d} = \mathbf{X}e^{j\omega t}, \quad \dot{\mathbf{d}} = j\omega\mathbf{X}e^{j\omega t}, \quad \ddot{\mathbf{d}} = -\omega^2\mathbf{X}e^{j\omega t}, \tag{6.0.4}$$

equations (6.0.3) and (6.0.4) can now be replaced back in equation (6.0.2) yielding

$$\{\underbrace{[\mathbf{K}^e + \mathbf{K}^v(j\omega)] + \Omega^2[\mathbf{K}_s - \mathbf{M}_s]}_{\mathbf{K}_{eq}} + 2j\omega\Omega\mathbf{G} - \omega^2\mathbf{M}\}\mathbf{X}(j\omega)e^{j\omega t} = \mathbf{F}e^{j\omega t} \tag{6.0.5}$$

where ω is the frequency of excitation and consequently the frequency of the response, and $\mathbf{F}$ and $\mathbf{X}$ are vectors possessing the amplitudes at each degree of freedom (DOF) of the excitation and the response respectively.

By definition the receptance FRF H_{rq} represents the displacement of the rth DOF due to an unitary load applied in the qth DOF and as such, $\mathbf{F}$ has all of its components null except for that that corresponds to the qth DOF. The FRF in a certain frequency range can then be obtained by solving the system of equations (6.0.5) repeatedly for various values of frequency and collecting the component in $\mathbf{X}$ that corresponds to the rth DOF.

Since the viscoelastic stiffness matrix is frequency dependent, it implies that the use of equation (6.0.2) is done in the frequency domain based on the Complex Modulus Approach, and that the material properties for the viscoelastic matrix need to be determined at each frequency defined in the frequency range. To do so, while computing and assembling the element matrices of each viscoelastic layer a unitary Young's modulus is assumed, then when the global matrices are defined, at each frequency defined between

the frequency range the complex modulus is determined, the viscoelastic stiffness matrix is updated with the complex extensional modulus $E^*(j\omega)$ and the FRF is determined.The procedure is known as direct frequency analysis (DFA) and it is shown schematically in figure 6.1.

This method is a very straightforward one, having as a main disadvantage the heavy computational cost and the time it takes to perform a full analysis, since it needs to solve a linear and complex system of equations (with the dimension of the spatial model) for each frequency.

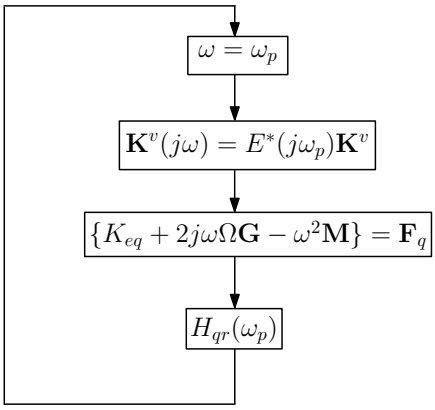

Figure 6.1: Diagram of the direct frequency analysis algorithm

As for the complex extensional modulus, it is determined for oscillatory forcing conditions as

$$E^*(j\omega) = 2(1 + \nu(j\omega))G^*(j\omega) \tag{6.0.6}$$

Note that for simplicity's sake the Poisson's ratio for the viscoelastic material is actually assumed real and frequency independent and with the following value $\nu = 0.49$. $G^*(j\omega)$ is the complex shear modulus and can be determined using a four-parameter constitutive model which is defined, according to Kergourlay [14] and Pritz [15], as

$$G^*(j\omega) = \frac{G_0 + G_\infty(j\omega\tau)^\alpha}{1 + (j\omega\tau)^\alpha} \tag{6.0.7}$$

where G_0 is the dynamic modulus at null frequency or, in other terms, the static modulus of elasticity, G_∞ represents the high frequency limit value of the dynamic modulus also known as relaxed modulus, τ represents the relaxation time and α is a constant that varies from zero to one ($0<\alpha<1$) [15]. The parameters are determined for an ISD112 at 27° by using an available laboratory fitting procedure and the data from the respective manufacturer nomogram [16], and their values are approximately found out to be

$$G_0 = 3.504 \times 10^5\ Pa, \quad G_\infty = 3.062 \times 10^9\ Pa$$

$$\tau = 8.230 \times 10^{-9}\ s, \quad \alpha = 0.675$$

The complex modulus $G^*(j\omega)$ can also be expressed in terms of the shear storage modulus $G'(\omega)$ and the loss factor $\eta(\omega)$ as follows

$$G^*(j\omega) = G'(\omega)[1 + j\eta(\omega)], \tag{6.0.8}$$

where the loss factor is defined as

$$\eta(\omega) = \frac{G''(\omega)}{G'(\omega)} \tag{6.0.9}$$

with G'' as the shear loss modulus. The shear storage and loss modulus are determined as

$$G' = \mathrm{Re}(G^*), \quad G'' = \mathrm{Im}(G^*) \tag{6.0.10}$$

6.1 Frequency response function analysis

To determine the effect of the viscoelastic treatment on the beam five treatments will be tested and the respective FRFs are compared with the FRF of the beam with no treatment (NT). The treatments are presented in table 6.1, where the thicknesses are in millimeters and the 'e' is for an elastic layer and 'v' is for a viscoelastic layer. The elastic layers are made out of aluminum ($\rho = 2700\ kg/m^3$, $E = 70\ GPa$, $\nu = 0.33$), the width of the beam is 8 mm and the length is 500 mm. Note that the last three treatments are exaggerated, as usually the thickness of the viscoelastic layer can only go as high as the thickness presented in treatment B. Moreover, the FRFs obtained are direct and the excitation force will be applied at the free end of the beam in the directions of y (chordwise FRF) and z (flapwise FRF) axes with the responses obtained in the same directions.

Table 6.1: Viscoelastic treatments analyzed

	A	B	C	D	E
h_2	0.254 e	0.508 e	1 e	-	1 e
h_1	0.127 v	0.254 v	2 v	2 v	2 v
base	3 e	3 e	3 e	3 e	3 e
h_{-1}	-	-	-	2 v	2 v
h_{-2}	-	-	-	-	1 e

Thicknesses in millimeters; e=elastic; v=viscoelastic

6.1.1 Results

It can be seen from figures 6.2 and 6.3 that the first two treatments A and B do not make much effect on the amplitudes of vibration when the exciting force is on the plane of rotation. This is because the beam is thick in that direction and as such the shear strain, which makes the viscoelastic effective, caused by that exciting force might not be to high. In addition, when modeling the multilayer finite element the horizontal displacement in the y direction was assumed constant for all of the layers which contributes for lowering the shear strain that the viscoelastic layer is subjected to. On the other hand, when considering a pre-twisted beam with a pre-twist of 30° and making the assumption of small angles, it can be seen that for the same FRF type the viscoelastic treatment makes effect and amplitudes drop. It is also noticeable comparing both figures, that the effect of the viscoelastic damping treatment decreases as the rotating speed of the beam increases. Even when applying the treatments C, D and E with the exaggerated viscoelastic layers, it is visible that the damping treatment doesn't make effect.

As for the FRF with the exciting force perpendicular to the plane of rotation, one can see from figure 6.4 that even for the first two damping treatments the amplitudes of vibration decrease which may lead one to conclude that the exciting force in the direction of the z axis causes significant shear strain. Also in this FRF type it can be seen from figure 6.5 that as the rotation speed of the beam increases the effect of the viscoelastic damping treatment decreases for the same frequency range. Possibly this is because for the same frequency band, the increase in the loss factor is always the same, and since the beam is stiffened due to the rotation the viscoelastic treatment doesn't make much effect, although further investigation of these results would be required to better understand this lack of damping from the treatment for a rotating beam. For a pre-twisted beam with a 30° angle of pre-twist and also assuming small angles, it is shown that the viscoelastic layer also produces effect on the amplitudes of vibration although it's reduced once again when the beam is rotating.

In figures 6.6 is presented the flapwise FRF using treatment A with different materials

- Steel (S), E=206 GPa, $\nu = 0.29$
- Aluminum (A), E=70 GPa, $\nu = 0.33$

It is quite clear the effect of using materials with different stiffnesses. As the base layer becomes more rigid comparatively to the constraining layer the viscoelastic suffers less shear stress and has less effect than when the beam is made of aluminum and the constraining layer of steel, configuration that increases the shear strain of the viscoelastic layer and thus increases the effectiveness of the damping treatment.

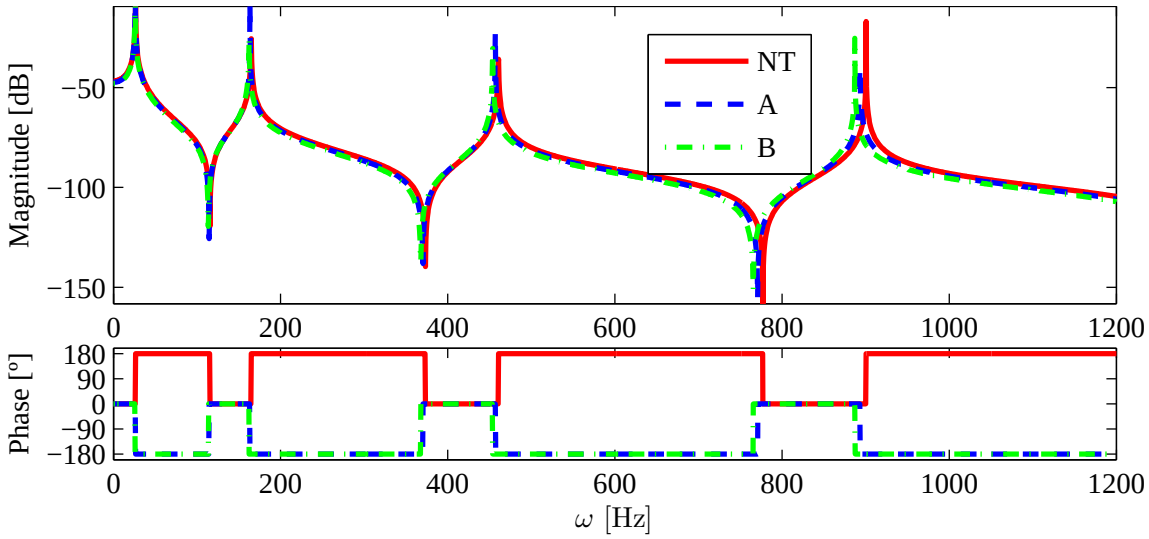

(a) Normal treatments

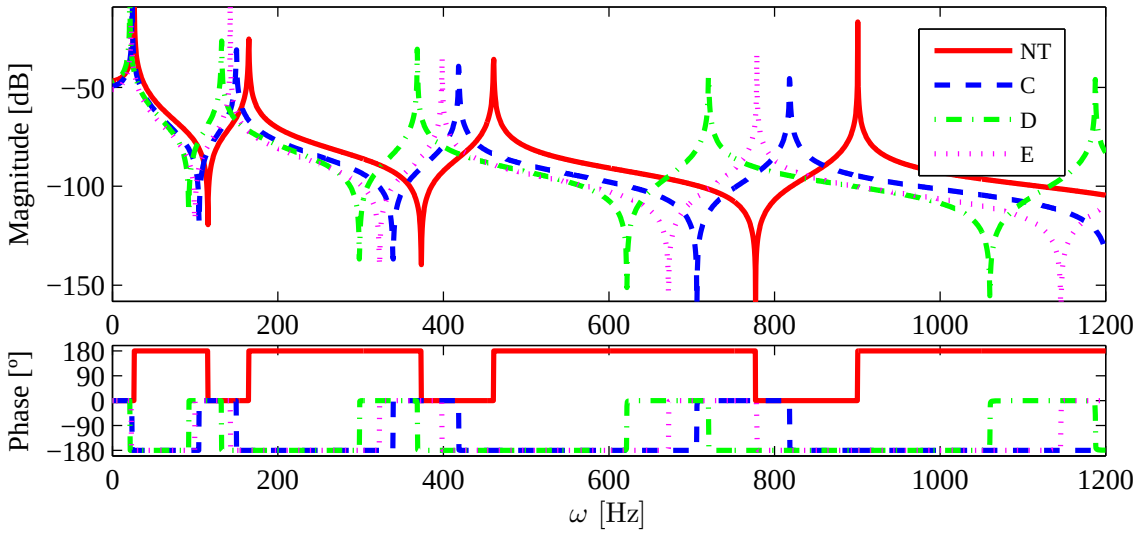

(b) Exaggerated treatments

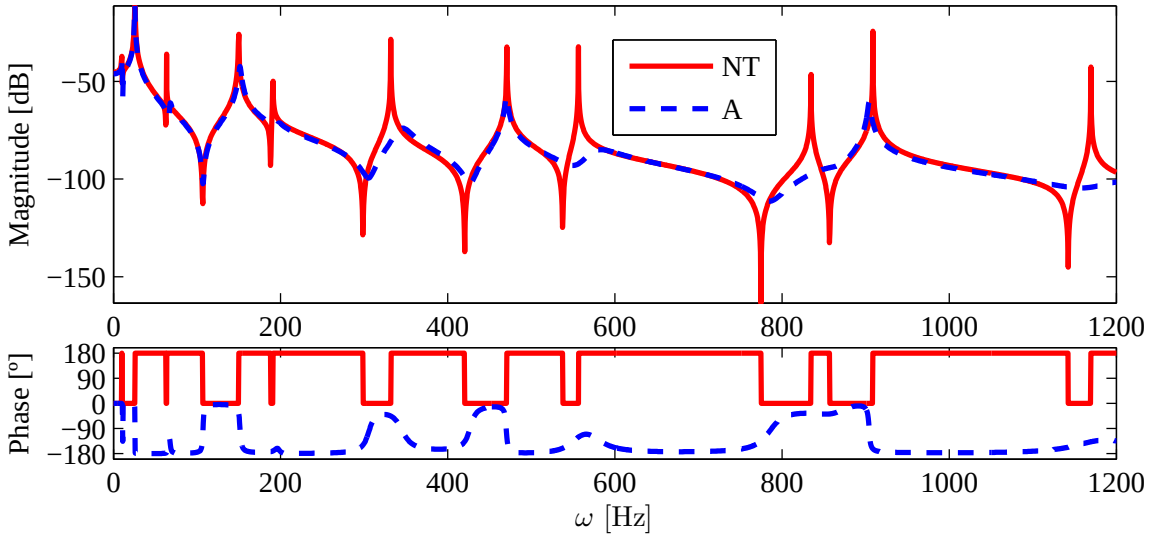

(c) Pre-twisted beam

Figure 6.2: FRF for the chordwise bending vibration ($\Omega = 0$ rpm)

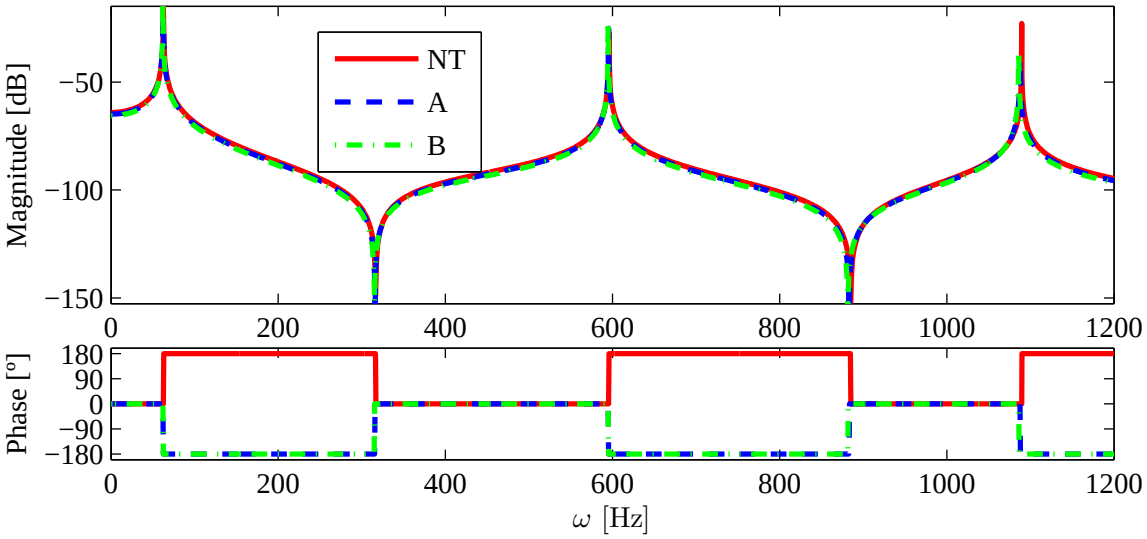

(a) Normal treatments

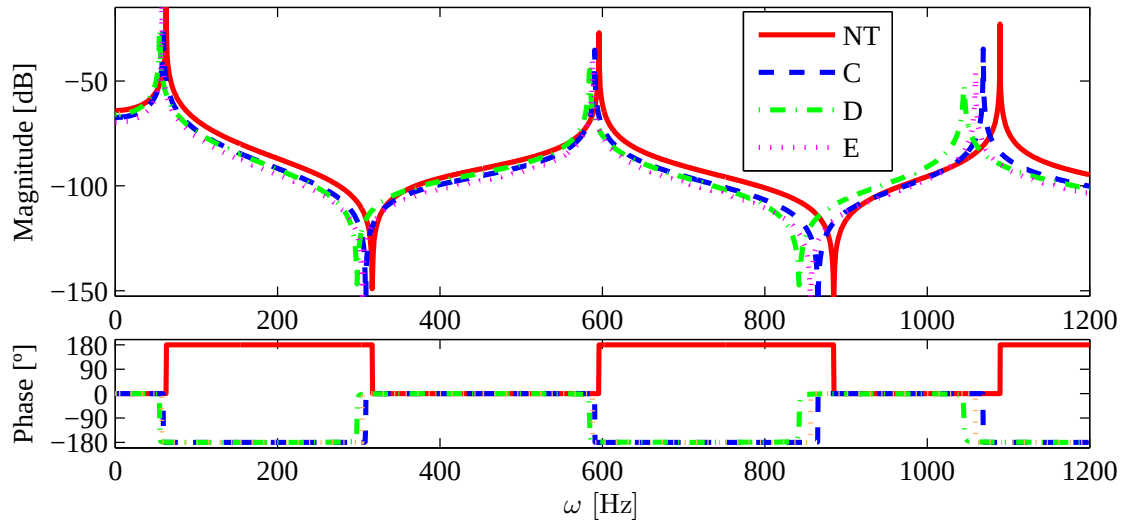

(b) Exaggerated treatments

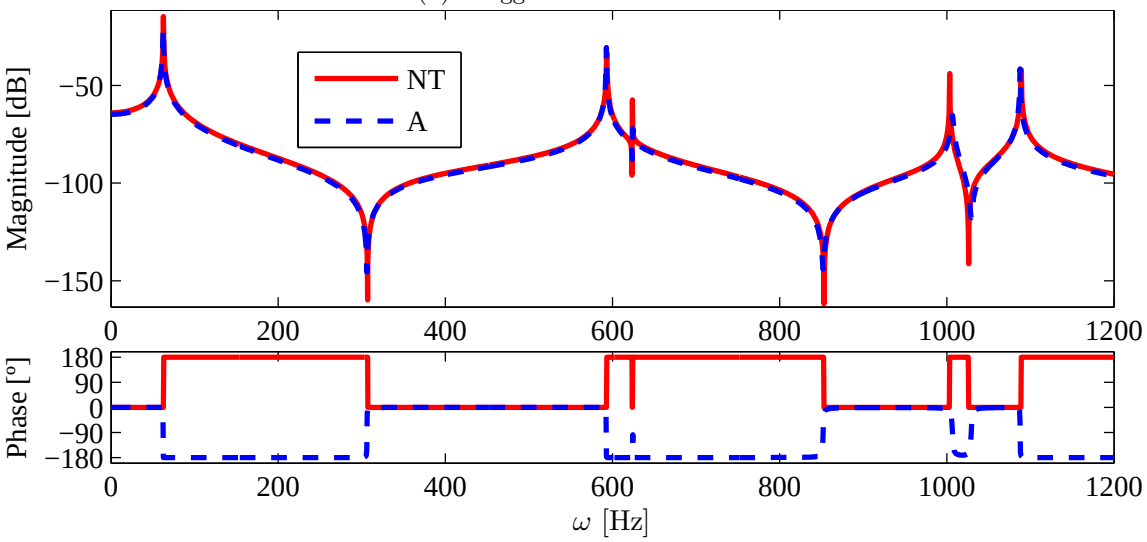

(c) Pre-twisted beam

Figure 6.3: FRF for the chordwise bending vibration ($\Omega = 15000$ rpm, $\delta = 0$)

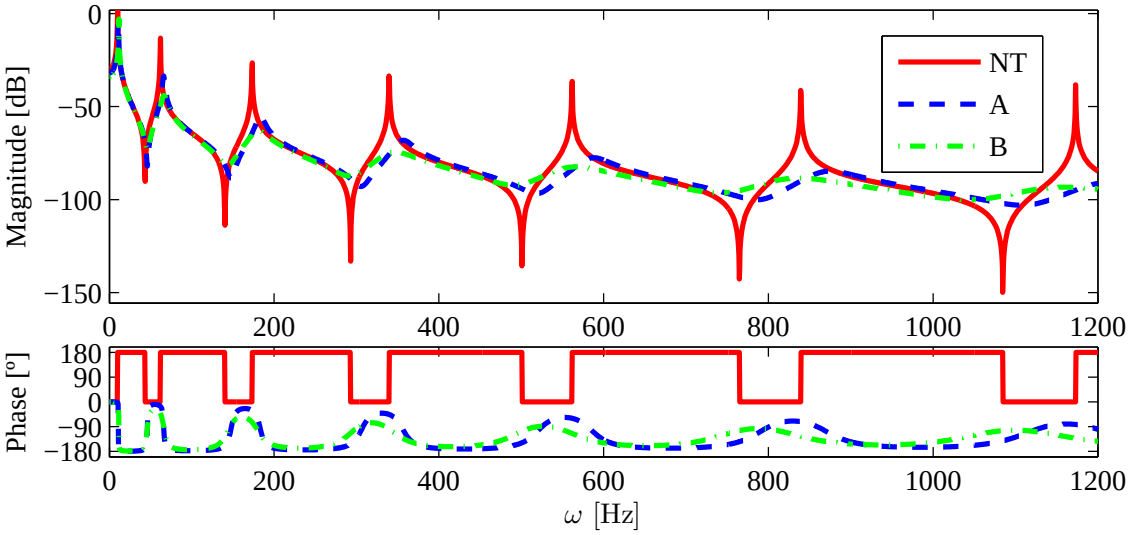

(a) Normal treatments

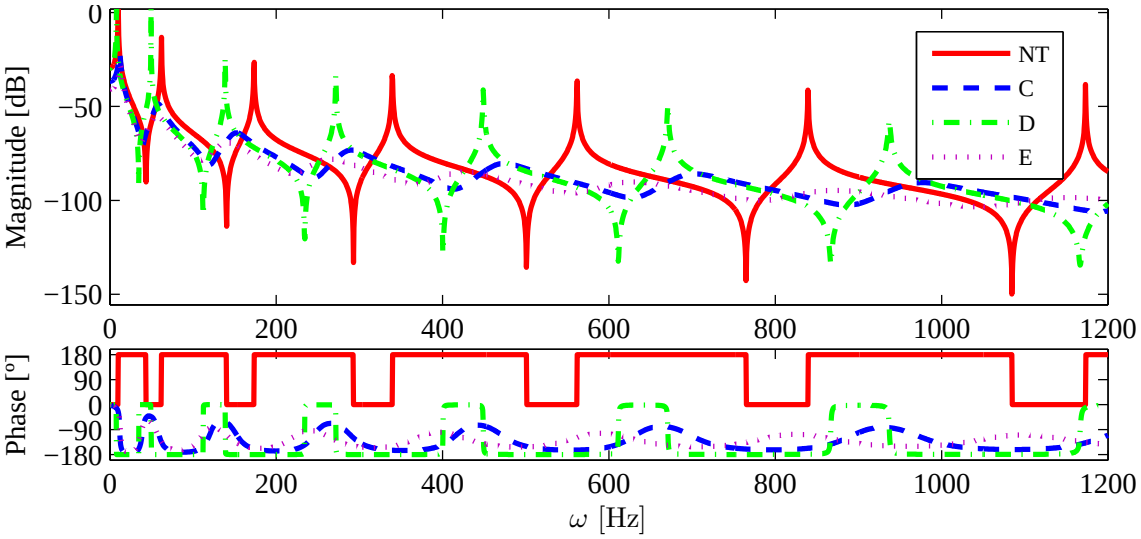

(b) Exaggerated treatments

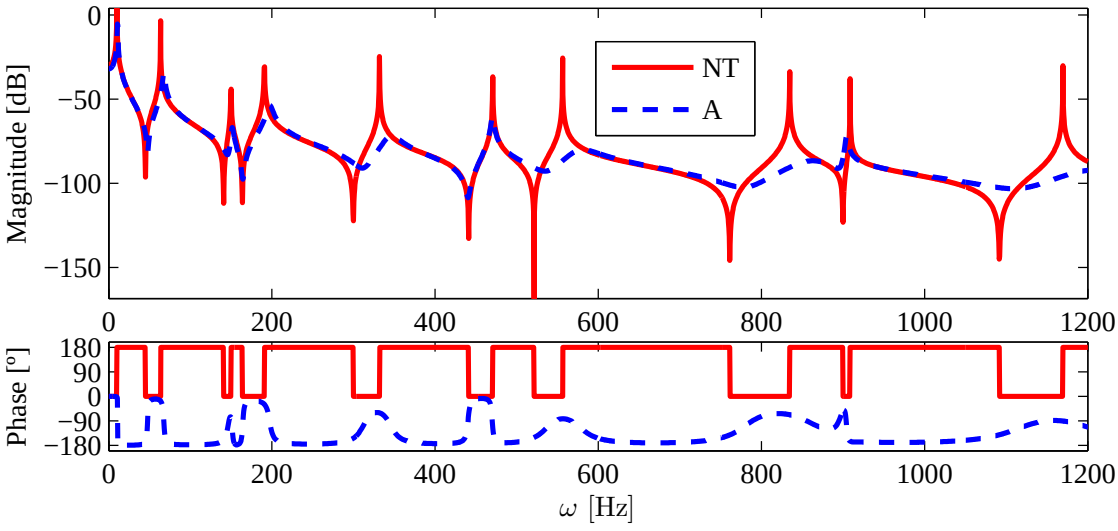

(c) Pre-twisted beam

Figure 6.4: FRFs for the flapwise bending vibration ($\Omega = 0$ rpm)

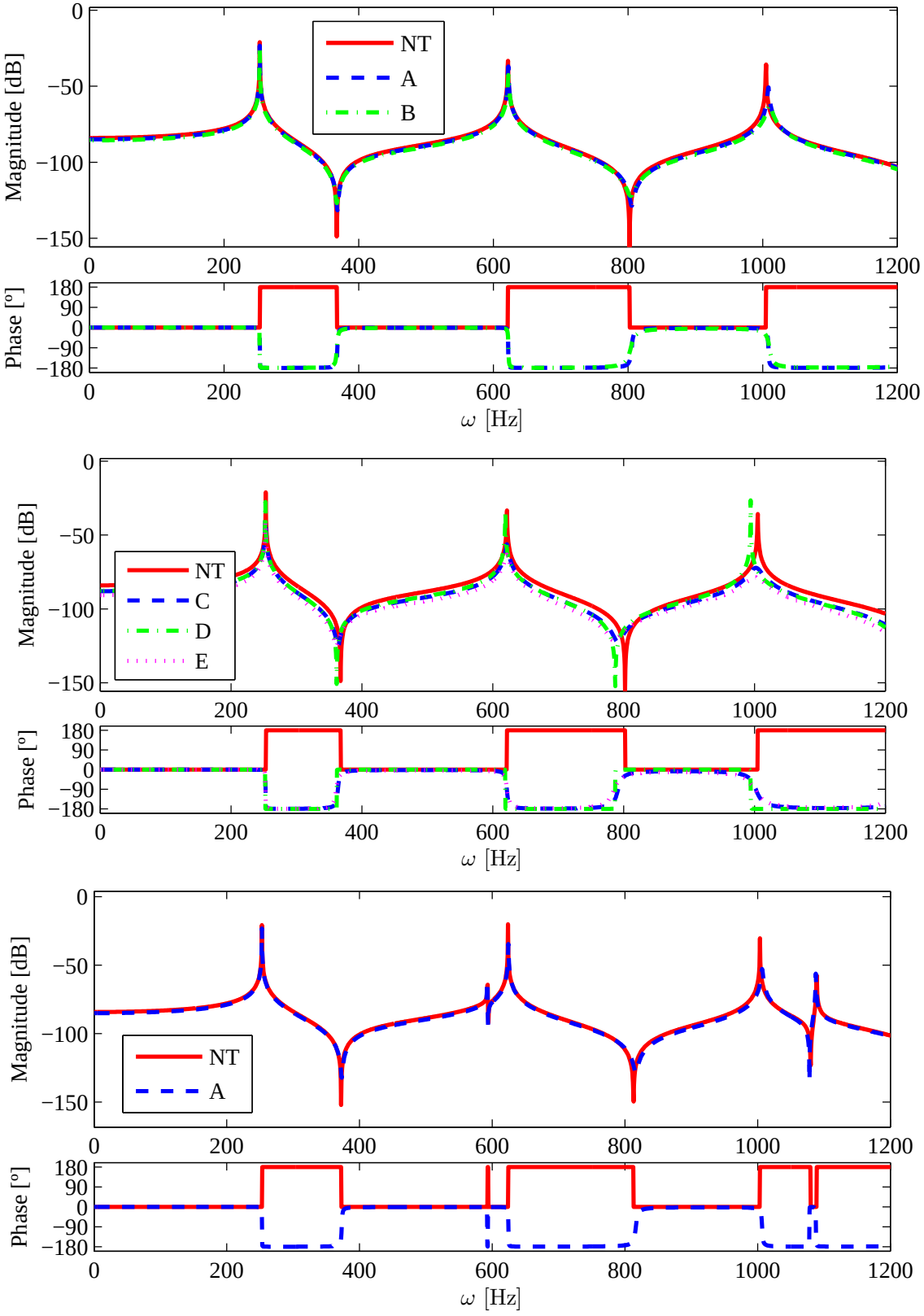

Figure 6.5: FRFs for the flapwise bending vibration ($\Omega = 15000$ rpm, $\delta = 0$)

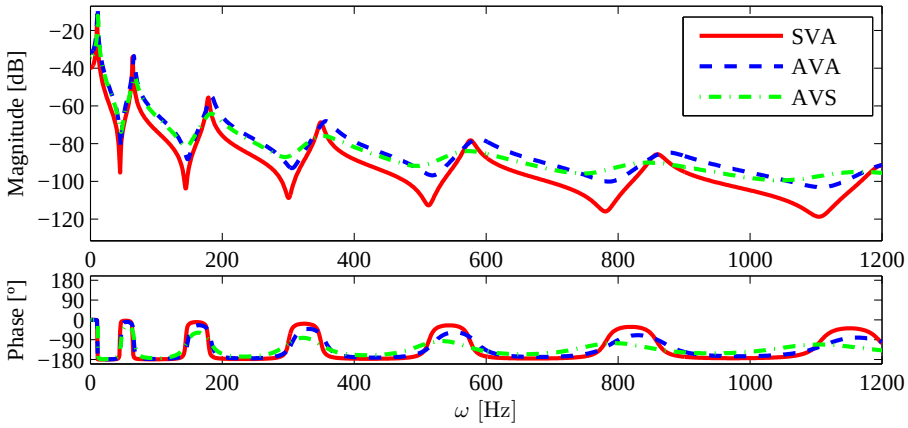

(a) $\Omega = 0$ rpm

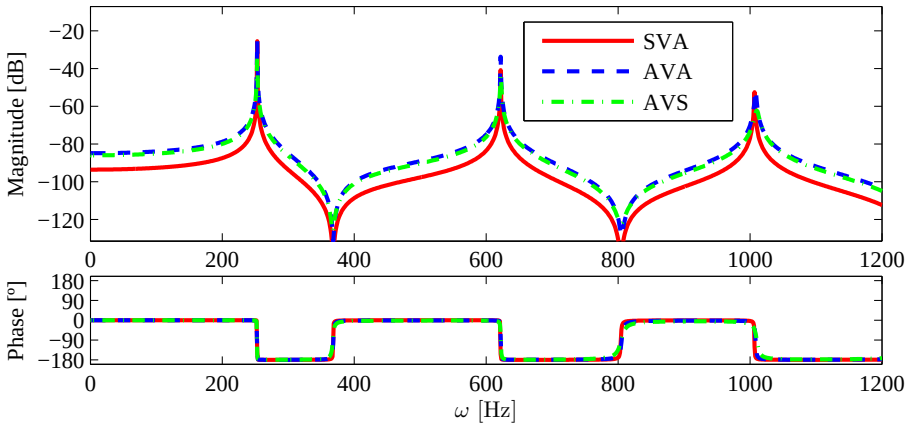

(b) $\Omega = 15000$ rpm, $\delta = 0$

Figure 6.6: Effect of the materials on the effectiveness of the viscoelastic damping for the flapwise bending vibration

Chapter 7

Laminated composite beams

In this chapter a multilayer element for a laminated composite beam is formulated using the layerwise displacement theory. The main point of the analysis is to understand the effect of the fiber angles in the natural frequencies of the composite cantilever rotating beam.

7.1 Beam constitutive matrix

According to Reddy [17], for an orthotropic material such as laminated composite the compliance matrix in the local material coordinate system can be defined as

$$\mathbf{S} = \begin{bmatrix} \frac{1}{E_1} & -\frac{\nu_{21}}{E_2} & \frac{\nu_{31}}{E_3} & 0 & 0 & 0 \\ -\frac{\nu_{12}}{E_1} & \frac{1}{E_2} & -\frac{\nu_{32}}{E_3} & 0 & 0 & 0 \\ -\frac{\nu_{13}}{E_1} & -\frac{\nu_{23}}{E_2} & \frac{1}{E_3} & 0 & 0 & 0 \\ 0 & 0 & 0 & \frac{1}{G_{23}} & 0 & 0 \\ 0 & 0 & 0 & 0 & \frac{1}{G_{13}} & 0 \\ 0 & 0 & 0 & 0 & 0 & \frac{1}{G_{12}} \end{bmatrix} \tag{7.1.1}$$

with E_{ij}, G_{ij} and ν_{ij} as the engineering constants for the composite material in the material local coordinates.

Since the orientation of the fibers relatively to the global set of axes or the problem set of axes can be arbitrary one needs to determine the elasticity constants in the problem coordinates through the constants in the material coordinate system. To do so the following transformation matrix, from the material to the problem coordinate system, is introduced and defined as [17]

$$\mathbf{T} = \begin{bmatrix} \cos^2\Gamma & \sin^2\Gamma & 0 & 0 & 0 & -\sin 2\Gamma \\ \sin^2\Gamma & \cos^2\Gamma & 0 & 0 & 0 & \sin 2\Gamma \\ 0 & 0 & 1 & 0 & 0 & 0 \\ 0 & 0 & 0 & \cos\Gamma & \sin\Gamma & 0 \\ 0 & 0 & 0 & -\sin\Gamma & \cos\Gamma & 0 \\ \sin\Gamma\cos\Gamma & -\sin\Gamma\cos\Gamma & 0 & 0 & 0 & \cos^2\Gamma - \sin^2\Gamma \end{bmatrix} \tag{7.1.2}$$

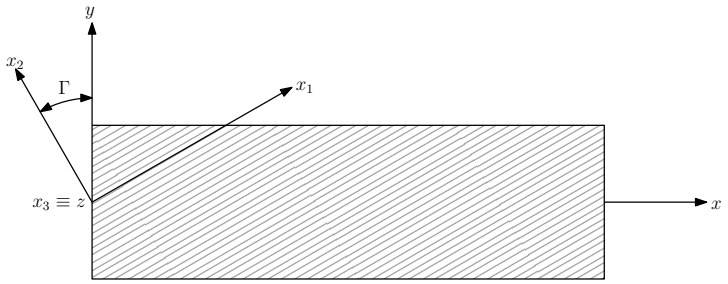

Figure 7.1: Material and problem axes

where Γ represents the rotation angle of the material set of axes relatively to the problem set of axes as illustrated in figure 7.1 Using the transformation matrix **T** from the material coordinte system to the problem coordinate system, the constitutive matrix **C** can now easily be obtained through the compliance matrix **S** in the material coordinate system as follows

$$\mathbf{C} = \mathbf{T}\mathbf{S}^{-1}\mathbf{T}^{T} \tag{7.1.3}$$

Using equation (7.1.3) one obtains a constitutive matrix that relates the full strain tensor $\boldsymbol{\varepsilon}$ with the full stress tensor $\boldsymbol{\sigma}$. Since we are considering the problem of a rotating cantilever beam, only the ε_{xx}, ε_{xz}, ε_{xy} strains and the σ_{xx}, σ_{xz}, σ_{xy} stresses are to be considered and thus we get

$$\begin{Bmatrix} \sigma^k_{xx} \\ \tau^k_{xz} \\ \tau^k_{xy} \end{Bmatrix} = \begin{bmatrix} C^k_{11} & 0 & C^k_{16} \\ 0 & C^k_{55} & 0 \\ C^k_{16} & 0 & C^k_{66} \end{bmatrix} \begin{Bmatrix} \varepsilon^k_{xx} \\ \dfrac{\gamma^k_{xz}}{2} \\ \dfrac{\gamma^k_{xy}}{2} \end{Bmatrix} \tag{7.1.4}$$

In table 7.1 are presented some composite material properties.

Table 7.1: Engineering constants for some composite materials

Material	E_1	E_2	E_3	G_{12}	G_{13}	G_{23}	ν_{12}	ν_{13}	ν_{23}	ρ
Gr.-Ep (AS)	137.9	8.96	8.96	7.10	7.10	6.21	0.30	0.30	0.49	1450
Gr.-Ep (T)	131.0	10.34	10.34	6.89	6.21	6.21	0.22	0.22	0.49	1450
Gl.-Ep (1)	53.8	17.93	17.93	8.96	8.96	3.45	0.25	0.25	0.34	1900
Gl.-Ep (2)	38.6	8.27	8.96	4.14	4.14	3.45	0.26	0.26	0.34	1900
Br.-Ep	206.8	20.68	20.68	6.89	6.89	4.14	0.30	0.25	0.25	1950

From Reddy [17] Gr.-Ep (AS) = Graphite-epoxy (AS/3501); Gr.-Ep (T) = Graphite-epoxy (T); Gl.-Ep (1)=Glass-Epoxy; Br.-Ep = Boron-epoxy. (units of E and G in GPa, ρ in kg/m^3)

7.2 Element formulation

The formulation of the layerwise element for a composite laminated beam is quite similar to that defined in chapter 5. However, the transformation matrix **T** in equation (7.1.2) is defined for the particular case of a rotation of the fibers about the vertical axis z that is coincident with the material vertical axis 3 and so the pre-twist analysis for the layerwise model of a rotating beam can no longer be made. As such the first area moments (static moments) as well as the product of inertia are null and thus don't take part in the respective equations. As for the second area moments they are determined for the case of a simple rectangular cross section as follows

$$I^k_y = \frac{bh^3}{12}, \quad I^k_z = \frac{b^3h}{12}$$

Seeing that the mass per unit volume of a composite material has nothing to do with the fiber angle of the ply, the kinetic energy for a generic layer composite beam is quite similar to that defined in subsection 5.2, hence all the matrices defined in equation (5.2.6) are still valid for the present problem.

As for the potential energy, considering the relation between the stresses and strain defined in equation (7.1.4), it can be expressed as

$$\Pi = \frac{1}{2}\int_V (C_{11}^k \varepsilon_{xx}^2 + C_{55}^k \gamma_{xz}^2 + C_{66}^k \gamma_{xy}^2 + 2C_{16}^k \varepsilon_{xx}\gamma_{xy})\, dV \tag{7.2.1}$$

where the strains in the previous equation are the same as those defined in equations (5.3.1). The potential energy is then given by

$$\begin{aligned}\Pi = \frac{1}{2}\int_V \Bigg\{ & C_{11}^k \left(s' + \frac{h_1}{2}\theta_1' + \sum_{j=2}^{k-1} h_j\theta_j' + \frac{h_k}{2}\theta_k' + z_k\theta_k' - y\psi' \right)^2 \\ & + C_{55}^k (w' + \theta_k)^2 + C_{66}^k (v' - \psi)^2 \\ & + 2C_{16}^k \left(s' + \frac{h_1}{2}\theta_1' + \sum_{j=2}^{k-1} h_j\theta_j' + \frac{h_k}{2}\theta_k' + z_k\theta_k' - y\psi' \right)(v' - \psi) \Bigg\}\, dV \end{aligned} \tag{7.2.2}$$

and applying the variational to it yields

$$\begin{aligned}\int_{t_i}^{t_f} \delta\Pi\, dt = \int_{t_i}^{t_f}\int_0^L \Bigg\{ & C_{11}^k \left(s' + \frac{h_1}{2}\theta_1' + \sum_{j=2}^{k-1} h_j\theta_j' + \frac{h_k}{2}\theta_k' \right)\delta\left(s' + \frac{h_1}{2}\theta_1' + \sum_{j=2}^{k-1} h_j\theta_j' + \frac{h_k}{2}\theta_k' \right) \\ & + C_{11}^k (I_y^k \theta_k' \delta\theta_k' + I_z^k \psi' \delta\psi') \\ & + C_{55}^k (w' + \theta_k)\delta(w' + \theta_k) + C_{66}^k (v' - \psi)\delta(v' - \psi) \\ & + C_{16}^k \left(s' + \frac{h_1}{2}\theta_1' + \sum_{j=2}^{k-1} h_j\theta_j' + \frac{h_k}{2}\theta_k' \right)\delta(v' - \psi) \\ & + C_{16}^k (v' - \psi)\delta\left(s' + \frac{h_1}{2}\theta_1' + \sum_{j=2}^{k-1} h_j\theta_j' + \frac{h_k}{2}\theta_k' \right) \Bigg\}\, dx\, dt \end{aligned} \tag{7.2.3}$$

By following the same procedure done in section 5.4, the weak form for the laminated composite beam can easily be derived as

$$\begin{aligned}\sum_{k=1}^{n} \int_0^L & \delta\Delta^T \mathbf{J}\ddot{\Delta} + 2\Omega\delta\Delta^T \mathbf{J_g}\dot{\Delta} + \Omega^2 (\mathcal{L}_s\delta\Delta)^T \mathbf{D_s}\mathcal{L}_s\Delta - \Omega^2\delta\Delta^T \mathbf{J_s}\Delta \\ & + (\mathcal{L}_\varepsilon\delta\Delta)^T \mathbf{D}_\varepsilon(\mathcal{L}_\varepsilon\Delta) + (\mathcal{L}_\gamma\delta\Delta)^T \mathbf{D}_\gamma(\mathcal{L}_\gamma\Delta) + (\mathcal{L}_{\varepsilon\gamma}\delta\Delta)^T \mathbf{D}_{\varepsilon\gamma}(\mathcal{L}_{\varepsilon\gamma}\Delta)\, dx \\ & = \sum_{k=1}^{n} \int_0^L \delta\Delta^T \mathbf{f}_s\, dx \end{aligned} \tag{7.2.4}$$

It is visible that the extensional and shear matrices defined in equation (5.3.6) are still applicable. In matrix (5.3.7) only E needs to be replaced by C_{11}^k, while in matrix (5.3.9) G needs to be replaced by C_{55}^k and C_{66}^k in their respective positions as

$$\mathbf{D}_\gamma = A^* \begin{bmatrix} 0 & 0 & 0 & 0 & 0 & \cdots & 0 & \cdots & 0 & 0 & \cdots & 0 \\ & C_{66}^k & 0 & -C_{66}^k & 0 & \cdots & 0 & \cdots & 0 & 0 & \cdots & 0 \\ & & C_{55}^k & 0 & 0 & \cdots & 0 & \cdots & C_{55}^k & 0 & \cdots & 0 \\ & & & C_{66}^k & 0 & \cdots & 0 & \cdots & 0 & 0 & \cdots & 0 \\ & & & & 0 & \cdots & 0 & \cdots & 0 & 0 & \cdots & 0 \\ & & & & & \ddots & \vdots & \ddots & \vdots & \vdots & \ddots & \vdots \\ & & & & & & 0 & \cdots & 0 & 0 & \cdots & 0 \\ & & & & & & & \ddots & \vdots & \vdots & \ddots & \vdots \\ & & & & & & & & C_{55}^k & 0 & \cdots & 0 \\ & & & & & & & & & 0 & \cdots & 0 \\ & & & & & & & & & & \ddots & \vdots \\ \text{sym.} & & & & & & & & & & & 0 \end{bmatrix} \tag{7.2.5}$$

The main difference present in the laminated composite beam is the coupling effect introduced between ε_{xx} and γ_{xy}, resulting in the following coupling matrix

$$\mathbf{D}_{\varepsilon\gamma}^k = C_{16}^k \begin{bmatrix} 0 & 1 & 0 & -1 & 0 & \cdots & 0 & \cdots & 0 & 0 & \cdots & 0 \\ & 0 & 0 & 0 & \frac{h_1}{2} & \cdots & h_j & \cdots & \frac{h_k}{2} & 0 & \cdots & 0 \\ & & 0 & 0 & 0 & \cdots & 0 & \cdots & 0 & 0 & \cdots & 0 \\ & & & 0 & -\frac{h_1}{2} & \cdots & -h_j & \cdots & -\frac{h_k}{2} & 0 & \cdots & 0 \\ & & & & 0 & \cdots & 0 & \cdots & 0 & 0 & \cdots & 0 \\ & & & & & \ddots & \vdots & \ddots & \vdots & \vdots & \ddots & \vdots \\ & & & & & & 0 & \cdots & 0 & 0 & \cdots & 0 \\ & & & & & & & \ddots & \vdots & \vdots & \ddots & \vdots \\ & & & & & & & & 0 & 0 & \cdots & 0 \\ & & & & & & & & & 0 & \cdots & 0 \\ & & & & & & & & & & \ddots & \vdots \\ \text{sym.} & & & & & & & & & & & 0 \end{bmatrix} \tag{7.2.6}$$

$$\mathcal{L}_{\varepsilon\gamma} = \operatorname{diag}\begin{bmatrix} \frac{\partial}{\partial x} & \frac{\partial}{\partial x} & 1 & 1 & \frac{\partial}{\partial x} & \cdots & \frac{\partial}{\partial x} & \cdots & \frac{\partial}{\partial x} & 1 & 1 \end{bmatrix} \tag{7.2.7}$$

After the introduction of the element displacements equation (7.2.4) can be written in a discretized way, yielding

$$\sum_{e=1}^{N} \delta\mathbf{d}_e^T \{\mathbf{m}_e\ddot{\mathbf{d}}_e + 2\Omega\mathbf{g}_e\dot{\mathbf{d}}_e + [\Omega^2(\mathbf{ks}_e - \mathbf{ms}_e) + \mathbf{k}_e]\mathbf{d}_e\}\, dx = \sum_{e=1}^{N} \Omega^2 \Delta^T \mathbf{f}_s \tag{7.2.8}$$

where all the element matrices in the previous equation are the same as the ones defined in equation (5.4.9) except for the stiffness matrix that now has to account for the coupling effect, becoming

$$\begin{aligned} \mathbf{k}_e &= \sum_{k=1}^{n} \int_{-1}^{+1} \mathbf{B}_\varepsilon^T \mathbf{D}_\varepsilon^k \mathbf{B}_\varepsilon + \mathbf{B}_\gamma^T \mathbf{D}_\gamma^k \mathbf{B}_\gamma + \mathbf{B}_{\varepsilon\gamma}^T \mathbf{D}_{\varepsilon\gamma}^k \mathbf{B}_{\varepsilon\gamma} det(\mathbf{J})\, d\xi \\ &= \sum_{k=1}^{n} \sum_{i=1}^{m} w_i \{\mathbf{B}_\varepsilon^T \mathbf{D}_\varepsilon^k \mathbf{B}_\varepsilon + \mathbf{B}_\gamma^T \mathbf{D}_\gamma^k \mathbf{B}_\gamma + \mathbf{B}_{\varepsilon\gamma}^T \mathbf{D}_{\varepsilon\gamma}^k \mathbf{B}_{\varepsilon\gamma}\} det(\mathbf{J}) \end{aligned} \tag{7.2.9}$$

7.3 Composite results

To obtain the results for the composite laminated beam the dimensionless quantities defined in chapter 4 and the layers for the composite beam are all assumed to have equal height. In this case the dimensionless

quantity T is defined as

$$T = \sqrt{\frac{\rho A L^4}{E_1 I_z}}$$

Furthermore, the following results are all obtained for $\vartheta = 1$ and using Br.-Ep for all of the layers. Other results for other materials or combination of materials could be obtained although, since the main interest is to evaluate the effect of the fibers' angle on the natural frequencies, the use of only one material is more appropriate so that other effects are not introduced.

In table 7.2 it is shown that the first four dimensionless natural frequencies for a rotating laminated composite beam converge as the number of elements increase. Analyzing table 7.3, it is quite noticeable that whether the beam possesses a symmetric or unsymmetric laminae, the natural frequencies are very similar. Considering figures 7.2a and 7.2b where two different laminae schemes are presented, it is observable the effect of the ply angle on the evolution of the natural frequencies. It is noted that as the angle of the ply increases the critical buckling speed decreases. The natural frequencies drop faster in the $(\Gamma/-\Gamma)_3$ scheme than in the $(0/\Gamma)_s$, mainly because in the former the angle changes for all of the layers reducing the bending stiffness while in the later the outer layers remain at zero degrees angle. Also as a general effect, the increase of the fibers' angle towards 90° tend to lower the natural frequencies although, it is interesting that the first flapwise bending natural frequency (second natural frequency for low rotating speeds) does not suffer any visible alteration whatsoever. It is also evident that the drop of the frequencies is faster when the angle approaches 45° than afterwards. In table 7.4, it is shown that the fibers' angle does alter the second natural frequency but this change is quite small. In fact, for the first symmetric scheme the effect of the angle is always negligible which makes sense since the outer layers are always with zero degrees angle and as such the change in middle layers doesn't affect significantly the flapwise bending stiffness. As for the unsymmetric scheme, the change in the angle of the fibers provides greater change in the natural frequencies but only for low rotating speeds, probably because for higher rotating speeds the centrifugal stiffening of the beam is dominant making the angle's effect negligible compared to it. Also important to these results is the centrifugal mass matrix $\mathbf{M}_s$ which is responsible for the buckling of the beam, has nothing to do with the angle of the fibers and more importantly, has negligible effects over the flapwise bending vibrations and very important influence on the chordwise bending vibrations (see section 4.2). As such, when the angle of the fibers is zero the stiffness matrix and the centrifugal stiffness matrix can compensate longer the centrifugal mass matrix before buckling occurs. On the opposite, when the angle approaches 90° the stiffness matrix can no longer compensate and the chordwise natural frequencies start to drop for low rotating speeds. Knowing that the centrifugal mass matrix has very little effect on the flapwise motion the centrifugal stiffness matrix can always compensate the loss of stiffness due to the fibers' angle.

Table 7.2: Convergence of the first four dimensionless natural frequencies for a laminated composite beam ($\delta = 0.1$, $\alpha = 70$, $(-10/45/-45/10)$)

γ	No. of elements	First	Second	Third	Fourth
0	10	2.8253	3.1796	16.8933	17.5880
	40	2.8221	3.1761	16.6051	17.2058
	70	2.8219	3.1759	16.5922	17.1888
	100	2.8219	3.1759	16.5890	17.1846
10	10	5.6010	11.4354	30.3806	31.4936
	40	5.6027	11.4356	30.0488	31.2193
	70	5.6028	11.4356	30.0339	31.2069
	100	5.6028	11.4356	30.0302	31.2038
50	10	11.9150	53.7579	110.7718	128.2164
	40	11.9038	53.7577	109.9506	127.9670
	70	11.9033	53.7576	109.9126	127.9559
	100	11.9032	53.7576	109.9032	127.9532

Table 7.3: Comparison for the first four dimensionless natural frequencies for symmetric and asymmetric schemes ($\delta = 0.1$, $\alpha = 60$)

	γ				
Scheme	0	2	10	50	100
First					
$(-45/45)_s$	1.9911	2.3283	4.9087	4.2252	-
$(-45/45)_2$	1.9443	2.3280	4.9091	4.2270	-
$(-30/30/-30)_s$	2.6704	2.9834	5.4820	9.4319	-
$(-30/30)_3$	2.6370	2.9833	5.4916	9.6447	-
Second					
$(-45/45)_s$	2.0306	3.0289	11.0904	53.6553	96.8911
$(-45/45)_2$	2.0324	3.0000	11.0809	53.6538	96.8919
$(-30/30/-30)_s$	2.7550	3.5091	11.2577	53.6974	107.1890
$(-30/30)_3$	2.7582	3.4868	11.2505	53.6963	107.1884
Third					
$(-45/45)_s$	11.1248	12.3317	27.4479	91.9395	107.1629
$(-45/45)_2$	10.9074	12.1364	27.4463	91.9412	107.1620
$(-30/30/-30)_s$	14.0592	15.0309	29.6865	103.7131	137.8786
$(-30/30)_3$	13.9277	14.9082	29.6764	104.2107	139.8444
Fourth					
$(-45/45)_s$	12.5340	13.4872	28.5391	108.4442	187.0866
$(-45/45)_2$	12.5343	13.4881	28.4575	108.4498	187.0888
$(-30/30/-30)_s$	16.7345	17.4557	29.8630	119.2192	195.1500
$(-30/30)_3$	16.7496	17.4710	29.8304	119.8530	195.7576

As for the viscoelastic treatment, it shown in figures 7.3 the effect of the angle of the fibers with the configuration of treatment A in table 6.1 and the angles as shown in the legend (the first refers to the base layer and the second refers to constraining layer). It is seen that as the angle of the fibers for the base layer approximate 90° and as the angles approximate zero degrees for the constraining layer, the damping treatment becomes more effective since. Like it was shown in figures 6.6, as the constraining layer becomes more rigid comparatively to the base layer, the viscoelastic layer suffers more shear deformation making the damping treatment more effective. Even though it is not showed, the viscoelastic treatment still showed no effect on chordwise bending vibration.

Table 7.4: Effect of the fibers' angles on the second natural frequency ($\delta = 0.3$, $\alpha = 60$)

	γ			
Scheme	0	2	10	50
$(0/0)_s$	3.3921	4.2109	12.6675	60.2184
$(0/45)_s$	3.2194	4.0869	12.6093	60.2030
$(0/90)_s$	3.1372	4.0176	12.5631	60.1906
$(10/-10)_3$	3.3829	4.1279	12.6366	60.2112
$(30/-30)_3$	2.7582	3.6567	12.4780	60.1734
$(50/-50)_3$	1.7998	3.0817	12.2862	60.1262

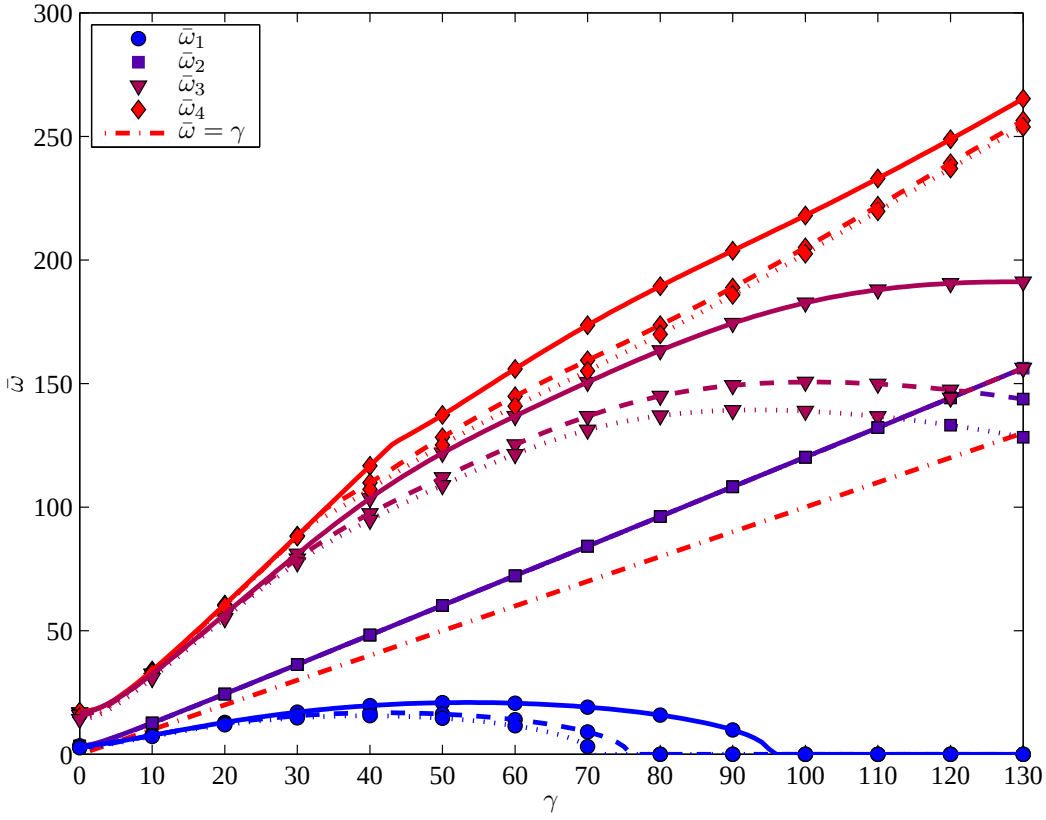

(a) Symmetric scheme $(0/\Gamma)_s$ ($-\Gamma = 0$, $--\ \Gamma = 45$, $:\ \Gamma = 90$)

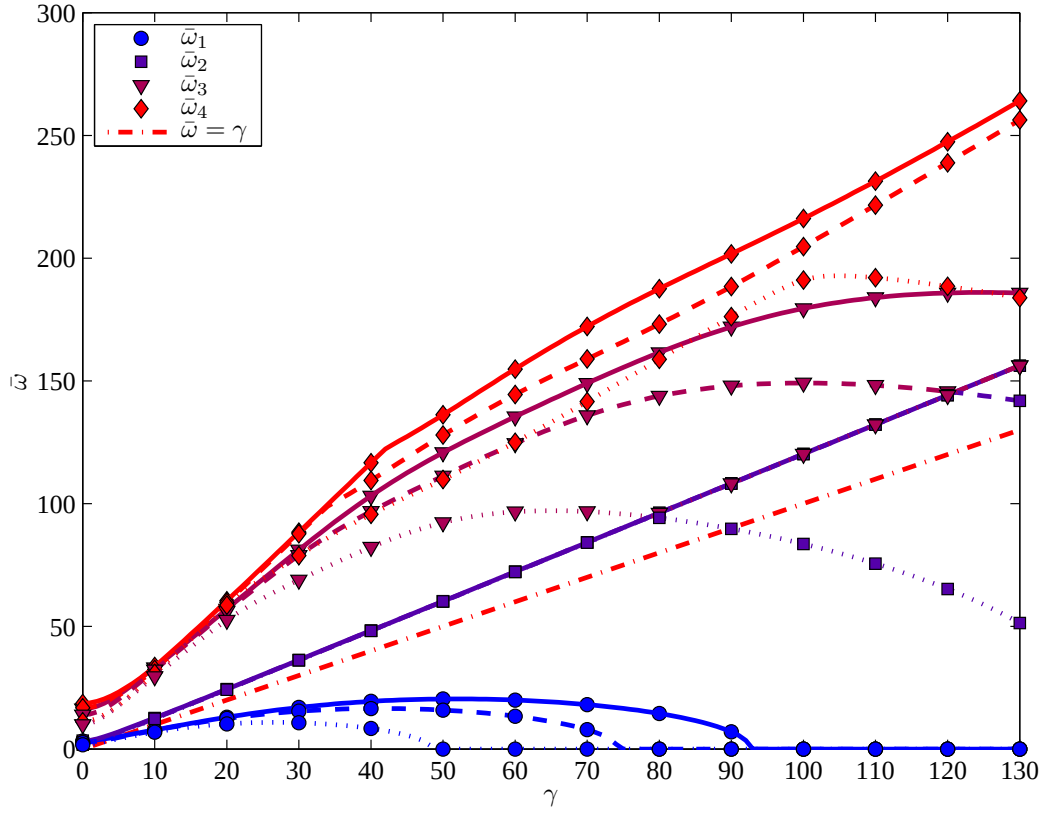

(b) Anti-symmetric scheme $(\Gamma/-\Gamma)_3$ ($-\Gamma = 10$, $--\ 30$, $:\ \Gamma = 40$)

Figure 7.2: Effect of the fibers' angle on the first four dimensionless natural frequencies ($\delta = 0.3$, $\alpha = 60$)

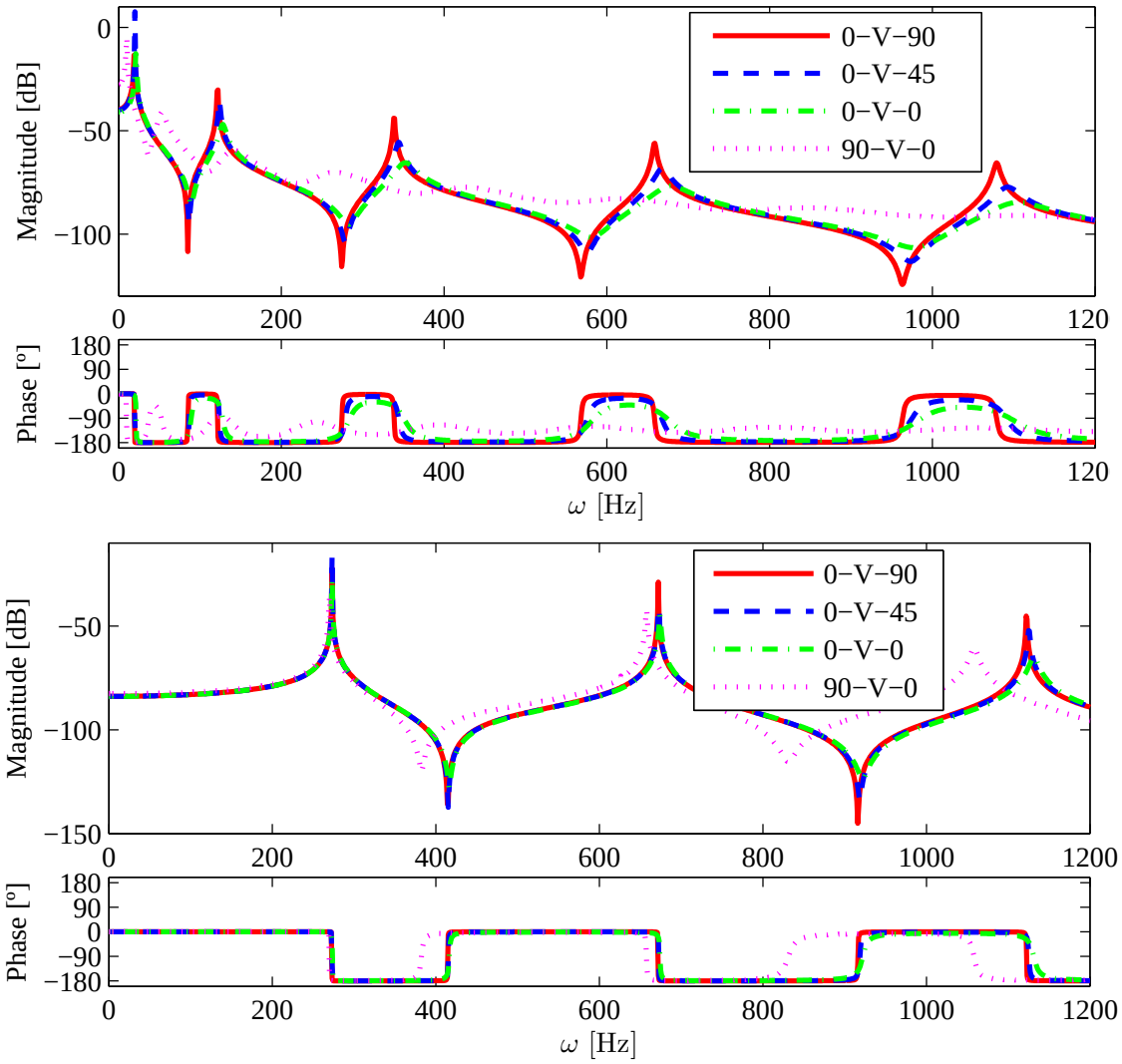

Figure 7.3: Effect of the fibers' angles on the effectiveness of the viscoelastic damping for the flapwise bending vibration ($\delta = 0.1$)

Chapter 8

Conclusion

8.1 Conclusions

This dissertation work presents a vibration analysis of a rotating cantilever beam considering the rotation induced dynamical effects, different deformation theories and different configurations using the finite element method, with a two node rotating beam finite element.

In chapter 2 the displacement and velocity fields, as well as the strain and stress fields are determined based upon the classic Cartesian system of coordinates. A new system of hybrid coordinates is introduced and derived based on the stretch of the neutral axis of the beam. Using this new set of hybrid deformation variables, the linear partial differential equations of motion are derived using the Euler-Bernoulli and Timoshenko beam theories where it is found out that there are two main motion types: the chordwise motion and the flapwise.

- Whether it is used the Euler-Bernoulli or the Timoshenko beam theory, it is found out that the governing equations that refer to the chordwise motion are uncoupled from those regarding the flapwise motion;
- Contrary to this fact, when developing the differential equations for the pre-twisted beam it is found out that both motion types are now coupled due to the inclusion of the product of inertia of the cross section of the beam which is an effect caused by the pre-twist angle.

In chapter 3 the weak forms are derived from the strong forms defined by the differential equations of motion and boundary conditions, using the weighted residuals method. From the weak forms the element matrices for discretized solution are defined and from the element matrices the global system of equations is determined. From the global matrices the eigenvalue problem is derived and it is found out that:

- while for the flapwise motion the global system of equations results in a generalized eigenvalue problem;
- the system of equations for the chordwise motions results in a non-linear complex eigenvalue problem due to the presence of the gyroscopic coupling matrix which needs to be linearized by adopting an identity equation and a state-space approach.

Chapter 4 provides numerical results from the finite element models. The following results were determined:

- Chordwise motion:
  - Natural frequencies don't increase monotonically due to gyroscopic coupling;
  - Existence of a tuned angular speed;
  - Presence of buckling speed and instability limit;
  - Slenderness and hub radius have great effect on the tuned rotating speed;

  - Buckling speed depends greatly on the slenderness bu not on the hub radius;
  - Gyroscopic coupling can be neglected provided that the angular speed is not high and/or that the beam is slender enough.

- Flapwise motion:
  - The natural frequencies increase monotonically with the increase of the rotating speed;
  - No tuned angular speed occurs;
  - The increase in the hub radius ratio increases the natural frequencies;
  - Slenderness has negligible effect on the first natural frequency but lowers the frequencies after the first mode.

- Pre-Twisted beam:
  - The previous effects are still valid;
  - The angle of the pre-twisted has a small effect over the natural frequencies;
  - The intersections of the flapwise and chordwise natural frequency become veering regions due to pre-twist angle.

In chapter 5 a multilayer finite element model using a layerwise theory is derived for a rotating pre-twisted beam composed of several layers. Results obtained are compared with those obtained for a simple beam.

- For the case of a non-pretwisted beam the layerwise model provides accurate results, in accordance with those obtained for a simple beam;
- However for a pre-twisted layerwise beam the results could not be properly validated as the results were very different from those determined for a simple pre-twisted beam. Under some assumptions for small angles of pre-twist the results were improved.

In chapter 6 it was demonstrated using the frequency response function that the viscoelastic damping treatment:

- has an effect over the flapwise bending vibration amplitudes;
- has negligible effects on the chordwise bending vibration amplitudes even with exaggerated treatments;
- produces effect even on the chordwise bending amplitudes if a pre-twist angle is introduced;
- loses effectiveness for elevated angular speeds of the beam;
- it's more effective with a constraining layer stiffer than the beam.

Finally, in chapter 7 a finite element model for composite laminated rotating beams was derived from the layerwise model introduced in chapter 5, making all the needed proper adjustments. The main point of this chapter was to analyze the effect of the fiber angles, and it was found out that:

- as the fibers approximate 90° angle, the natural frequencies start to drop;
- moreover, the beam becomes more unstable since it was noted that the buckling speed decreases;
- it was also found out that whether the laminated beam is symmetric or unsymmetric, the natural frequencies are similar.

It is hoped that this work provides a contribution to the literature regarding the study of rotating beams, mainly considering the most important subjects of the dissertation which are the development of a pre-twisted multi-layered element using a layerwise displacement theory, introduction of the passive vibration control over the vibration amplitudes using viscoelastic treatment and the analysis of laminated composite beams. These subjects are still on an earlier stage of development as, to author's knowledge, little information on the matter or even none is available in the literature and as such these subjects still need further study and development hoping that this work provides a starting point.

8.2 Development Suggestions

Several other studies can be made from the present one and as such, some suggestions are made for further development of the present work:

- Better study of the effect of the viscoelastic damping for a rotating beam with higher rotating speeds;
- Implementation of an iterative model for modal analysis of a rotating beam with viscoelastic damping;
- Further analysis of the pre-twisted multilayer element model for higher pre-twist angles;
- Development of a finite element layerwise model considering different chordwise bending displacements for each layer
- Proper validation of the laminated composite rotating beam, possibly with a commercial program;
- Experimental analysis and validation of the results presented;
- Introduction of the active vibration control using piezoelectric damping layers;
- Expansion of the present work to rotating cantilever plates and disks.

References

[1] H. H. Yoo, R. R. Ryan, and R. A. Scott. Dynamics of flexible beams undergoing overall motions. *Journal of Sound and Vibration*, 181(2):261–278, 1995.

[2] H. H. Yoo and S. H. Shin. Vibration analysis of rotating cantilever beams. *Journal of Sound and Vibration*, 212(5):807–828, 1998.

[3] S. S. Rao and R. S. Gupta. Finite element vibration analysis of rotating Timoshenko beams. *Journal of Sound and Vibration*, 242(1):103–124, 2001.

[4] J. Chung and H. H. Yoo. Dynamic analysis of a rotating cantilever beam by using the finite element method. *Journal of Sound and Vibration*, 249(1):147–164, 2002.

[5] O. Ozdemir Ozgumus and M. O. Kaya. Flapwise bending vibration analysis of a rotating double-tapered Timoshenko beam. *Archive of Applied Mechanics*, 78(5):379–392, 2008.

[6] T.-L. Zhu. The vibrations of pre-twisted rotating Timoshenko beams by the Rayleigh-Ritz method. *Comput. Mech.*, 47(4):395–408, 2011.

[7] Hong Hee Yoo, Jung Hun Park, and Janghyun Park. Vibration analysis of rotating pre-twisted blades. *Computers and Structures*, 79(19):1811–1819, 2001.

[8] H. H. Yoo, J. Y. Kwak, and J. Chung. Vibration analysis of rotating pre-twisted blades with a concentrated mass. *Journal of Sound and Vibration*, 240(5):891–908, 2001.

[9] Hong Hee Yoo, Seung Hyun Lee, and Sang Ha Shin. Flapwise bending vibration analysis of rotating multi-layered composite beams. *Journal of Sound and Vibration*, 286(4?5):745–761, 2005.

[10] Leonard Meirovitch. *Fundamentals of Vibrations*. McGraw-Hill, New York, 2001.

[11] J. N. Reddy. *Applied Functional analysis and Variational methods in engineering*. McGraw-Hill, New York, 1986.

[12] J. N. Reddy. *Energy principles and variational methods in applied mechanics*. John Wiley & Sons, Inc., New York, 2002.

[13] G. R. Liu and S. S. Quek. *The Finite Element Method A Practical Course*. Butterworth-Heinemann, Oxford; Boston, 2003.

[14] Gérald Kergourlay. *Mesure et prédiction vibroacoustique de structures viscoélastiques: Application à une enceinte acoustique*. PhD thesis, Ecole Centrale Paris, 2004.

[15] T. Pritz. Analysis of four-parameter fractional derivative model of real solid materials. *Journal of Sound and Vibration*, 195(1):103–115, 1996.

[16] 3M (1993). Scotchdamp Vibration Control Systems: Product Information and Perfomance Data. Technical report, 3M Industrial Tape and Specialties Division, St. Paul, Minnesota, US.

[17] J. N. Reddy. *Mechanics of laminated composite plates and shells: theory and analysis*. CRC Press, Boca Raton, 2004.

Appendix A

Area moments

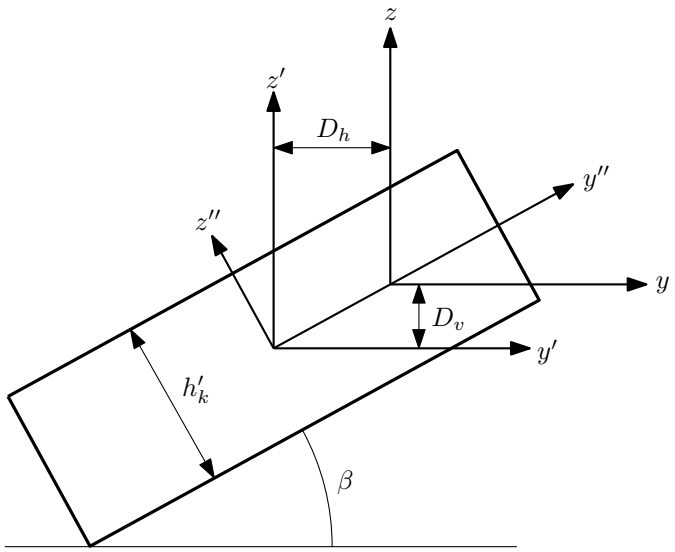

$$S_{y''} = \int_A z''\,dA = 0 \tag{A.0.1a}$$

$$S_{z''} = \int_A y''\,dA = 0 \tag{A.0.1b}$$

$$I_{y''z''} = \int_A y''z''\,dA = 0 \tag{A.0.1c}$$

$$I_{y''} = \int_A z''^2\,dA = \frac{bh^3}{12} \tag{A.0.1d}$$

$$I_{z''} = \int_A y''^2\,dA = \frac{b^3h}{12} \tag{A.0.1e}$$

$$y' = y''\cos\beta - z''\sin\beta \tag{A.0.2a}$$

$$z' = y''\sin\beta + z''\cos\beta \tag{A.0.2b}$$

$$S_{y'} = \int_A z'\,dA = \int_A y''\sin\beta + z''\cos\beta\,dA = 0 \tag{A.0.3a}$$

$$S_{z'} = \int_A y'\,dA = \int_A y''\cos\beta - z''\sin\beta\,dA = 0 \tag{A.0.3b}$$

$$\begin{aligned} I_{y'z'} &= \int_A y'z'\,dA \\ &= \int_A y''^2 \cos\beta \sin\beta + y''z'' \cos^2\beta - y''z'' \sin^2\beta - z''^2 \sin\beta\cos\beta)\,dA \\ &= (I_{z''} - I_{y''}) \sin\beta\cos\beta \end{aligned} \tag{A.0.4}$$

$$\begin{aligned} I_{y'} &= \int_A z'^2\,dA \\ &= \int_A y''^2 \sin^2\beta + z''^2 \cos^2\beta + 2y''z'' \sin\beta\cos\beta\,dA \\ &= I_{z''} \sin^2\beta + I_{y''} \cos^2\beta \end{aligned} \tag{A.0.5}$$

$$\begin{aligned} I_{z'} &= \int_A y'^2 \\ &= \int_A y'' \cos^2\beta + z''^2 \sin^2\beta - 2y''z'' \cos\beta\sin\beta\,dA \\ &= I_{z''} \cos^2\beta + I_{y''} \sin^2\beta \end{aligned} \tag{A.0.6}$$

$$y = y' - D_h \tag{A.0.7a}$$
$$z = z' - D_v \tag{A.0.7b}$$

$$S_y = \int_A z\,dA = \int_A z' - D_v\,dA = -D_v A \tag{A.0.8a}$$
$$S_z = \int_A y\,dA = \int_A y' - D_h\,dA = -D_h A \tag{A.0.8b}$$

$$I_{yz} = \int_A yz\,dA = y'z' - y'D_v - z'D_h + D_h D_v = I_{y'z'} + D_h D_v \tag{A.0.9}$$

$$I_y = \int_A z^2\,dA = \int_A z'^2 + D_v^2 - 2z'D_v\,dA = I_{y'} + AD_v^2 \tag{A.0.10}$$

$$I_z = \int_A y^2\,dA = \int_A y'^2 + D_h^2 - 2y'D_h\,dA = I_{z'} + AD_h^2 \tag{A.0.11}$$

$$D_h = \left(\frac{h'_1}{2} + \sum_{j=2}^{k-1} h'_j + \frac{h'_k}{2}\right) \sin\beta \tag{A.0.12a}$$
$$D_v = D_h \tan\beta \tag{A.0.12b}$$